SISSA

International School for Advanced Studies
(SISSA/ISAS)

Maria Elisabetta Pezzoli

PhD Thesis:

Disorder and Interaction:

ground state properties

of the disordered Hubbard model

Supervisors: Prof.Michele Fabrizio and Dr.Federico Becca

October 2008

Contents

Introduction

The reductionist hypothesis is accepted without question by the great majority of the physicist community. The behavior of all the animate or inanimate matter is assumed to be controlled by the same set of fundamental laws, which, except under certain extreme conditions, we feel that we know very well. Nevertheless the reductionist hypothesis does not by any means imply a "constructionist" one: the ability to reduce everything to simple fundamental laws does not imply the ability to start from these laws and reconstruct the universe. In condensed matter physics there exist many examples where the behavior of a large and complex aggregate of elementary particles was not anticipated from basic quantum mechanics [1] . The off-diagonal long range order underneath superconductivity and superfluidity is just an example of a phenomenon that is practically impossible to deduce from the Schrödinger equation, but becomes accessible once the perspective is enlarged to account for the collective behavior of matter. Even if we had at our disposal techniques that would allow us to treat a large number of elementary constituents of matter and their fundamental interactions, we are not certain that we could reconstruct all the phenomena we observe. Indeed, some physical properties shown by condensed matter may have their foundation in the complex of particles and their mutual interactions considered as a whole. Anyway, since we are not able to calculate everything starting from first principles, the only possibility we have to unveil the physics behind some materials properties is to address directly the collective behavior of matter. The physics of strongly correlated and many body systems deals with these properties which "emerge" from the particles and their mutual interaction considered as a whole.

Another vital aspect of quantum matter is phase coherence. Phase coherence is at the origin of the quantum mechanical behavior observed in macro-

scopic measures, such as transport measures, on mesoscopic electronic devices. For instance, rings of the micrometer size, made out of two-dimensional electron gas on GaAs-AlGaAs heterostructures, show the beautiful magneto-resistance oscillations typical of the Aharonov Bohm effect [2]. In this context the role of disorder is fundamental. Disorder can destroy phase coherence and thus it may cancel the beautiful quantum features that could be observed in macroscopic measures. Nevertheless, at the meantime disorder itself can be at the origin of quantum properties of matter. Non-interacting electrons back-scatter off impurities and, in this backscattering process, they preserve phase memory. The time-reversed paths that contribute to back-scattering interfere constructively with one-another and conspire to localize electrons. For this reason, a disordered non interacting gas of electrons is always insulating in one and two dimensions, while a critical amounts of disorder is required in three dimensions.

The physics of disordered systems without interactions and of interacting but clean systems, has been studied since long and great achievements have been obtained, so that today we feel that we gained a good insight in both fields. Nevertheless, strong disorder together with strong interaction are much harder to tackle. In fact, disorder and Coulomb interaction compete against each other. On the one hand, electrons would like to localize in places which are energetically favorable. On the other hand, such localization generally inhibits the electrons from being well separated from each other, which would better accommodate their mutual Coulomb interaction. This frustration entails complex physical behavior that gives rise to a plethora of exciting new phenomena; one for all the possible existence of a metal-insulator transition in two dimensions, which was believed impossible [3].

Traditionally, disorder is included as a perturbative correction in strongly interacting theories or, conversely, interaction is treated as a perturbation in non-interacting theories of disordered systems. Nevertheless, neither of these perturbative approaches can account for the interaction-disorder frustration described above. Renormalization group theories based on a quantum-field theory approach succeeded in describing the metal-insulator transition in disordered weakly-interacting systems [4, 5, 6]. In the meantime, Dynamical Mean Field Theory (DMFT) was developed and provided new insights into the long-standing issue of the interaction-induced metal-to-insulator transition,the so

called *Mott transition* [7]. Very recently DMFT has been extended to include disorder effects so to address the interplay between disorder and strong interaction [8]. However this scheme neglects spatial correlations and becomes exact only in the limit of infinite-coordination lattices. Since spatial charge fluctuations are very important to determine the transport properties, an alternative method that could allow to treat disorder and strong correlations on equal footing would be highly desirable.

In this thesis we consider a variational wave function approach as a possible route to describe the competition between disorder and strong electron-electron interaction in two dimensions. In particular we aim to obtain a transparent and physically intuitive understanding of the competition between these two localizing forces within the simplest model where they both are active, namely the disordered Hubbard model at half filling and in a square lattice. Our approach is based on an approximate form of the ground-state wave function, which we believe contains the physically relevant ingredients for a correct description of both the Mott and the Anderson insulators, where electrons are localized by the Coulomb repulsion and by disorder, respectively. For strongly interacting fermionic systems, a standard variational wave function is constructed by a correlation term acting on a Slater determinant, the latter being an uncorrelated metallic state. Previous variational calculations showed that a long-range density-density correlation factor, so called Jastrow factor, is needed to correctly describe the Mott insulator [9]. This term, which is collective by definition, correlates spatially charge fluctuations, thus preventing their free motion that would otherwise imply metallic conductance. For this reason, our variational wave function does include such a term. Anderson localization is instead mostly a matter of single-particle wave functions, hence it pertains to the uncorrelated Slater determinant which the Jastrow factor acts onto. We consider both the case in which we enforce paramagnetism in the wave function and the case in which we allow for magnetic ordering.

Summarizing briefly our results, we find that, when the variational wave function is forced to be paramagnetic, the Anderson insulator to Mott insulator transition is continuous. This transition can be captured by studying several quantities. In particular, a novel one that we have identified and that is easily accessible variationally is the *disconnected* density-density fluctuation at long

wavelength, defined by

$$\lim_{q \to 0} N_q^{\text{disc}} = \lim_{q \to 0} \overline{\langle \hat{n}_q \rangle \langle \hat{n}_{-q} \rangle},$$

where $\hat{n}_q$ is the Fourier transform of the charge density at momentum q, $\langle \ldots \rangle$ denotes quantum average at fixed disorder and the overbar represents the average over disorder configurations. We find that $N_{q \to 0}^{\text{disc}}$ is everywhere finite in the Anderson insulator and vanishes critically at the Mott transition, staying zero in the Mott insulator.

When magnetism is allowed and the hopping only connects nearest neighbor sites, upon increasing interaction the paramagnetic Anderson insulator first turns antiferromagnetic and finally the magnetic and compressible Anderson insulator gives way to an incompressible antiferromagnetic Mott insulator. The optimized uncorrelated Slater determinant is always found to be the eigenstate of a disordered non-interacting effective Hamiltonian, which suggests that the model is never metallic. Finally, when magnetism is frustrated by a next to nearest neighbor hopping, the overall sequence of phases does not change. However, the paramagnetic to magnetic transition within the Anderson insulator basin of stability turns first order. Indeed, within the magnetically ordered phase, we find many almost degenerate paramagnetic states with well defined local moments. This is suggestive of an emerging glassy behavior when the competition between disorder and strong correlation is maximum.

Overview

The thesis is organized as follows:

In **chapter 1** we discuss the physics of disordered systems giving a brief overview on the Anderson metal-insulator transition. Subsequently we describe the most significative experimental examples of effects induced by the competition between disorder and interaction, i.e. the existence of a metal in a two-dimensional disordered electron system and the non Fermi-Liquid behavior of doped Si:P semiconductors. We conclude the chapter introducing the disordered Hubbard model.

In **chapter 2** we describe our variational wave function and the criteria we adopt in order to detect the conducting properties given only the ground-state wave function. The second part of the chapter is a more technical one, where we discuss the Variational Monte Carlo method and the Stochastic Reconfiguration optimization algorithm.

In **chapter 3** we show our variational results for the paramagnetic sector of the disordered Hubbard model. We show that disorder is screened due to the Coulomb repulsion and that, for interaction higher than a critical value, a charge gap opens up in the excitation spectrum and thus the wave function becomes an incompressible Anderson insulator.

In **chapter 4** we consider the magnetic properties of the ground state of the disorder Hubbard model and we discuss the magnetic phase diagram of the model both with only first-neighbors hopping and with a frustrating second neighbors hopping term t'. In both cases we show that a finite value of the interaction is needed in order to have a finite magnetization. Moreover we show that an intermediate phase with finite magnetization, but, at the same time, finite compressibility, is stabilized between the paramagnetic Anderson insulator and the magnetic Mott insulator. From our calculations it emerges that, in presence of a finite t', this intermediate phase is reduced.

Chapter 1

Interplay of disorder and electron-electron interaction.

Since their early applications, independent-electron approaches, like Hartree-Fock of density-functional theory within the local density approximation, have led to a fairly complete understanding of the electronic properties of many different materials. Within these schemes the metallic or insulating behavior is determined only by the existence of an energy gap between highest occupied single-particle levels and lowest unoccupied ones. A necessary but not sufficient condition for an insulating behavior is therefore an even number of electrons per unit cell. When this number is odd, one should expect always a metallic behavior unless symmetry breaking phenomena, like magnetism, intervene to increase the unit cell, e.g. doubling it as in the case of Neèl order, so to fulfill the above criterium. However, the independent-electron approaches fail in describing the insulating character of a wide range of materials. The first compound that attracted the attention of the scientific community for its unexpected insulating behavior was NiO. NiO is a transition metal-oxide with one conduction electron per unit cell, and therefore, according to band theory, it should be a metal. Nevertheless it shows an insulating behavior, which is ascribed to the predominant d character of the valence electrons, as Mott pointed out in his pioneering work [10]. In order to explain the NiO insulator, Mott imagined a crystalline array of atomic potentials with one electron per atom and a Coulomb interaction between the electrons. If the lattice spacing is suffi-

ciently large, the overlap between the atomic wave functions is small, giving a very small energy gain due to delocalization of charges throughout the lattice. In this case, the dominant energy contribution comes from the Coulomb repulsion, which favors electron localization. Today it is well accepted that, when the electron interaction is sufficiently strong, the independent electron picture fails and the system can be insulating even with an odd number of electrons per unit cell. These systems, whose insulating character is induced by electron correlations, are called *Mott insulators*. Typical experimental examples are the transition metal oxides, such as the aforementioned *NiO*, layered organic materials [11, 12] and, recently, advances in the laser techniques permitted to realize Mott insulators with cold atomic gases trapped in optical lattices [13, 14].

However interaction is not the only source of localization. There are systems that are insulators neither because of a filled conducting band nor because of a strong repulsive interaction, but because of disorder. These systems are called *Anderson insulators*. In the conventional view of an Anderson insulator, electrons are treated as non interacting particles that become "localized" by the scattering off impurities or defects. The non-interacting assumption can be extended to take into account weak correlations that introduce renormalized disorder and temperature dependent Fermi liquid parameters [37, 38]. However, when strong correlation becomes so strong to push the system towards a Mott transition, the above framework becomes poorly justified.

Conversely, the traditional description of a Mott transition in a clean system, as the one provided by dynamical mean field theory [7], is likely to be not sufficient when disorder is taken into account, since it is difficult to imagine how quasiparticles with a vanishing residue could cope with a finite disorder strength upon approaching a Mott transition.

The above discussion justifies the need of an alternative approach that could deal simultaneously with the physics of Anderson's and Mott's localization.

In this chapter we will briefly survey the theory of the Anderson localization and emphasize experimental evidences of the emerging relevant role of correlations.

1.1   Anderson localization

In his famous paper on the "Absence of Diffusion in certain Random Lattices",
Anderson presented a simple model to show that, in lattices where the energy
varies randomly from site to site, particle diffusion may not take place [15]. He
introduced a simple tight-binding Hamiltonian

$$H = -t \sum_{\langle ij \rangle, \sigma} \left(\hat{c}^{\dagger}_{i,\sigma} \hat{c}_{j,\sigma} + h.c. \right) + \sum_{i} \epsilon_i \hat{n}_i, \qquad (1.1)$$

where t is the hopping amplitude, $\hat{c}^{\dagger}_i (\hat{c}_i)$ creates (destroys) an electron with
spin σ on site r_i, $\hat{n}_i$ it the electron number operator and ϵ_i are random on-site
energies distributed according to some distribution function characterized by
a width D.

For $D << t$, the Kohn-Luttinger theory of transport is applicable [16]. Bloch
waves lose phase coherence on a length of the order of the mean free path l,
which in this case is much longer than the de Broglie wavelength, thus jus-
tifying a semiclassical description of electron motion. Between two successive
scattering events, electrons move ballistically and one recovers the conventional
resistive behavior.

When $D \gg t$, the Hamiltonian (1.1) describes electrons moving in random
potential-wells that are typically very deep compared to the kinetic energy.
Anderson pointed out that, in this case, a single-particle wave functions may
become localized, in the sense that its envelope decays exponentially from some
point in space r_0, i.e.,

$$\psi_n(r) \simeq e^{-\frac{|r - r_0|}{\xi}}, \qquad (1.2)$$

where ξ is the localization length, and $\psi_n(r) = \langle r | \psi_n \rangle$, see Fig.(1.1). The
existence of localized states is better understood in the limit of very strong dis-
order. The zeroth-order description amounts to neglect the kinetic energy; the
eigenstates are simply localized orbitals within each potential well. Perturba-
tion theory in the hopping generates an admixture between different orbitals.
The main point is that such admixture can not produce an extended state
built of a linear combinations of infinitely many localized orbitals. The reason
is that orbitals that are nearby in space, so that the wave functions overlap
significantly, have in general very different energies, so that the admixture is
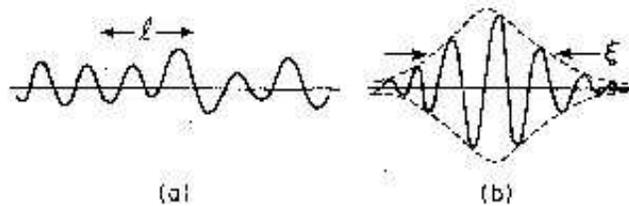
Figure 1.1: Typical wave functions of (a) extended state with mean free path l; (b) localized state with localization length ξ.

small because of the large energy denominator. On the other hand, states that are nearly degenerate, are in general very far apart in space, so that the overlap is significantly small. Thus, in the strongly disordered limit, the wave function will be exponentially localized. A way to measure numerically the localization of a single particle wave function on a discrete lattice is to calculate the Inverse Participation Ratio ($I.P.R.$), which is defined as

$$I.P.R. = \sum_i |\langle i|\psi_n\rangle|^4, \tag{1.3}$$

where $\langle i|\psi_n\rangle$ satisfies the normalization condition. The $I.P.R.$ is a dimensionless number in the range $[0, 1]$. It is equal to one for a completely localized state, and for an extended state it goes to zero in the limit $N \to \infty$. Indeed, for an orbital n completely localized on one site j, $\langle i|\psi_n\rangle \sim \delta_{i,j}$ and, substituting in Eq. (1.3), we find that $I.P.R. = 1$. On the contrary, for a plain wave $\langle i|\psi_n\rangle \sim 1/\sqrt{N}$ and thus

$$I.P.R. \sim \sum_i \frac{1}{N^2} = \frac{1}{N}, \tag{1.4}$$

which leads to $\lim_{N\to\infty} I.P.R. = 0$.

The properties of disordered systems depend crucially on the dimensionality. In three dimensions, the disorder can drive a metal-to-insulator transition. In fact, in the presence of disorder, the density of states acquires tails of localized states – localization occurs first where the density of states is low, see Fig.(1.2) [17]. If D is not so large as to localize the whole band, then ener-
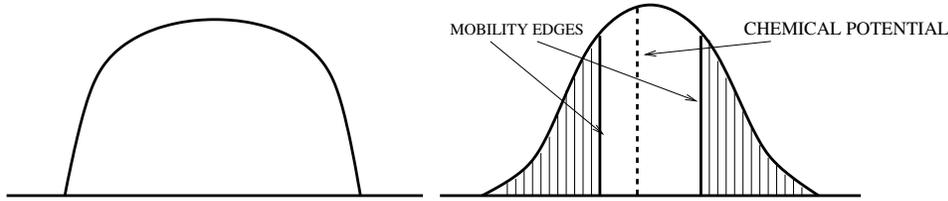
Figure 1.2: Left: density of states of a clean system. Right: density of states in presence of disorder.

gies E_c, called *mobility edges*, separate localized states in the band tails from extended ones in the band center, and the metal-insulator transition can be triggered by sweeping the chemical potential across the "mobility edge" E_c. The chemical potential can be moved across the mobility edge by doping the system; alternatively the metal-insulator transition can be achieved by increasing the density of impurities/defects, i.e., by increasing the region of localized states.

In one dimension, all single-particle wavefunctions are localized, however weak the disorder is, as Mott and Twose rigorously proved [18]. It turns out that two dimensions ($2d$) is the lower critical dimension for a metal-insulator transition, as conjectured by Abrahams *et al.* on the basis of a scaling ansatz [19]. Hence, also in $2d$ all single-particle wavefunction are localized by arbitrarily weak disorder. A key prediction of the scaling theory was that, in thin metallic films, the resistance at moderately low temperatures should logarithmically increase with decreasing temperature, a prediction that has become known as the *weak localization* effect. Experiments performed in the early 1980s on different $2d$ systems confirmed these predictions [20, 21, 22]. The agreement between theoretical expectations and experimental results was convincing, and for nearly two decades, the question of whether a conducting state is possible in $2d$ was considered settled up. The weak localization in two dimension is a result of a non-interacting theory. Nevertheless, subsequent theoretical works showed that weak electron-electron interaction has perturbatively a localization effect [23], which adds to the weak localization phenomenon (for a review on disordered electronic systems see e.g. Ref.[24]).

1.2   Metal-insulator transition in $2d$

Even though the weak localization theory in $2d$ was widely accepted, from time to time some indications appeared that this approach might not be always correct. Finkelstein [25] and Castellani *et al.* [26] considered the interplay of disorder and interactions using perturbative renormalization group methods and they showed that, for weak disorder and sufficiently strong interactions, a $2d$ system scales toward a state with finite nonzero conductivity as temperature is lowered. Unfortunately, the conclusion was not very definite since the theory's range of validity was exceeded as this "metallic" region was approached. Only with the groundbreaking experimental work of Kravchenko and coworkers, the validity of the weak localization in $2d$ was really put into question [3, 27]. Kravchenko has been the first to observe and claim that, above some critical density n_c, high-mobility silicon MOSFET's display a metallic behavior, i.e. resistivity that decreases with decreasing temperature down to the lowest accessible ones, see Fig.(1.3). Below this critical density, the behavior of the resistance looks insulating, thus suggesting that a metal-insulator transition occurs by varying the density. At the critical density, the resistivity is found to be independent of temperature and of order of the quantum resistance unit, $h/e^2 = 25.6\,k\Omega$. These findings were later confirmed in other high-mobility $2d$ devices. A common feature of all the systems that show such a behavior is the low carrier density n_e below $10^{11}\mathrm{cm}^{-2}$. Instead of being small compared to the Fermi energy, at these electron densities the electron-electron interaction energy E_{e-e} is the dominant energy scale. Estimates for Si MOSFET's at $n_e = 10^{11}\mathrm{cm}^{-2}$ yield

$$E_{e-e} \sim \frac{e^2}{\epsilon}(\pi n_e)^{\frac{1}{2}} \simeq 10\,\mathrm{meV} \tag{1.5}$$

while

$$E_F = \frac{\pi\hbar^2 n_e}{2m^*} \simeq 0.58\,\mathrm{meV}, \tag{1.6}$$

where e is the electron charge, ϵ is the dielectric constant, E_F is the Fermi energy, and m^* the effective electron mass (for a MOSFET on a (100) surface, a valley degeneracy of two is taken into account when calculating the Fermi energy). The dimensionless parameter $r_s = E_{e-e}/E_F$ thus assumes values above 10, indicating a strongly interacting regime [28]. Therefore, what distin-
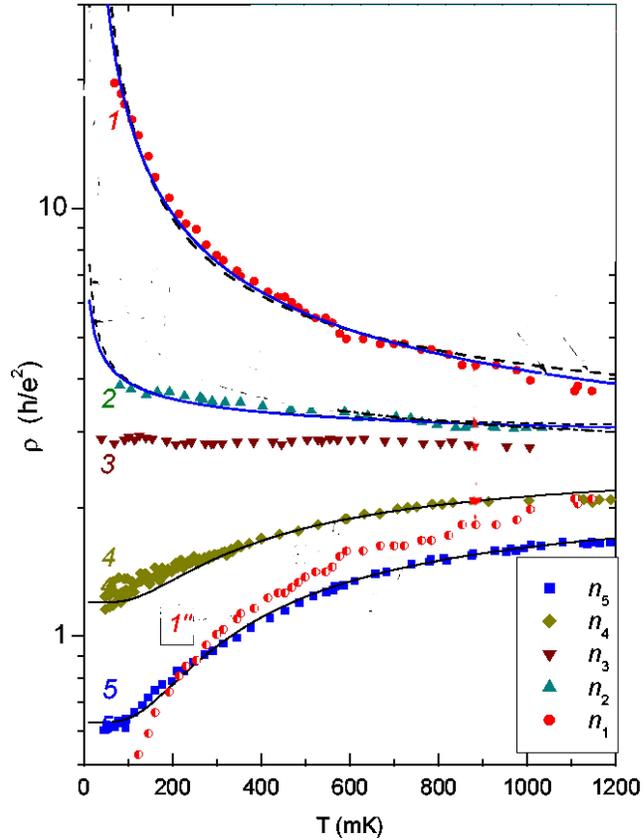
Figure 1.3: $\rho(T)$ for electron densities across the metal-insulator transition. The critical electron density value is $n_c = n_3 = 7.25 \times 10^{10} \mathrm{cm}^{-2}$ and $n_1 < n_2 < n_3 < n_4 < n_5$ [27]

.

guishes these samples from those studied in the 1980s is that the strength of interaction. Thus it is straightforward wondering whether it is just the strong interaction that is responsible of the observed behavior. The old problem of the interplay between disorder and electron-electron interaction is present here in an extreme limit and it yields to many questions that are still far from being solved.

Various explanations of the observed metallic behavior – downturn of conductance lowering temperature – have been suggested during the years, ranging from non-Fermi-liquid hypotheses, to emerging superconductivity and to tem-

perature dependent scattering on charged traps and/or temperature dependent screening; nevertheless the stabilization of a metallic phase in $2d$ is still controversial [29, 4, 30]. Within a perturbative renormalization-group approach, Castellani *et al.* succeeded in describing a stable metallic state in $2d$; in particular, they showed that, in the case of weak disorder, the theory remains under control over a wide temperature range if a renormalization of the energy scale (relative to the length scale) is properly taken into account [5]. Later, by a two-loop renormalization-group calculation in the limit of large valley degeneracy, Punnose and Finkel'stein unveiled the existence of a strong-coupling fixed point that describes a genuine $2d$ metal-insulator transition [6], which was subsequently claimed to be in accord with experiments [31]. However, more recent experiments on p-type GaAs/AlGaAs quantum wells have raised several questions on the correct interpretation of the observed transition, in particular about the role of inhomogeneities in such a very diluted systems where screening is extremely poor [32, 33].

In connection with the topic pertinent to this thesis, it is worth noticing that, in spite of the fact that interaction in these high-mobility devices is undoubtedly strong, it is less clear whether Mott physics plays any relevant role. It is conceivable that, because of the low carrier density, these systems are very close to a Wigner crystalization, which may be viewed as the analogous of a lattice Mott transition in the continuum. However this analogy is quite weak, since when dealing with Wigner crystalization and disorder one has to really worry about inhomogeneities, glassy behavior, clustering [33], all features that go beyond the simple Mott phenomenon but may be crucial to explain the observed behavior.

1.3   Phosphorus doped Silicon

The systems where the Mott physics seems to be really working are phosphorus-doped and boron-doped silicon, Si:P and Si:B. In Si:P and Si:B three-dimensional impurities states form a narrow conducting band in the electronic gap. The impurities are displayed randomly, so that the disorder can lead to an Anderson metal-insulator transition. At the same time, conduction electrons are strongly interacting, since the impurity band is narrow, hence could be driven

to a Mott transition, which is supposedly the case for uncompensated Si:P upon varying doping. Therefore Si:P and Si:B are clear examples systems in which both disorder and interaction are strong, and indeed the competition between these two localizing forces yields to the appearance of unexpected features. Experiments on doped semiconductors show thermodynamic anomalies that cannot be consistently explained within the field-theoretical approach, developed by Finkel'stein [34]. This approach achieved important improvements over previous perturbative works and quickly led to a faithful description of the metal-insulator transition for disordered interacting systems in the presence of magnetic impurities or a magnetic field [35]. These results were soon supplemented by a derivation in terms of many-body perturbation theory [5] and by interpretations in terms of a Fermi liquid theory [36, 37]. However, in the absence of either magnetic impurities or magnetic fields, a full understanding of the metal-insulator transition has proved much harder [4]. Fig.(1.4) shows electron-spin-resonance (ESR) results for the magnetic susceptibility of three samples of Si:P,B [39]. We note two surprising features. (i) The magnetic susceptibility is power law diverging as the temperature $T \to 0$ in the insulating as well as in the metallic phase. (ii) The behavior of the magnetic susceptibility is smooth across the transition. This suggests that whatever is causing the magnetic anomalies does not critically depend on what is happening to the charges, a property shared by the Mott localization. Indeed, the activated conductivity observed below the critical density in Si:P suggests the existence of a Mott-Hubbard gap, hence an insulating phase that is most likely a disordered Mott insulator. On the contrary, compensated Si:(P,B) shows in the insulating phase a more conventional Efros-Shklovskii variable-range-hopping behavior of conductance, which suggests that a Mott-Hubbard gas still exists and explains the local moments, but the metal-insulator transition is primarily an Anderson transition of itinerant quasiparticles. A similar anomalous behavior as that of the magnetic susceptibility[41] is present also in the specific heat, shown for Si:P in Fig.(1.5) as a function of temperature and for three electron densities $n_e/n_c = 0.78, 1.09$, and 1.25, where n_c is the critical value at the metal-insulator transition [40]. The phonon contribution, proportional to T^3, is shown as dashed lines for each of the three samples. The solid line represents the "free"-electron contribution $c_{v0} = \gamma_0 T$, which was calculated using the Si
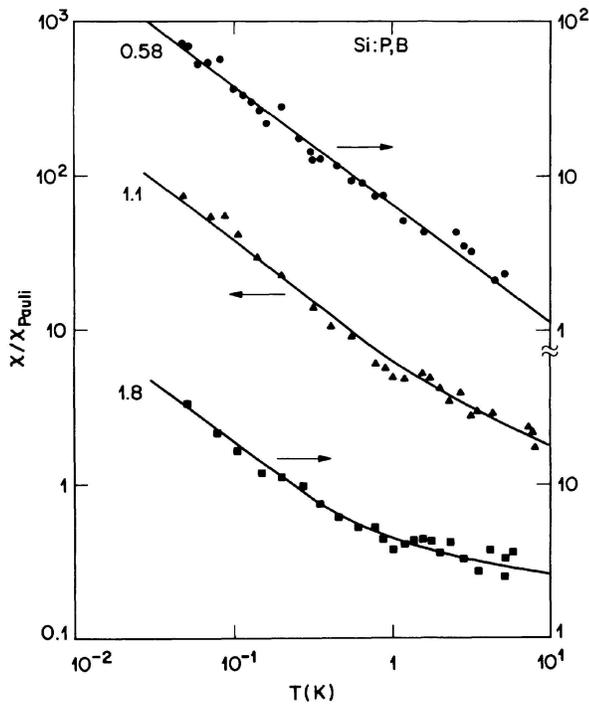
Figure 1.4: Temperature dependence of normalized susceptibility $\chi/\chi_{\mathrm{Pauli}}$ of three samples Si:P,B with different normalized electron densities $n_e/n_c = 0.58, 1.1, 1.8$. Solid line through data are a guide for the eye [39]

.

conduction-band mass, consistent with specific heat measurements well above n_c. These curves show that the specific heat coefficient diverges too at low temperatures both in the insulating and in the metallic side of the transition, pointing to the existence of a very large number of degrees of freedom at low temperatures.

The singular behavior of both specific heat coefficient and magnetic susceptibility in the insulating phase of Si:P is consistent with the model of a disordered quantum antiferromagnet

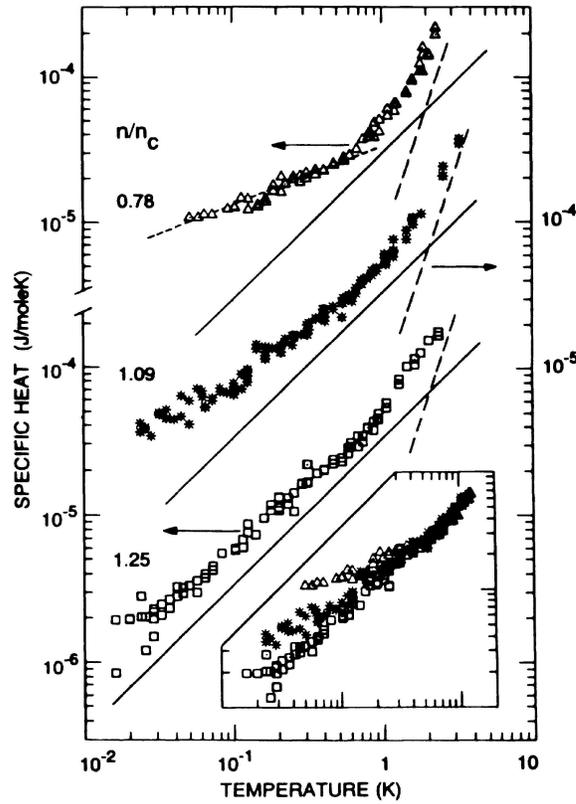$$H = \frac{1}{2} \sum_{i \neq j} J_{i,j} S_i S_j, \tag{1.7}$$

Figure 1.5: Specific heat of Si:P as a function of temperature. Dashed lines represent the phonon contribution AT^3 for $\theta_D = 640K$ and the solid line are the expected specific heat $\gamma_0 T$ for degenerate electrons with effective mass $m_0^* = 0.34m_0$. The lighter dashed line over the $T, 0.7K$ data of the $n_e/n_c = 0.78$ sample represent a $T^{0.4}$ power-law fit. Inset: Different low-temperature behaviors of three samples. [40]

.

proposed by Bhatt and Lee [42]. In Eq.(1.7) $J_{i,j}$ is an exponential function of the distance $|r_i - r_j|$, with r_i being the positions of the donor atoms. Within the Bhatt and Lee scenario, which implicitly assumes that the insulator is Mott-like, there exist a hierarchy of energy/temperature scales that control the quenching of the impurity spins. Specifically, at any finite temperature T there is a finite concentration $N_{free}(T)$ of spins that are still free, hence contribute in a Curie-Weiss fashion to the susceptibility, $\chi(T) \sim N_{free}(T)/T$, and carry

a finite entropy $S(T) = N_{free}(T) \ln 2$. This implies a well defined relationship between specific heat and magnetic susceptibility, specifically if $\chi(T) \sim T^{-\alpha}$ then $c_v \sim T^{1-\alpha}$, which is actually verified in the insulating phase[40, 43, 44, 45].

Extending the Bhatt-Lee scenario on the metallic side of the transition, one could imagine a kind of two fluid model, where itinerant electrons coexist with localized moments, which can be shown to arise within Hartree-Fock approximation by the interplay of interaction and disorder [46], the two constituents being coupled by a Kondo exchange. This assumption would still lead to the same relationship as before – $\chi(T) \sim T^{-\alpha}$ implies $c_v \sim T^{1-\alpha}$ – even if one takes into account, although in an approximate manner, Kondo screening effects [47, 48]. However, experiments do not seem to be in agreement, as they show a specific heat coefficient much greater than one would expect by the magnetic susceptibility through the above relationship, suggesting that there are other low energy degrees of freedom that accumulate at low energy besides the local moments.

Therefore, if, one one hand, there are plenty of evidences that in doped semiconductors the Mott and the Anderson localization phenomena are both active, on the other hand there is still not a satisfactory theory that explains all the observed properties. Like in the aforementioned example of high-mobility $2d$ electron gas systems, even in this, apparently simpler case, many ingredients conspire to complicate the physics. Local moments in the disordered metal should be a source of spin-flip scattering in a strictly two-fluid model – local moments plus non-interacting itinerant quasiparticles coupled one to another by a Kondo exchange. The convention scaling theory of Anderson localization would then predict a positive magneto-conductance, which is not observed. Therefore, the two-fluid scenario is not truly correct – the two constituents are not really distinct; local moments couple one to another by RKKY exchange; residual interactions between quasiparticles may not be negligible. In conclusion, the need of a better understanding of the interplay between disorder and strong correlations overbearingly emerges even in the case of doped semiconductors.

1.4 The disordered Hubbard model

The simplest model that contains both correlations and disorder is the one band disordered Hubbard model

$$H = -\sum_{i \neq j, \sigma} t_{i,j} \left(\hat{c}_{i,\sigma}^{\dagger} \hat{c}_{j,\sigma} + h.c. \right) + \frac{U}{2} \sum_i (\hat{n}_i - 1)^2 + \sum_i \epsilon_i \hat{n}_i \qquad (1.8)$$

where i and j denote sites r_i and r_j, $\hat{c}_{i,\sigma}^{\dagger}(\hat{c}_{i,\sigma})$ creates (destroys) an electron with spin σ on the site r_i and $\hat{n}_i = \sum_{\sigma} \hat{c}_{i,\sigma}^{\dagger} \hat{c}_{i,\sigma}$ is the density operator at site r_i. The term *one-band* refers to the assumption that only one Wannier state per site is considered. This approximation is valid when the Fermi energy lies within a single conduction band, implying an irrelevant contribution of the other bands. Since only one atomic level per atom is considered, each lattice site can appear in four different quantum states: empty, occupied by one spin-up electron, occupied by one spin-down electron, doubly occupied. The first term is responsible for the band energy gain that favors delocalization over the whole lattice. The hopping parameter $t_{i,j}$, $i \neq j$, controls the bandwidth of the system and depends on the weighted overlap of close-by orbitals:

$$t_{i,j} = \int dr \, \phi_i(r)^* \left(\frac{\nabla^2}{2m} + V_{ion} \right) \phi_j(r), \qquad (1.9)$$

where $\phi_i(r)$ is a Wannier orbital centered on site r_i and V_{ion} is the potential created by the positive ions forming the lattice. The Hubbard U comes from the Coulomb repulsion of two electrons sharing the same orbital:

$$U = \int dr_1 dr_2 \, |\phi_j(r_1)|^2 \frac{e^2}{|r_1 - r_2|} |\phi_j(r_2)|^2. \qquad (1.10)$$

This term is only an approximation of the true Coulomb interaction, since it completely neglects the long-range components that are present in realistic systems. The disorder can be introduced in the model through a random hopping matrix $t_{i,j}$ (*off-diagonal disorder*) and/or through random on-site energies ϵ_i (*diagonal disorder*). In what follows we assume only diagonal disorder, namely the hopping parameters $t_{i,j}$ depend only on the distance between site r_i and r_j and the on-site energies are picked up from a flat distribution between $-D$ and D.

In the limit $D = 0$, i.e., when all the energies ϵ_i are equal, the model reduces to the single band Hubbard model. The Hubbard model was independently introduced by Hubbard [49], Gutzwiller [50] and Kanamori [51], in 1963 in order to understand magnetism in transition metals. Currently it is widely used to study strongly-correlated systems, nevertheless it has been solved exactly only in the one-dimensional case [52], since, in spite of its simplicity, the Hubbard model is far from being trivial. Its phase diagram depends on the electron density $n_e = N/L$ (with N the number of electrons and L the number of lattice sites), and the ratio U/t. Moreover, different lattice geometries and different-range hopping terms (first, second, etc. neighbors) can influence the resulting phase diagram. In the generic case and at half-filling, one electron per site, this model must display a Mott metal-to-insulator transition by increasing U, characterized by the opening of a charge gap in the spectrum. Since the Mott insulator has local moments, most likely a magnetic ordering intervenes below a critical temperature that might contaminate the nearby metallic phase, unless in the case of a paramagnetic-metal to a magnetic-Mott-insulator first order transition. In particular examples of nested band dispersions, the magnetic insulator might exhaust all the phase diagram for any $U > 0$, as it is the case for strictly nearest neighbor hopping.

For $U = 0$ but $D > 0$, the model (1.8) is equivalent to the Anderson model (1.1), discussed at the beginning of the chapter. As we discussed, this model is always insulating. However, as we mentioned, the probability to find unoccupied single-particle eigenstates arbitrarily close to the chemical potential, although very far apart in distance from almost degenerate occupied states, is finite in the thermodynamic limit. Therefore, unlike a Mott insulator, the Anderson insulator has a finite compressibility – absence of energy gap for charge excitations.

When both U and D are finite, a plethora of different phases may emerge: magnetically disordered Anderson insulators with or without local moments; magnetically ordered Anderson insulators; magnetically ordered or disordered Mott insulators; and eventually paramagnetic or magnetic metals with or without free local moments. The aim of this work is to identify in simple cases what are the phases that are actually stable at zero temperature.

Chapter 2

The Variational approach

The aim of this thesis is to study the interplay of disorder and electron-electron interaction in two dimensions. As we discussed in the previous chapter, the simplest model to describe such a system contains a kinetic term, an on-site Coulomb repulsion and on-site disordered potentials :

$$H = -t \sum_{<i,j>,\sigma} \left(\hat{c}_{i,\sigma}^\dagger \hat{c}_{j,\sigma} + h.c. \right) + \frac{U}{2} \sum_i (\hat{n}_i - 1)^2 + \sum_i \epsilon_i \hat{n}_i \qquad (2.1)$$

where U is the on-site electron-electron repulsion and t the hopping amplitude. ϵ_i are the on-site potential energies, which are chosen randomly from a flat distribution between $-D$ and D. We focus our work on the two-dimensional case at half filling, i.e., we study a square lattice with N sites and N electrons. Indeed, this is the case in which the interplay between disorder and interaction has its more spectacular effects.

For $D = 0$ the model (2.1) reduces to the well-known Hubbard model :

$$H = -t \sum_{<i,j>,\sigma} \left(\hat{c}_{i,\sigma}^\dagger \hat{c}_{j,\sigma} + h.c. \right) + \frac{U}{2} \sum_i (\hat{n}_i - 1)^2. \qquad (2.2)$$

Despite its simplicity, the exact ground state of the Hubbard Hamiltonian in two dimensions is not known. Nevertheless, important insights into the ground-state properties can be assessed by the *variational method* where the exact ground state is approximated by a trial state. In this approach, the expectation value of the Hamiltonian can be calculated with the important fact that for all wave functions the variational energy gives an upper bound of

the exact one. Therefore, given a trial wave function $|\psi_t(\alpha)\rangle$ depending on a set of parameters $\{\alpha_k\}$ with $k = 1, ...n$, the best approximation to the ground state is given by the parameters that minimize the variational energy

$$E_{var}(\alpha) = \frac{\langle\psi_t(\alpha)|\hat{H}|\psi_t(\alpha)\rangle}{\langle\psi_t(\alpha)|\psi_t(\alpha)\rangle}. \tag{2.3}$$

The key point is to find a variational ansatz that contains the electronic correlation between electrons in a proper way; in fact a good form of the proposed wave function allows one to derive the physical properties of the corresponding phases in a straightforward way.

In the first part of the following chapter, we will introduce appropriate trial states $|\psi_t(\alpha)\rangle$, that can be easily treated by numerical methods. First of all we will discuss the Gutwiller wave function supplemented with a long-range Jastrow factor as variational ansatz for the Hubbard model without disorder. Then, we will extend this wave function to inhomogeneous systems, in order to study the properties of the Hamiltonian (2.1). We will also discuss how to understand the low-energy properties of the system from the correlation functions of the ground-state wave function.

The second part of the chapter is a more technical one: we will discuss how to calculate the expectation value of the energy, or of an observable in general, by aims of the quantum Monte Carlo technique. Finally, we will introduce the optimization algorithm, i.e., the Stochastic Reconfiguration method, and we will discuss some minimization examples.

2.1 The variational wave function for a clean system

In a milestone paper, Gutzwiller suggested an elegant way to define a correlated wave function. Indeed, the main effect of local interaction, such as the electron-electron repulsion in the Hubbard model, is to reduce the probability to find doubly occupied sites. Therefore, a good guess for the trial ground state is

$$|\psi_G\rangle = \exp[-g\sum_i \hat{n}_i^2]|SD\rangle, \tag{2.4}$$

where g is a variational parameter and $|SD\rangle$ an uncorrelated Slater determinant, like for example a free fermion wave function [53]. For $g = 0$ the Gutzwiller wave function reduces to the non-interacting ground state, the Slater determinant $|SD\rangle$, while for $g = \infty$ it describes a state without double occupancies, corresponding to the atomic limit obtained for $U/t = \infty$. At half filling, the latter state is an insulator since charge fluctuations are completely forbidden and each site is occupied by one electron. Since the Gutzwiller wave function may describe both the uncorrelated and the infinitely correlated limits, one would expect that it may be also accurate for finite values of U/t, making it possible to describe the Mott-insulator transition that takes place in the paramagnetic sector. However, exact analytical calculations in $1D$ and quantum Monte Carlo studies in higher dimensions [54, 55, 56], showed that the Gutzwiller wave function is always metallic and becomes insulating only for $U/t = \infty$. In fact for any finite U, g is also finite and thus there is a finite number of doubly occupied sites (*doblons*) and empty sites (*holons*). Since there is no correlation between empty and doubly occupied sites, these objects are free to move, implying a finite conductibility. Indeed, at half-filling, holons are positively charged objects with respect to the average of one electron per site, while doblons are negative charged objects, and once an electric field is applied to the system, holons and doblons flow in opposite directions and a finite charge current is generated. For $U/t = \infty$ all the charge fluctuations are completely suppressed and indeed the variational parameter g becomes infinite. Therefore, in this limit the Gutzwiller wave function becomes an insulator, which, however, is non realistic, since charge fluctuations are completely frozen.

In order to obtain an insulating state at finite U, the wave function must contain long-range correlations between holons and doblons. In this respect, recently Capello *et al.* [9] proposed as variational ansatz

$$|\psi_J\rangle = \mathcal{G}\mathcal{J}|SD\rangle, \tag{2.5}$$

where $\mathcal{G}$ is the Gutzwiller factor defined in Eq. (2.4), $|SD\rangle$ a non-interacting Slater determinant, and $\mathcal{J}$ is the Jastrow factor

$$\mathcal{J} = \exp[\frac{1}{2}\sum_{i,j} v_{i,j}(\hat{n}_i - 1)(\hat{n}_j - 1)], \tag{2.6}$$

with $v_{i,j}$ variational parameters that depend upon the distance, i.e., $v_{i,j} = v(|r_i - r_j|)$. Capello *et al.* showed that the density correlations introduced by the Jastrow factor are indeed the important correlations between holons and doblons that make it possible to obtain a Mott insulating state. In fact, we can re-express the density-density term in Eq.(2.6) in the following form

$$(\hat{n}_i - 1)(\hat{n}_j - 1) = \hat{d}_i \hat{d}_j + \hat{h}_i \hat{h}_j - \hat{h}_i \hat{d}_j - \hat{h}_j \hat{d}_i \tag{2.7}$$

where $\hat{d}_i = \hat{n}_{i,\uparrow} \hat{n}_{i,\downarrow}$ and $\hat{h}_i = (1 - \hat{n}_{i,\uparrow})(1 - \hat{n}_{i,\downarrow})$ are the operator that counts the doblons and the holons on the site r_i, respectively. Thus it follows that a negative Jastrow parameter $v_{i,j} < 0$ implies a long-range attraction between holons and doblons and a long-range holon-holon and doblon-doblon repulsion.

The Jastrow factor (2.6) was first introduced as variational ansatz in the continuum [57] . Several numerical works, sustained by analytical calculations, proved that it describes accurately the low-energy properties of liquid Helium [58, 59]. Afterwards, the Jastrow factor applied to a Slater determinant $|SD\rangle$ has been proposed also for fermionic problems [60, 61, 62]. The most successful example is given by the Fractional Quantum Hall effect that can be explained using the Laughlin variational wave function. Indeed, this state can be easily written as the product of one-body and two-body Jastrow factors

$$\psi_L(z_i) = \exp[\frac{1}{\nu} \sum_{i \neq j} \ln(z_i - z_j)] \exp[\sum_l |z_l|^2] \tag{2.8}$$

where ν is the filling factor (that must be odd in order to obtain the correct symmetry properties) and $z_j = x_j + iy_j$ is the complex adimensional coordinate of the jth particle [63]. In all these examples the functional form of the Jastrow wave function is kept fixed: in fact the Jastrow factor in its most generic form (2.6) involves many variational parameters, whose number grows with the lattice size. Keeping fixed the functional form of $v_{i,j}$ implies a wave function that is easy to handle, but however it may give a result that is biased by the choice of the functional form and the variational flexibility may be lost.

Recently, thanks to recent developments of the minimization technique (see below), it has been possible to afford a full optimization of the Jastrow factor, despite a large number of parameters. The full optimization permitted to show that the Jastrow factor is the key ingredient to describe a Mott insulator

in a variational approach, despite the fact that it was generally considered irrelevant for the description of strongly correlated systems (its use was believed to influence only the accuracy in energy). Indeed, the Gutzwiller wave function supplemented with a long-range Jastrow factor is able to describe the metal-insulator transition without any symmetry breaking. For instance, this wave function is able to reproduce all the known phases of the one dimensional $t - t'$ Hubbard model. [9, 64].

2.1.1 Criteria to distinguish the metallic and insulating phases

The Kohn criteria. Transport measures distinguish a metal from an insulator, nevertheless in a variational approach the conductivity is not accessible and other criteria must be employed.

In a milestone paper, Kohn [65] pointed out that the qualitative difference in the conducting properties of a system reflects a different arrangement of electrons in the ground state. In particular, a metallic wave function is sensible to a change in the boundary conditions, while an insulating state is not, since in insulators all electron states are localized. Therefore, the conducting properties of a system can be studied assuming periodic boundary conditions, threading the system with a flux Φ and looking at the change in the ground-state energy. In fact, it can be proved that

$$\omega_D^* \sim \frac{d^2 E_0}{d\Phi^2} \tag{2.9}$$

where ω_D^* is the weight of the Drude peak of the optical conductivity and E_0 the ground-state energy. Thus there is a tight connection between the DC conductivity and the behavior of the ground-state energy with respect to a change of Φ, in other words $\frac{d^2 E_0}{d\Phi^2} \neq 0$ becomes a criterion to distinguish the metal from the insulating phase, without disorder, at temperature $T = 0$.

It has been proved that the variational wave functions of the Gutzwiller type, thus including also the Jastrow wave function, are always metallic according to the Kohn criteria [66]. In particular it has been showed that for the Gutzwiller wave function $|\psi_G\rangle$

$$\omega_D^* = -4\pi T_g \tag{2.10}$$

where T_g is the kinetic energy evaluated using $|\psi_G\rangle$. Since for every finite U, T_g is finite, it follows that ω_D^* is always finite. Therefore, one would be tempted to believe that it is impossible to describe an insulator within the variational approach. Indeed, these type of wave functions fail in describing an insulating state according to the Kohn criteria because the "Gutzwiller/Jastrow" prescription gives an approximation $E(\Phi)$ to the ground-state energy $E_0(\Phi)$ whose accuracy varies with Φ leading to an incorrect estimate of $d^2E_0/d\Phi^2$. However, this is not the end of the story. In fact, the previous statement is based on the assumption that the functional form of the Jastrow factor does not change in the presence of Φ. Instead, in presence of a finite flux, it may acquire an odd part under inversion, making it possible to correctly reproduce the behavior of the ground-state energy. In particular in order to describe in a proper way the response to the flux Φ, we should add to the Jastrow factor the term

$$J_\Phi = \exp[\sum_{i,j} w_{i,j} \hat{h}_i \hat{d}_j] \tag{2.11}$$

where $\hat{h}_i(\hat{d}_i)$ is the holon (doblon) operator and $w_{i,j}$ acquire an antisymmetric component, i.e., $w_{i,j} - w_{j,i} \neq 0$ when $\Phi \neq 0$.

In practice, with the variational method it is more convenient to discriminate the Mott insulator from the metal through correlation functions that can be calculated in the absence of a flux, as it is very unhandy to follow the changes of the variational wave function due to the presence of a finite flux Φ.

The f-sum rule. Following always the Kohn idea that the transport properties are reflected in the arrangement of electrons in the ground state, it is possible to show that the metal-insulator transition can be determined from the different behavior of the static structure factor N_q:

$$N_q = \langle \hat{n}_{-q} \hat{n}_q \rangle - \langle \hat{n}_q \rangle \langle \hat{n}_{-q} \rangle \tag{2.12}$$

where $\hat{n}_q$ is the Fourier transform of the local density operator $\hat{n}_i = \hat{n}_{i,\uparrow} + \hat{n}_{i,\downarrow}$ and $\langle ... \rangle$ indicates the average over the optimized wave function. Naturally, in a clean system $\langle n_q \rangle = \delta_{q,q_B}$ where $q_B = 2\pi(n,m)$, with n,m integer numbers, are the reciprocal lattice vectors corresponding to the Bragg peaks.
We can estimate the average energy Δ_q of the low-lying excitations through

the relation

$$\Delta_q = \frac{\int_0^\infty \frac{d\omega}{\pi}\, \omega S_q(\omega)}{\int_0^\infty \frac{d\omega}{\pi} S_q(\omega)}, \tag{2.13}$$

where $S_q(\omega)$ is the dynamical structure factor, related to the static structure factor through the relation

$$N_q = \int_0^\infty \frac{d\omega}{2\pi} S_q(\omega). \tag{2.14}$$

After some simple calculations, from Eq.(2.13) we obtain that

$$\lim_{q\to 0} \Delta_q \sim \frac{q^2}{N_q}. \tag{2.15}$$

Therefore the charge excitation spectrum, and thus the metallic or insulating behavior of the system, can be inferred from the behavior of N_q for $q \to 0$: in fact since the numerator behaves like q^2, $N_q \sim q$ means that the system is gapless (the average energy of an excitation is zero), while $N_q \sim q^2$ is a necessary condition for the charge gap to be finite (for a detailed demonstration, see appendix A). This argument, generally known as *f-sum rule* was first introduced in Ref.[67]. Within the variational approach, the use of a long-range Jastrow factor ensures that the f-sum rule holds also variationally, once we assumed that $n_q|\psi_t\rangle$ represents the excited state, with $|\psi_t\rangle$ the approximated ground-state wave function. In fact from the condition that determines the variational minimum

$$\frac{\partial E_{var}}{\partial v_q} = 0 \qquad\qquad \forall q, \tag{2.16}$$

we find the f-sum rule relation

$$\Delta_q = E_q - E_0 \sim \frac{q^2}{N_q}, \tag{2.17}$$

where E_q and E_0 are respectively the variational energy of $n_q|\psi_t\rangle$ and $|\psi_t\rangle$ and N_q is the density-density correlation factor calculated over $|\psi_t\rangle$. As an example, we show in Fig.(2.1) the variational results for the Hubbard model (2.2): for $U < U_c^{\mathrm{MI}} = (8.5 \pm 0.5)\, t$ we have that $N_q \sim q$, while for $U/t \geq 9$, $N_q \sim q^2$.

The metal-insulator transition and the Jastrow factor. From the f-sum rule discussed above, it is possible to make a link between the properties
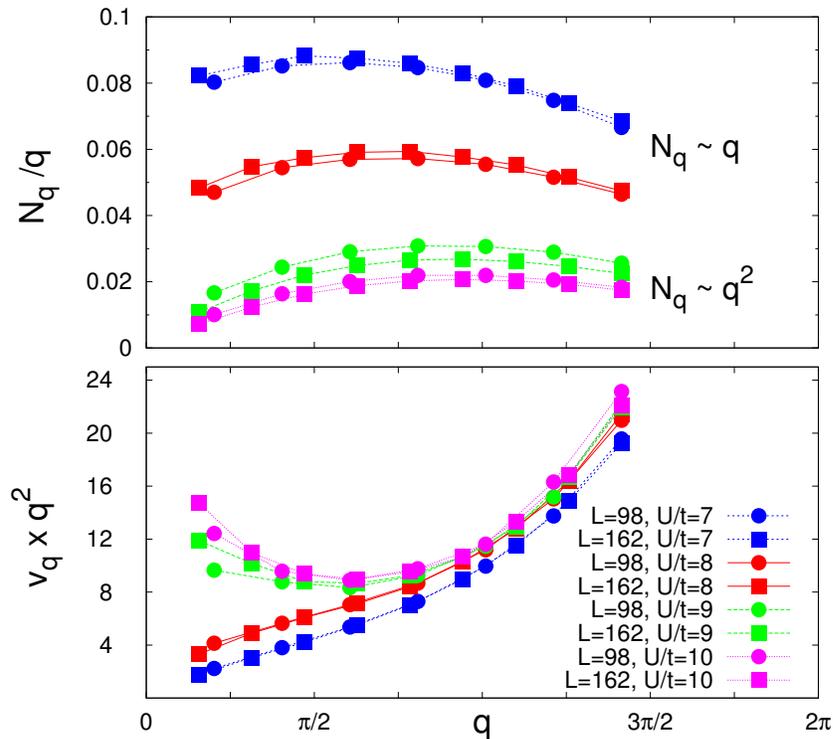
Figure 2.1: Upper panel: static structure factor N_q divided by $|q|$ as a function of $|q|$ for different values of the interaction U. Lower panel: optimized Jastrow potential v_q multiplied by $|q|^2$ as a function of $|q|$ for different values of the interaction U. Calculations have been done for different lattice sizes: $L = 98$ (circles) and $L = 162$ (squares).

of the excitation spectrum and the correlation function calculated from the ground-state wave function. Then, we can infer that the static structure factor behaves like $N_q \sim q$ for a metal and $N_q \sim q^2$ for an insulator. In the following, we will make a further step and show that, within a Jastrow-Slater variational state, there is a tight connection between N_q and the Jastrow parameters. In particular, we show that in order to correctly reproduce the static structure factor of an insulator, without breaking any symmetry, a long-range component of the Jastrow is necessary.

Let $|x\rangle$ be an electronic configuration in real space. For all that operators

θ that depend only on such positions, for example the charge-density structure factor itself, the quantum average

$$\langle \theta \rangle = \frac{\langle \psi | \theta | \psi \rangle}{\langle \psi | \psi \rangle} \tag{2.18}$$

can be written in terms of the classical distribution $|\psi(x)|^2 = \frac{|\langle x | \psi \rangle|^2}{\sum_{x'} |\langle x' | \psi \rangle|^2}$, as

$$\langle \theta \rangle = \sum_x \langle x | \theta | x \rangle |\psi(x)|^2. \tag{2.19}$$

Since $|\psi(x)|^2$ is a positive quantity, we can define an appropriate correspondence between the wave function $|\psi\rangle$ and an effective potential $V(x)$:

$$|\psi(x)|^2 = e^{-V(x)}. \tag{2.20}$$

In the limit of strong interaction the charge fluctuations are small and thus we can safely assume that only the two-body term is relevant; therefore, we can write the potential in the quadratic form:

$$V(x) \simeq \sum_{q \neq 0} v_q^{eff} n_q(x) n_{-q}(x) \tag{2.21}$$

with $n_q(x)$ Fourier transform of the local density of the configuration $|x\rangle$. If we consider $n_q(x)$ as continuous complex variable, the classical average $N_q = \sum_x n_q(x) n_{-q}(x) e^{-V(x)}$ turns into a standard Gaussian integral, yielding to

$$N_q \sim \frac{1}{v_q^{eff}}. \tag{2.22}$$

It follows immediately that in order to obtain the insulating behavior of the static structure factor, $N_q \sim q^2$, the effective potential (2.21) must diverge as:

$$v_q^{eff} \sim \frac{1}{q^2} + \text{less singular terms.} \tag{2.23}$$

If we choose as variational ansatz the Jastrow wave function $|\psi\rangle = \mathcal{J}|SD\rangle$, it turns out that the potential $V(x)$ contains the contributions coming from the Slater determinant $|SD\rangle$ and the Jastrow factor $\mathcal{J}$. If we want to describe the Mott transition without any symmetry breaking, the non-interacting $|SD\rangle$ is a metallic state at half filling. The static structure factor of a metal behaves like

$N_q \sim q$ and thus $|SD\rangle$ will contribute to the effective potential of Eq.(2.21) only with less singular terms, typically of order $O(1/q)$. Therefore, in this approach the Jastrow factor is the key ingredient to obtain a Mott insulator: at the Mott transition the Jastrow changes form, i.e., $v_q \sim 1/q^2$ for small momenta, and in this way it opens up a charge gap in the system.

In Fig.(2.1) we report $v_q \times q^2$, where v_q is the Fourier transform of the optimized $v_{i,j}$ for the Hubbard Hamiltonian (2.2). For $U/t \leq 8$ the Jastrow factor behaves like $v_q \sim 1/q$, while for $U/t \geq 9$, $v_q \sim 1/q^2$. Thus, only by looking at the behavior of the Jastrow term, we are able to conclude that at $U_c^{\mathrm{MI}} = (8.5 \pm 0.5)\, t$ the system becomes a Mott insulator, in agreement with the behavior of the static structure factor N_q, see upper panel of Fig.(2.1).

2.2 The variational wave function with disorder

In order to study the competing role of disorder and electron-electron interaction, we use a trial wave function that includes both correlations through a long-range Jastrow term and the possibility to have local non-homogeneous densities. Our variational ansatz is

$$|\psi\rangle = \mathcal{J} \, \Pi_i \mathcal{G}_i |SD\rangle. \tag{2.24}$$

$|SD\rangle$ is the ground state of a system of N electrons described by the non interacting mean-field Hamiltonian

$$H_{\mathrm{MF}} = -t \sum_{<i,j>,\sigma} \left(\hat{c}_{i,\sigma}^\dagger \hat{c}_{j,\sigma} + h.c. \right) + \sum_{i,\sigma} \tilde{\epsilon}_{i,\sigma} \hat{n}_{i,\sigma}, \tag{2.25}$$

being $\tilde{\epsilon}_{i,\sigma}$ variational parameters. We are going to study the ground-state properties of the Hamiltonian (2.1) both in the paramagnetic and in the magnetic sectors. In order to study the paramagnetic Anderson-Mott transition, we impose the wave function (2.24) to be paramagnetic, by fixing the variational parameters $\tilde{\epsilon}_{i,\downarrow} = \tilde{\epsilon}_{i,\uparrow}$. On the contrary, to study the magnetic properties of the ground state of (2.1), we consider a variational wave function that can break the spin-rotational symmetry, namely we allow the variational parameters to

be $\tilde{\epsilon}_{i,\downarrow} \neq \tilde{\epsilon}_{i,\uparrow}$. The local Gutzwiller factors $\mathcal{G}_i$ are defined as

$$\mathcal{G}_i = \exp[-g_i \hat{n}_i^2], \tag{2.26}$$

and $\mathcal{J}$ is the long-range Jastrow term

$$\mathcal{J} = \exp\left[\frac{1}{2}\sum_{i,j} v_{ij}(\hat{n}_i - 1)(\hat{n}_j - 1)\right]. \tag{2.27}$$

While the Gutzwiller factors have been defined with a different parameter g_i for each site in order to capture the non-homogeneous character of the system, we will consider only translational invariant $v_{i,j} = v(|r_i - r_j|)$. This choice is done in order to reduce the number of variational parameters and so to make the problem tractable from a numerical point of view. Nevertheless, we expect that this choice will not give a strong bias, since the Jastrow factor plays a primary role in the strong coupling regime where the disorder effects are highly suppressed; therefore a translational invariant Jastrow factor should be a fairly good approximation.

To summarize, the variational parameters are: N Gutzwiller factors g_i, N auxiliary energies $\tilde{\epsilon}_i$ for the paramagnetic wave function (for the magnetic wave function we have $2N$ parameters corresponding to $\tilde{\epsilon}_{i,\uparrow}$ and $\tilde{\epsilon}_{i,\downarrow}$) and the Jastrow parameters $v_{i,j}$. In principle, we could also allow for site dependent hopping amplitudes in the mean field Hamiltonian (2.25), however we checked that this further variational freedom does not qualitatively modify the final results. In table (2.1) we report a comparison between the optimized energy

	hop. par.	no hop. par.
U=1	$-2.31373(7)$	$-2.31356(7)$
U=8	$-0.3615(1)$	$-0.3576(1)$
U=12	$0.3855(2)$	$0.3885(2)$

Table 2.1: Optimized energies with and without site dependent hopping amplitudes as variational parameters. The optimization is done for $D/t = 5$ and 18 sites..

corresponding to the variational wave function defined in (2.24) and (2.25) and

the energy corresponding to a wave function including also the site dependent hopping amplitudes. The values are reported for one disorder configuration: a larger variational freedom leads to a better estimate of the ground-state energy, however the loose in accuracy is never larger than 7%. Moreover, computing physical properties of the system, we observe that there is not qualitatively difference from the two solutions. For example in Fig.(2.2) we report the
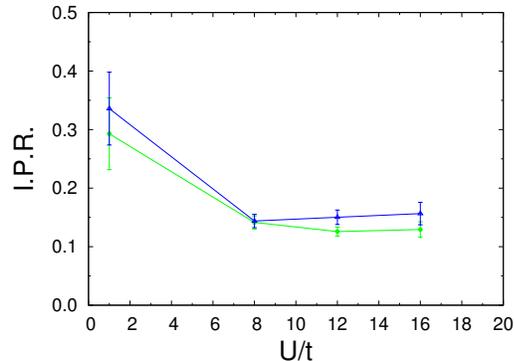

Figure 2.2: I.P.R. with disordered hopping amplitudes (blue curve) and without disordered hopping amplitudes (green curve), for $D/t = 5$ and 18 sites.

results for the inverse participation ratio $I.P.R. = \sum_i |\langle i|\psi_f\rangle|^4$, where $|\psi_f\rangle$ is the normalized eigenvector corresponding to the Fermi level of the disordered Hubbard Hamiltonian (2.1).

2.2.1 The static structure factor N_q with disorder

In a disordered system q is not a good quantum number, nevertheless the average over different disorder configurations restores the translational invariance. This fact implies that the density-density structure factor N_q is a meaningful quantity to assess physical properties. After averaging, the *f-sum rule* should be a good criterium also to distinguish the compressible Anderson insulator from the incompressible Mott insulator. In particular, we expect that $N_q \sim q$ for the Anderson insulator and $N_q \sim q^2$ for the Mott insulator.

In the following, in order to gain a better understanding on the static structure factor, we focus on the non-interacting case. While in a ordered system
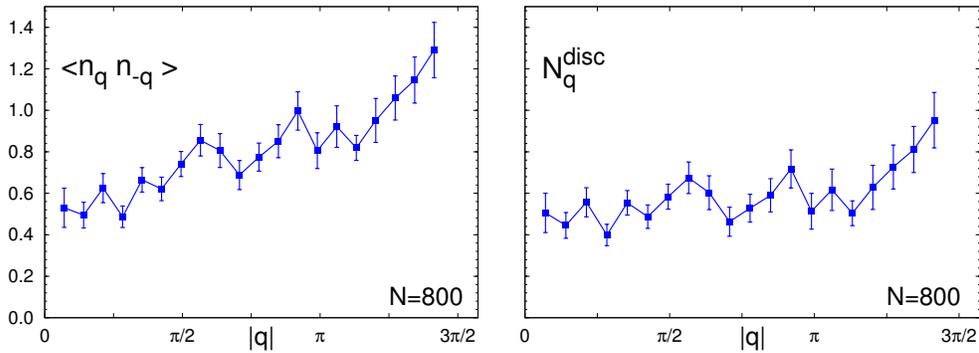
Figure 2.3: Density-density correlation function $\langle \hat{n}_q \hat{n}_{-q} \rangle$ for the Anderson insulator. Left panel: $\langle \hat{n}_q \hat{n}_{-q} \rangle$ vs. q in the (1,1) direction. Right panel: disconnected part N_q^{disc} vs. q. Data points are averaged over 48 disorder realizations for a lattice of size $N = 800$.

$\langle \hat{n}_q \rangle = \delta_{q,q_B}$ with $q_B = 2\pi(n, m)$, in presence of disorder $\langle \hat{n}_q \rangle$ is finite since the translational invariance is broken. This implies that, for a given disorder configuration, $\langle \hat{n}_q \rangle \neq 0$, but, after the disorder average $\overline{\langle \hat{n}_q \rangle} = 0$. However, $N_q^{\text{disc}} = \overline{\langle \hat{n}_q \rangle^2}$ may be finite and, in fact, as Belitz pointed out [68], it is related to the elastic scattering of electrons that can transfer momentum without transferring energy, due to the coupling to a random potential. Because of that, in a disordered system, it is meaningful to subtract N_q^{disc} from the definition of the static structure factor

$$N_q = \langle \hat{n}_{-q} \hat{n}_q \rangle - \langle \hat{n}_q \rangle \langle \hat{n}_{-q} \rangle. \tag{2.28}$$

We use the notation $N_q^{\text{disc}} = \overline{\langle \hat{n}_q \rangle^2}$, since in the Feynman diagram representation of the density-density correlation function $\langle \hat{n}_q \hat{n}_{-q} \rangle$, N_q is the connected part, while $\langle \hat{n}_q \rangle^2 = \langle \hat{n}_q \rangle \langle \hat{n}_{-q} \rangle$ represents the disconnected part.

In Fig.(2.3) we report the "total" density-density correlation function $\langle \hat{n}_q \hat{n}_{-q} \rangle$ and the disconnected term N_q^{disc} calculated for a system of $N = 800$ sites and with disorder strength $D/t = 5$, averaged over 48 disorder realizations. In almost all our work we choose $D/t = 5$, which is indeed a *strong* disorder: in this way the localization length at $U = 0$ is small compare to the numerically accessible system sizes and thus the interplay between disorder and interaction is more evident.

In Fig.(2.4) the static structure factor N_q is shown: $N_q \rightarrow 0$ for $q \rightarrow 0$ as
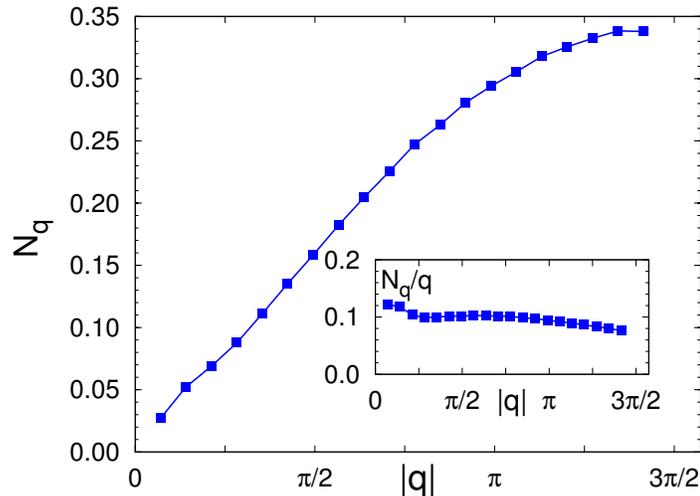

Figure 2.4: Connected part N_q of the density-density correlation function for the Anderson insulator plotted against q in the (1,1) direction. In the inset we show N_q/q, from which is clear that $N_q \sim q$. Data points are averaged over 48 disorder realizations for a lattice of size $N = 800$.

we expect from the particles number conservation (see appendix A) and, most interestingly, $N_q \sim q$ in agreement with the fact that the Anderson insulator is gapless.

2.3   The Variational Monte Carlo method

The first step in a variational approach is to define a good trial state $|\psi_t(\alpha)\rangle$, which is a function of a set of variational parameter $\alpha = \{\alpha_k\}$ for $k = 1, \ldots, p$, in order to include the particle-particle correlations in a proper form. Nevertheless, once a correlated wave function is defined, the problem of computing the expectation value of the Hamiltonian (the variational energy) is not easy because of the presence of correlation factors (the Gutzwiller and Jastrow terms) that make it not possible to apply the Wick theorem, like for mean-field states. In particular for the Hubbard model, since each site can be either singly occupied, by a spin up or down, or empty or doubly occupied, the generic state

reads $|x\rangle = |\uparrow, \uparrow, 0, \downarrow, \uparrow, 2, 2, \uparrow, \downarrow, ...\rangle$ and thus the Hilbert space contains 4^N different configuration states, where N is the number of lattice sites. Therefore, for N larger than 20, the problem becomes numerically intractable.

In the following, we show how to approach this problem through a Monte Carlo sampling of this huge Hilbert space. To this purpose, by using the completeness of the basis $\mathbb{I} = \sum_x |x\rangle\langle x|$, we can write the expectation value of a generic observable $\hat{O}$ like:

$$\langle O \rangle = \frac{\langle \psi_t(\alpha)|\hat{O}|\psi_t(\alpha)\rangle}{\langle \psi_t(\alpha)|\psi_t(\alpha)\rangle} = \frac{\sum_x O(x)\psi_\alpha^2(x)}{\sum_x \psi_\alpha^2(x)} \tag{2.29}$$

where $\psi_\alpha(x) = \langle x|\psi_t(\alpha)\rangle$ and $O(x)$ is defined in the following way:

$$O(x) = \frac{\langle x|\hat{O}|\psi_t(\alpha)\rangle}{\langle x|\psi_t(\alpha)\rangle}. \tag{2.30}$$

Following Eq. (2.29), we can recast the calculation of $\langle O \rangle$ as the average of a random variable $O(x)$ over a probability distribution p_x given by:

$$p_x = \frac{\psi_\alpha^2(x)}{\sum_x \psi_\alpha^2(x)}. \tag{2.31}$$

Within the Monte Carlo algorithm, it is possible to generate a sequence of configuration $|x_n\rangle$, with $n = 1, \ldots, M$, the so called Markov chain, distributed according to the desired probability p_x. Then, since $O(x)$ can be easily computed for any given configuration $|x_n\rangle$, we can evaluate the expectation value of the observable $\hat{O}$ as the mean of the random variable $O(x)$ over the visited configurations:

$$\overline{O} = \frac{1}{M}\sum_{n=1}^{M} O(x_n). \tag{2.32}$$

We would like to mention that in this section the overbar denotes the statistical average, while usually we denote with an overbar the disorder average. In order to obtain the wanted Markov chain, the first step in any Variational Monte Carlo algorithm consists in choosing the initial coordinates $\{r_i\}_0$ for the N particles on the lattice, i.e., the initial configuration $|x_0\rangle$, either randomly (within the choice of $\psi^2(x) \neq 0$) or taking them from a previous Monte Carlo simulation. Then a new trial configuration $|x^T\rangle$ is chosen by moving a particle from its old position to another site.

The Markov chain is then constructed following the Metropolis algorithm. Given the nth configuration of the Markov chain $|x_n\rangle$, the proposed one $|x^T\rangle$ will be accepted, i.e., $|x_{n+1}\rangle = |x^T\rangle$, with a probability $\mathcal{P}$ equal to

$$\mathcal{P} = \min[1, \mathcal{R}] \quad \text{with } \mathcal{R} = |\frac{\psi_\alpha(x^T)}{\psi_\alpha(x_n)}|^2 \tag{2.33}$$

where $\psi_\alpha(x_n)$ and $\psi_\alpha(x^T)$ are the variational wave functions associated with the configurations $|x_n\rangle$ and $|x_T\rangle$, respectively. In practice, a positive random number $0 \leq \eta \leq 1$ is extracted: if $\eta \leq \mathcal{R}$ the proposed move is accepted and $|x_{n+1}\rangle = |x^T\rangle$, otherwise the proposed move is refused and $|x_{n+1}\rangle = |x_n\rangle$. After a certain number of steps, the configurations $|x_n\rangle$ generated at each step n are independent from the initial condition $|x_0\rangle$ and are distributed according to the probability p_x defined above. Notice that this algorithm does not require to know the normalization of the wave function since it always deals with the ratios. This is a big advantage of Monte Carlo methods since the normalization constant implies a sum over the total (huge) Hilbert space.

Once the Markov chain is constructed, it is possible to compute the stochastic average (2.32). Indeed the central limit theorem ensures that:

$$\lim_{M \to \infty} \overline{O} = \sum_x p_x O(x). \tag{2.34}$$

The statistical error related to the fact that we are sampling a finite set of configurations scales like $1/\sqrt{M}$, if the configurations $|x_n\rangle$ are independent from each other. Therefore, for large enough and no correlated samplings, the stochastic average calculated with the Metropolis algorithm gives a reliable estimate of the true expectation value of the system.

In order to ensure uncorrelated samples, the *bin technique* is generally used. This corresponds to average first among M_{bin} configurations:

$$\overline{O}_{\text{bin}}^i = \frac{1}{M_{\text{bin}}} \sum_{n=1}^{M_{\text{bin}}} O(x_n^i), \tag{2.35}$$

where $|x_n^i\rangle$ is the nth configuration state of the ith bin. In this way the quantities $\overline{O}_{\text{bin}}^i$ are less correlated than the original ones. Then one can compute the average value as

$$\overline{O} = \frac{1}{N_{\text{bin}}} \sum_{i=1}^{N_{\text{bin}}} \overline{O}_{\text{bin}}^i, \tag{2.36}$$

where $N_{\text{bin}} = M/M_{\text{bin}}$. The variance can be evaluated in the standard way as

$$\sigma^2(\overline{O}) = \frac{1}{N_{\text{bin}}} \sum_{i=1}^{N_{\text{bin}}} \left(\overline{O}_{\text{bin}}^i - \overline{O} \right)^2. \tag{2.37}$$

In a system with finite disorder, once the expectation value $\overline{O}$ has been computed, the average over different disorder configurations must be evaluated. Therefore, we fix a disorder configuration and we compute $\overline{O}$ as explained above. Then we repeat the same calculation for several disorder realizations and we average the obtained results. We notice that, especially for small Coulomb interactions, different disorder configurations may give rather different results on physical quantities.

2.4 The Stochastic Reconfiguration method

In the previous section, we explained how to compute the variational energy for each set of variational parameters $\alpha = \{\alpha_k\}$ $i = 1, \ldots, p$ by aims of the Metropolis algorithm. The variational parameters have to be adjusted in order to find the wave function that is closer to the exact ground state. In the following we show how to optimize the variational wave function minimising the energy through the Stochastic Reconfiguration algorithm, introduced in Ref. [69].

First of all we reintroduce the notation $|\psi_t(\alpha)\rangle$ for the variational wave function depending on the set of parameters $\alpha = \{\alpha_k\}$ $k = 1, \ldots p$; let $|\psi_t(\alpha^0)\rangle$ be the wave function depending on the initial set of variational parameters. If we consider a small variation of the parameters $\alpha_k = \alpha_k^0 + \delta\alpha_k$, we can linear expand the corresponding wave function $|\psi_t(\alpha)\rangle$ in the following way

$$|\psi_t(\alpha)\rangle = \left(|\psi_t(\alpha^0)\rangle + \sum_{k=1}^{p} \delta\alpha_k \frac{\partial}{\partial\alpha_k} |\psi_t(\alpha^0)\rangle \right). \tag{2.38}$$

We define on each configuration $|x\rangle$ the local operators O^k, corresponding to $O^k(x)$ through the relation $\langle x|O^k|x'\rangle = O_k(x)\,\delta_{x,x'}$ where

$$O^k(x) = \frac{\partial}{\partial\alpha_k} \ln \psi_t(x). \tag{2.39}$$

Then we can rewrite $|\psi_t(\alpha)\rangle$ in a more compact form:

$$|\psi_t(\alpha)\rangle = \sum_{k=0}^{p} \delta\alpha_k \, O^k |\psi_t(\alpha^0)\rangle \tag{2.40}$$

where we imposed $O^0 = \mathbb{I}$ and $\delta\alpha_0 = 1$ for convenience. However, the normalization of $|\psi_t(\alpha)\rangle$ will naturally lead to $\delta\alpha_0 \neq 1$. In this case, the variation of the parameters will be obviously scaled like

$$\delta\alpha_k \rightarrow \frac{\delta\alpha_k}{\delta\alpha_0} \tag{2.41}$$

and $|\psi_t(\alpha)\rangle$ will be proportional to $|\psi_t(\alpha^0)\rangle$ for small $\delta\alpha_k/\delta\alpha_0$. It has to be noticed that Eq. (2.40) can be read as the expansion of $|\psi_t(\alpha)\rangle$ on the subspace spanned by the basis set $\{|\psi_t(\alpha^0)\rangle, O^k|\psi_t(\alpha^0)\rangle\}$ with $k = 1, \ldots, p$, namely the subspace defined by the variational parameters.

Now the key point is to determine the new parameters so to have a lower variational energy. The Stochastic Reconfiguration algorithm is based on the projection method idea: the exact ground state can be filtered out by iteratively applying the Hamiltonian to the trial wave function. In particular, we can apply one step of the power method starting from $|\psi_t(\alpha^0)\rangle$

$$|\psi_t'(\alpha)\rangle = (\Lambda - H)|\psi_t(\alpha^0)\rangle, \tag{2.42}$$

where Λ is a large positive constant in order to lower the energy. The equations for determining the new parameters can be found by imposing that $|\psi_t'(\alpha)\rangle$ coincides with $|\psi_t(\alpha)\rangle$ in the subspace spanned by the vectors $\{O^k|\psi_t(\alpha^0)\rangle\}$ with $k = 1, \ldots, p$. Then, by combining Eqs. (2.42) and (2.40) and projecting the result on the kth component of the Hilbert space, we obtain

$$\langle\psi_t(\alpha^0)|O^k(\Lambda - H)|\psi_t(\alpha^0)\rangle = \sum_{k'=0}^{p} \delta\alpha_{k'} \, \langle\psi_t(\alpha^0)|O^k O^{k'}|\psi_t(\alpha^0)\rangle. \tag{2.43}$$

Thus we found a system of $(p+1)$ linear equations that can be solved to calculate the parameters $\delta\alpha_k$.

Substituting $k = 0$ in the system (2.43) we obtain the relation for $\delta\alpha_0$

$$\delta\alpha_0 = \Lambda - E - \sum_{k=1}^{p} \delta\alpha_k \langle O_k \rangle \tag{2.44}$$

that inserted in Eq. (2.43) for $k \neq 0$ returns

$$\langle H \rangle \langle O_k \rangle - \langle O_k H \rangle = \sum_{k'=1}^{p} \langle O_{k'} O_k \rangle \delta \alpha_{k'} - \sum_{k'=1}^{p} \langle O_{k'} \rangle \langle O_k \rangle \delta \alpha_{k'} \qquad (2.45)$$

where $\langle ... \rangle$ indicates the average over $|\psi_t(\alpha^0)\rangle$. We recognise the first part of Eq. (2.45) to be the *generalised forces*

$$f^k = -\frac{1}{2} \frac{\partial E}{\partial \alpha_k} = \langle H \rangle \langle O_k \rangle - \langle O_k H \rangle \qquad (2.46)$$

and we define the positive definite $p \times p$ matrix

$$s_{l,k} = \langle O_l O_k \rangle - \langle O_l \rangle \langle O \rangle. \qquad (2.47)$$

With this notation the Eq. (2.43) can be rewritten in the compact form

$$\sum_{l=1}^{p} \delta \alpha_l \, s_{l,k} = f^k. \qquad (2.48)$$

Finally, the parameters variations $\delta \alpha_k$ can be rescaled by an *acceleration* constant δt, i.e., $\delta \alpha_k \rightarrow \delta \alpha_k / \delta t$. Thus the Stochastic Reconfiguration algorithm becomes

$$\delta \alpha_k = \delta t \sum_l s_{k,l}^{-1} f^l; \qquad (2.49)$$

from this relation we observe that the role of the *acceleration* δt is to control the extension of the optimisation steps.

The positive definiteness of the matrix $s_{k,l}$ ensures that the algorithm converges. In fact the energy variation corresponding to a small change in the parameters is:

$$\Delta E = -\delta t \sum_{k=1}^{p} \sum_{l=1}^{p} s_{k,l}^{-1} f^k f^l + O(\delta t^2), \qquad (2.50)$$

which is always negative for small enough δt, unless the minimum condition of $f^k = 0$ is reached.

It has to be noticed that the Stochastic Reconfiguration method is very similar to the simpler Steepest Descent method. In fact substituting $s_{k,l}$ with the identity $\delta_{k,l}$, Eq. (2.49) defines the Steepest Descent algorithm

$$\delta \alpha_k = f^k \delta t. \qquad (2.51)$$

The fundamental difference between the Stochastic Reconfiguration minimisation and the Steepest Descent method is the definition of the distance Δ_α between a new set of parameters $\{\alpha_{k'}\}$ and the previous one. The distance Δ_α is crucial for the stability of the optimisation method: in fact in these iterative methods the new parameters have to be chosen close enough to the old ones in terms of the prescribed distance. As it is explained in Ref. [70], within the Stochastic Reconfiguration scheme Δ_α is chosen to be the square distance between the wave functions $\psi_t(\alpha'_k)$ and $\psi_t(\alpha_k)$ corresponding to the two different sets of parameters. On the contrary, in the Steepest Descent method the distance is simply defined as

$$\Delta_\alpha^{SD} = \sum_{k=1}^{p} (\alpha'_k - \alpha_k)^2. \tag{2.52}$$

Sometimes a small change in the parameters corresponds to a large change of the wave function, and conversely a large change of the variational parameters can imply only a small change in the wave function. The Stochastic Reconfiguration method takes into account this effect through a better definition of the distance Δ_α. In Fig.(2.5) we report the comparison between the energy evolution as a function of the minimisation iterations using the Stochastic Reconfiguration algorithm and the Steepest Descent algorithm. It is immediate to notice that the energy is already converged at the 100th iteration in case of the Stochastic Reconfiguration algorithm, while in the Steepest Descent case it still has to converge at the iteration number 300.

The algorithm takes the name *Stochastic* since both the forces and the matrix $s_{k,l}$ are determined stochastically, evaluating the averages in Eqs. (2.46) and (2.47) within the Monte Carlo scheme as explained in the previous section. For example within the Monte Carlo scheme, the forces are equal to

$$f^k = \frac{1}{M_{\text{weight}}} \sum_{i=1}^{M_{\text{weight}}} O^k(x_i) E_{LOC}(x_i) - O^k H(x_i) \tag{2.53}$$

where $E_{LOC}(x_i) = \langle x_i|H|\psi\rangle/\langle x_i|\psi\rangle$, $O^k H(x_i) = \langle x_i|O^k H|\psi\rangle/\langle x_i|\psi\rangle$ and M_{weight} is the number of sampled configurations. This indeed implies that the forces f^k are always determined with some statistical noise η_k. It follows that even when the variational minimum is reached, the parameters will fluctuate around
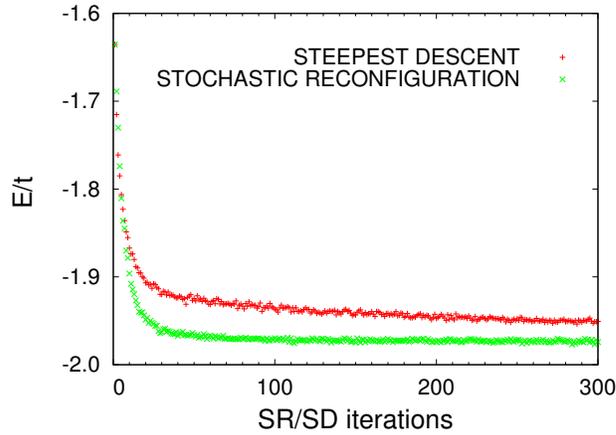
Figure 2.5: Comparison of the Monte Carlo energy evolution as a function of the minimisation iterations using the Stochastic Reconfiguration algorithm (green points) and the Steepest Descent algorithm (red points). The optimization is done for $U/t = 6$ and $D/t = 5$ for a lattice of size $N = 50$.

their mean value. Therefore, it is necessary to average over a certain number of iterations in order to find the optimal parameters that are close to the energy minimum. The evolution of the variational parameters during the minimisation iterations can be described by the Langevin dynamics where the statistical noise plays the role of the thermal noise:

$$\frac{\partial \alpha_k}{\partial t} = f_k + \eta_k. \tag{2.54}$$

By increasing the number of sampled configurations M_{weight} the statistical noise diminishes, namely $\eta_k \sim 1/\sqrt{M_{\text{weight}}}$. Therefore, there is an optimal value of M_{weight} that guarantees a fast convergence and prevent the parameters from being biased by the statistical error. Moreover, the optimal number of sampled configurations M_{weight} depends on the value of the electron-electron interaction U and of the disorder D (in units of the hopping t).

In Fig.(2.6), we show the different energy evolutions for different values of the number of sampled configurations M_{weight}, for $U/t = 4$ and $D/t = 5$ on a lattice of $N = 98$ sites. We observe that the convergence is faster for $M_{\text{weight}} = 4000$: it could be quite unexpected that $M_{\text{weight}} = 4000$ is better than $M_{\text{weight}} = 7000$ and $M_{\text{weight}} = 9000$. A possible reason could be the presence
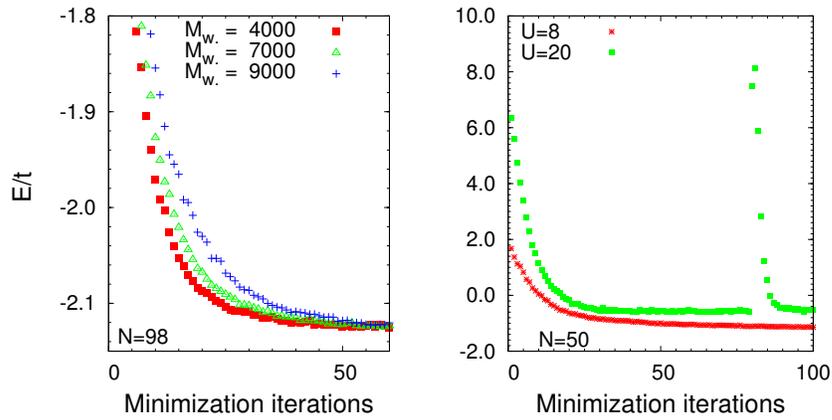
Figure 2.6: Left panel: comparison of the Monte Carlo energy evolution as a function of the minimisation iterations. Different curves correspond to different values of the number of sampled configurations $M_{\text{w.}}$. The optimization is done for $U/t = 4$ and $D/t = 5$ for a lattice of size $N = 98$. Right panel: energy evolution with a fixed number of sampled configurations $M_{\text{weight}} = 4000$ for $U/t = 8$ (red curve) and $U/t = 20$ (green curve). The optimization is done for $D/t = 5$ on a lattice of $N = 50$ sites.

of local minima in the energy landscape: in this case generalized forces, with larger statistical noise, can lead to the true minima faster. In Fig.(2.6) we also report also the energy evolutions for $U/t = 8$ and $U/t = 20$. In both cases $M_{\text{weight}} = 4000$. It is immediate to notice that $M_{\text{weight}} = 4000$ is sufficient for $U/t = 8$, but not for $U/t = 20$.

To summarize, a single iteration step of the Stochastic Reconfiguration minimization scheme can be described as follows: i) a set of variational parameters is given $\{\alpha_k\}$ after the i-th iteration, ii) we calculate f^k and $s_{k,l}$ statistically through a small Monte Carlo simulation, iii) a new set of variational parameters α_k is determined from Eq. (2.49) with a suitable choice of δt.
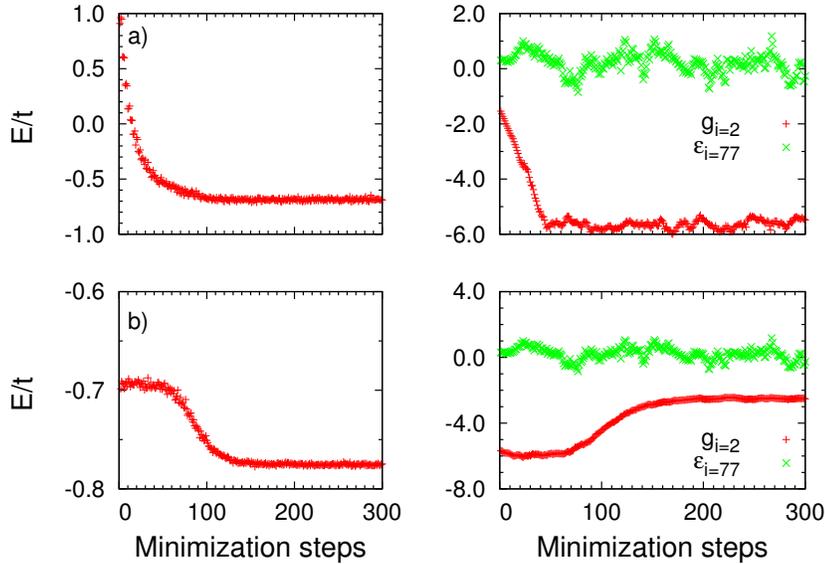
Figure 2.7: a) Energy evolution (left panel) and two parameters evolution (right panel) as a function of the minimization steps for the paramagnetic solution. b) Energy evolution (left panel) and two parameters evolution (right panel) as a function of the minimization steps for the magnetic solution. The optimization is done for $U/t = 16$ and $D/t = 5$ for a lattice of size $N = 98$.

In Fig.(2.7) we report some examples of energy and parameters convergence both for the paramagnetic (a) and the magnetic (b) solution. We argue that the energy evolution in the magnetic case is due to the following mechanism: the

initial parameters $\tilde{\epsilon}_i$ are in a paramagnetic configuration, i.e., $\tilde{\epsilon}_{i,\uparrow} = \tilde{\epsilon}_{i,\downarrow}$, which corresponds to a local minimum so that at the beginning of the simulation the parameters do not change much. Moving from the local minimum, thanks to the statistical noise, the algorithm finds out that with $\tilde{\epsilon}_{i,\uparrow} \neq \tilde{\epsilon}_{i,\downarrow}$ the energy is lowered. At the end of the simulation the energy is converged to a lower minimum corresponding to the antiferromagnetic solution.

Chapter 3

The paramagnetic Anderson-Mott transition

Disorder and electron-electron interactions are both legitimate routes to localization. In the first case, the single-particle eigenstates are localized because of the scattering with impurities, but the charge gap vanishes and the system is compressible; in the second case, the strong Coulomb repulsion localize electrons and a gap in the excitation spectrum opens, making the system incompressible. As we discussed in the first chapter, the interplay between disorder and interaction is one of the most challenging problems in condensed matter. On a theoretical ground, some insights in such a difficult problem can be gained studying the Anderson-Mott transition in the paramagnetic sector, where indeed the charge gap opens up just because of the electron-electron interaction and not because of the onset of long-range magnetic order. Any approach based on a single-particle description, like unrestricted Hartree-Fock [71], can uncover the Mott transition only if spin-rotational symmetry is explicitly broken, which introduces spurious effects due to magnetism. More sophisticated approaches, like those based on dynamical mean-field theory (DMFT) [7], can in principle manage without magnetism [8, 72, 73, 74, 75, 76], but they may miss important spatial correlations, since these are treated in a mean-field-like fashion.

In this chapter, we demonstrate that, within a variational approach, it is possible to describe the Anderson-Mott transition in the paramagnetic sector.

We concentrate our analysis on the case of a disordered Hubbard Hamiltonian defined by

$$H = -t \sum_{<i,j>,\sigma} \left(\hat{c}_{i,\sigma}^{\dagger} \hat{c}_{j,\sigma} + h.c. \right) + \frac{U}{2} \sum_i (\hat{n}_i - 1)^2 + \sum_i \epsilon_i \hat{n}_i, \qquad (3.1)$$

where the hopping term is restricted to nearest neighbor sites of a square lattice. In the following, we consider the half filled case, where the number of sites N is equal to the number of electrons. We define a paramagnetic wave function $|\psi\rangle = \mathcal{J} \Pi_i \mathcal{G}_i |SD\rangle$, where $|SD\rangle$ is the ground state of the mean-field Hamiltonian

$$H_{\mathrm{MF}} = -t \sum_{<i,j>,\sigma} \left(\hat{c}_{i,\sigma}^{\dagger} \hat{c}_{j,\sigma} + h.c. \right) + \sum_{i,\sigma} \tilde{\epsilon}_{i,\sigma} \hat{n}_{i,\sigma}. \qquad (3.2)$$

The paramagnetic character of the variational state is enforced by fixing $\tilde{\epsilon}_{i,\uparrow} = \tilde{\epsilon}_{i,\downarrow}$. In this way, the Slater determinant does not break the spin symmetry. Moreover, $\mathcal{J}$ is the Jastrow factor $\mathcal{J} = \exp[1/2 \sum_{i,j} v_{i,j} (\hat{n}_i - 1)(\hat{n}_j - 1)]$ and $\mathcal{G}_i$ are the local Gutzwiller terms $\mathcal{G}_i = \exp[-g_i \hat{n}_i^2]$ discussed in the previous chapter.

In the following, we construct the paramagnetic phase diagram of the disordered Hubbard model (3.1) and we show that, within this approach, the Mott transition is continuous, in agreement with DMFT results. Moreover, we find that the charge gap opening in the Mott insulator is accompanied by the vanishing of $\lim_{q \to 0} \overline{\langle \hat{n}_q \rangle \langle \hat{n}_{-q} \rangle}$, the overbar denoting the impurity average. Therefore, this quantity, that is related to the compressibility fluctuations, can be interpreted as an order parameter, which permits to distinguish the two insulators, Anderson versus Mott, in a variationally easy way. We also discuss the disorder suppression due to the interaction in the strong-coupling regime and thus the effect of an increasing localization length induced by the interaction. Finally, we define local quantities, e.g., the local kinetic energy, in order to detect the inhomogeneous character of the system and to assess the possibility that different lattice sites approach the Mott transition in different ways.

Actually, from our calculation, the following picture of the Anderson-Mott transition emerges: given a finite disorder D, with increasing electron-electron interaction, the localization length of the single-particle eigenstates increases

and, in this sense, the non-interacting ground state $|SD\rangle$ becomes more metallic. However, the Gutzwiller and Jastrow factors build strong charge correlations in the full variational wave function. Therefore, above a critical value of the interaction $U \geq U_c^{\mathrm{MI}}$, a charge gap opens up, making the ground state an insulator. In the regime $U \sim D$, we observe that the kinetic energy has a maximum and indeed also the single-particle eigenfunctions are maximally extended. Nevertheless, we do not find any evidence in favor of a stabilization of a metallic phase.

3.1 Results for the $2d$ Hubbard model with diagonal disorder

In the previous chapter we discussed that in a clean system it is possible to discriminate variationally metals from Mott insulators by looking at the equal-time density-density structure factor $N_q = \langle \hat{n}_q \, \hat{n}_{-q} \rangle - \langle \hat{n}_q \rangle \langle \hat{n}_{-q} \rangle$. Indeed, $N_q \sim q$ implies the existence of gapless states, while $N_q \sim q^2$ indicates that charge excitations are gaped. Moreover, we saw that there is a tight connection between the long-wavelength behavior of N_q and the Fourier transform of the Jastrow factor v_q, namely $v_q \sim 1/q$ for a metal and $v_q \sim 1/q^2$ for an insulator. We discussed that this distinction should equally work in our model after disorder average.

In Fig.(3.1), we report the variational results of N_q for different values of the interaction U and $D/t = 5$ (as we already discussed, we take such a large value of D in order to have a localization length that, at $U = 0$, is smaller than the numerically accessible system sizes). The results are averaged over different disorder realizations, which range between 6 and 24, depending on the strength of the interaction U. In addiction, the Fourier transform v_q of the optimized Jastrow parameters $v_{i,j}$ is reported in Fig.(3.2) for different values of the interaction U and for different lattice sizes. A clear change of the behavior is observed at $U_c^{\mathrm{MI}}/t = (11.5 \pm 0.5)$ in both quantities, similarly to what was found in the clean Hubbard model [77]. For small values of the interaction strength, i.e., for $U < U_c^{\mathrm{MI}}$, we have that $N_q \sim q$ and $v_q \sim 1/q$, whereas $N_q \sim q^2$ and $v_q \sim 1/q^2$ in the strong-coupling regime $U > U_c^{\mathrm{MI}}$. The
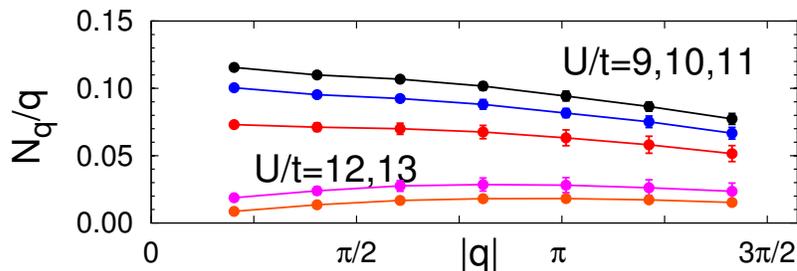
Figure 3.1: Static structure factor N_q divided by q plotted versus q in the $(1,1)$ direction, for different values of the interaction U and $D/t = 5$. The change in the small wave-vector behavior permits us to identify the Mott transition at $U_c^{MI} = (11.5 \pm 0.5)t$. Data points are averaged over several disorder realizations for a lattice of size $N = 98$.
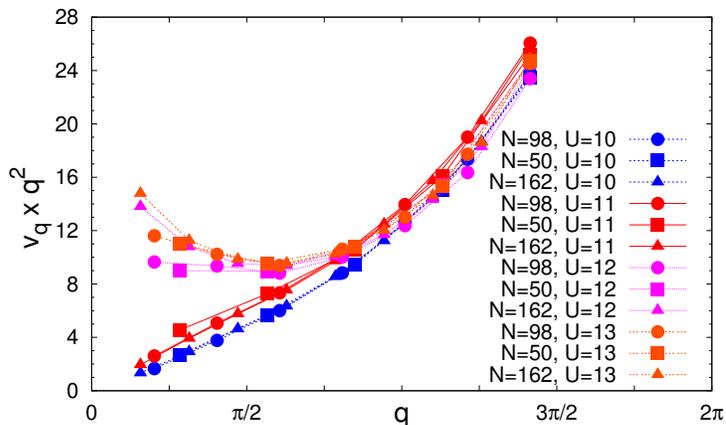

Figure 3.2: Jastrow parameters v_q multiplied by q^2, plotted in the direction $(1,1)$ for disorder $D/t = 5$ and for different values of the interaction U. Calculations have been done for different lattice sizes: $N = 50$ (squares), $N = 98$ (circles), $N = 162$ (triangles).

latter behavior is symptomatic of the presence of a charge gap hence of a Mott insulating behavior [9]. In Fig.(3.3) we report the Fourier transform of the Jastrow parameters for different values of the interaction U and the disorder D. For $D/t = 4$ we find that $U_c^{MI} \cong 11\ t$, whereas for $D/t = 6$ we have
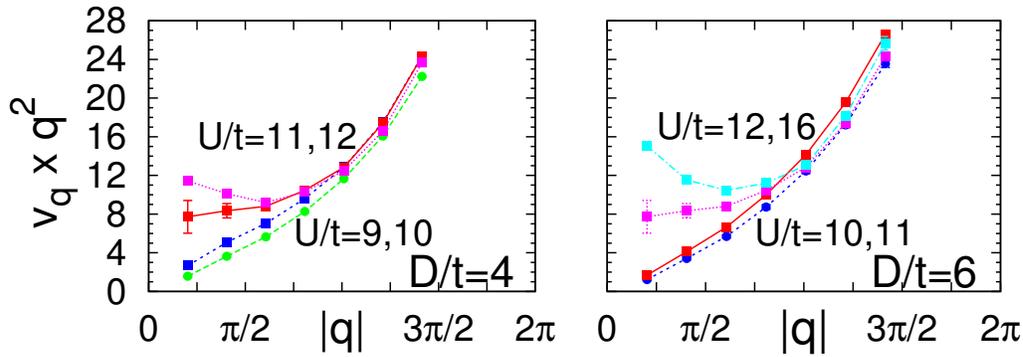
Figure 3.3: Fourier transform of the Jastrow parameters $v_q \times q^2$ for $N = 98$, different values of the interaction U, $D/t = 4$ (left panel), and $D/t = 6$ (right panel). For $D/t = 4$ we find $U_c^{MI}/t \sim 11$ and for $D/t = 5$ $U_c^{MI}/t \sim 12$.

$U_c^{MI} \cong 12\,t$. Moreover we notice that, for the clean case $D = 0$ and within the same approach, a metal-insulator transition at $U_c^{MI} = (8.5 \pm 0.5)t$ was found [77], indicating that disorder competes with U and pushes the Mott transition to higher U. We sketch the resulting phase diagram in the (U, D) plane in Fig.(3.4). We would like to emphasize that the present results are qualitatively similar to those obtained within the clean Hubbard model. In particular, we find that the transition is likely to be continuous, since the linear coefficient of N_q goes continuously to zero at the phase transition. Additional evidence in favor of a second-order transition will be given by considering compressibility fluctuations that will be presented in the following paragraph.
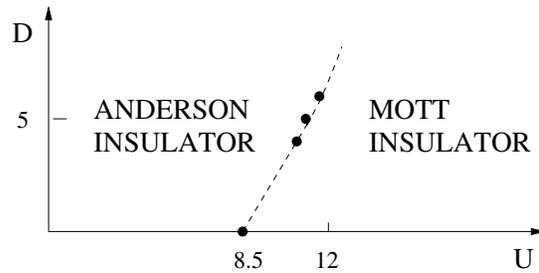
Figure 3.4: Phase diagram for the paramagnetic Anderson-Mott transition.

It is worth pointing out that, unlike in the case of a clean system, for

$U < U_c^{\mathrm{MI}}$, $N_q \sim q$ is not associated to a metallic behavior but only to a gapless spectrum, also characteristic of an Anderson insulator. Our variational Monte Carlo results compare well with those obtained within recent extensions of DMFT to account for disorder effects [76]. Also within this approach, the paramagnetic Mott and Anderson insulators are continuously connected by a second-order phase transition. In addition, although there are discrepancies in the critical values of the interaction, we notice that the slope of the transition line $U_c^{\mathrm{MI}} = U_c^{\mathrm{MI}}(D)$ found within our approach is similar to the one obtained within DMFT.

3.2 The compressibility fluctuations

In the previous paragraph, we showed that our variational approach is able to describe the paramagnetic Anderson-Mott transition. Here, we identify a novel order parameter, namely the disconnected term of the density-density correlations N_q^{disc}, which gives strong evidence in favor of a truly continuous phase transition between the Anderson and the Mott insulators. This quantity, at long wave-length, can easily distinguish between the two insulating states. In the previous chapter we discussed that $N_q^{\mathrm{disc}} = \langle \hat{n}_q \rangle \langle \hat{n}_{-q} \rangle$ is rather different for clean and disordered systems. In the former ones, N_q^{disc} gives rise to the elastic scattering Bragg peaks δ_{q,q_B}, with $q_B = 2\pi(n, m)$, while in the latter ones it is finite for every finite momentum q. From the diagrammatic

Figure 3.5: a) Feynman diagram representation of $\langle \hat{n}_q \rangle$ and $\langle \hat{n}_{-q} \rangle$. Rectangles indicate vertex corrections including both interaction and impurity insertions. Lines indicate fully renormalized Green's functions. b) The average over disorder couples $\langle \hat{n}_q \rangle$ and $\langle \hat{n}_{-q} \rangle$. The dotted line denotes one impurity line connecting the two Feynman diagrams representing $\langle \hat{n}_q \rangle$ and $\langle \hat{n}_{-q} \rangle$.

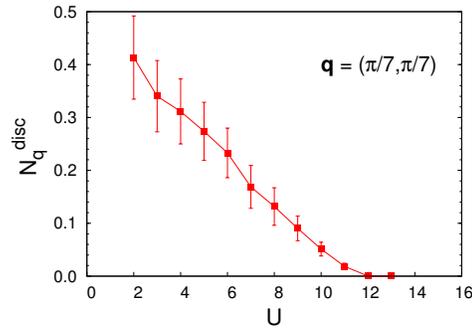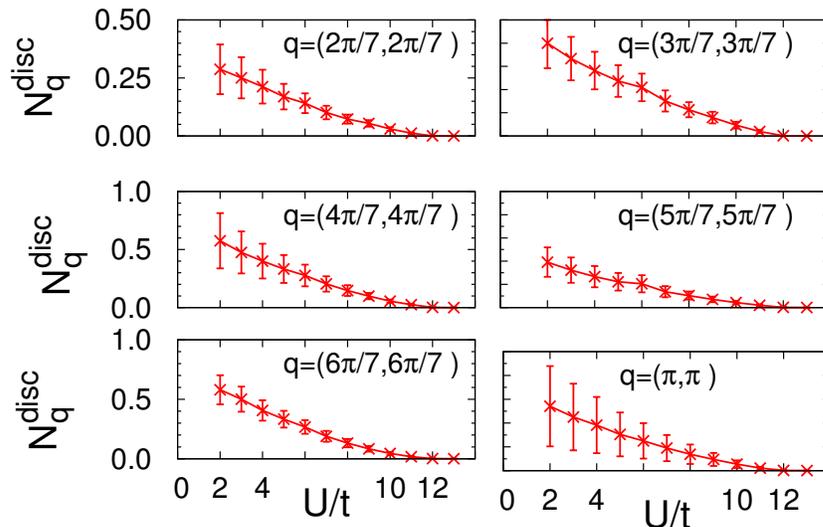representation of N_q^{disc}, one can realize that, for $q \to 0$, it is closely related to

Figure 3.6: Disconnected part of the density-density correlation function N_q^{disc} versus the interaction U. Data points are averaged over different disorder realizations and error bars indicate the standard deviation of the average distribution.

the electron compressibility fluctuations. In fact, the two quantum averages $\langle \hat{n}_q \rangle$ and $\langle \hat{n}_{-q} \rangle$ correspond to the two tadpoles Feynman diagrams, shown in Fig.(3.5), where the solid lines represent fully renormalized Green's functions, i.e., including both disorder and interaction corrections. The average over disorder couples the two tadpoles, see Fig.(3.5). The net result is two "bubbles" connected by impurity lines, which could be regarded as compressibility fluctuations. Therefore, N_q^{disc} is a faithful order parameter for the phase transition between the Anderson insulator, which is compressible, and the Mott insulator, which is incompressible. Fig.(3.6) shows that N_q^{disc}, calculated for the smallest wave-vector available in a finite lattice and averaged over disorder, goes *continuously* to zero at the phase transition. This identifies a simple and variationally accessible way to distinguish between an Anderson insulator and a Mott insulator.

Moreover, as can be extracted from Fig.(3.7), the general trends of N_q^{disc} for all momenta are very much alike, although disorder fluctuations are larger for larger q vectors. This fact demonstrates that the fluctuations $\overline{\langle \hat{n}_i \rangle \langle \hat{n}_j \rangle}$ become local as U increases and eventually vanish at the Mott transition.

Figure 3.7: Disconnected part of the density-density correlation function N_q^{disc} versus the interaction U calculated for different wave vectors q along the (1,1) direction. Data points are averaged over different disorder realizations and error bars indicate the standard deviation of the average distribution.

3.3 Static screening of disorder

The suppression of disorder due to the interaction is an idea that has been discussed by several authors. The connection between disorder screening and delocalization effects, possibly leading to a metallic phase for $U \sim D$, is probably the most interesting aspect that may emerge from this issue. It has to be emphasized that here we are considering the ground-state properties of the disordered Hubbard model, and thus we are referring to static screening of disorder, namely the change and redistribution of the on-site energies by the electron-electron repulsion U. In the following, we will discuss how disorder gets screened by interaction, both in the atomic limit, which is relevant at strong coupling, and within Hartree-Fock approximation, which properly describes the weak-coupling regime. These results have been recently discussed by Henseler *et al.* [78] and are in good agreement with recent numerical works [71, 79, 80]. However, as we discuss below, in all these approaches the disorder

suppression breaks down at large values of the interaction U, a result that we argue is not realistic. Indeed, our variational results, indicate that disorder is highly suppressed also in the Mott regime, in contrast to other approaches.

Let us start with the atomic limit. In this case the Hamiltonian reduces to

$$H = \sum_i \epsilon_i \hat{n}_i + \frac{U}{2} \sum_i (\hat{n}_i - 1)^2. \tag{3.3}$$

In the absence of interaction (i.e., $U = 0$) all the localized states with energy $\epsilon_i < 0$ are doubly occupied and the others are empty. When the interaction is considered, each doubly-occupied site pays a cost in energy equal to $U/2$. If $U > 2D$, all sites are singly occupied and the Mott insulator is recovered. On the other hand, if $U \leq 2D$, those sites with energy $\epsilon_i < -U/2$ are doubly occupied, those with energy $-U/2 < \epsilon_i < U/2$ are singly occupied and the others are empty, see Fig.(3.8). Therefore, the knowledge of the bare energy
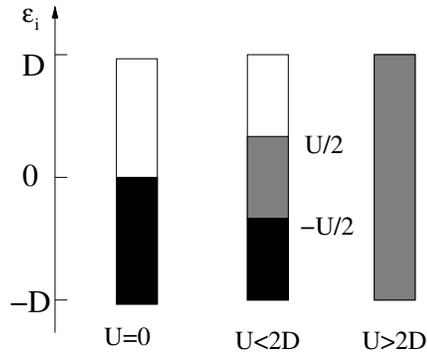
Figure 3.8: Energy level occupation in the atomic ground state with doubly occupied (black), singly occupied (grey), and empty levels (white). Since we are in the strongly localized regime each level correspond to a site. The case on the left corresponds to the Anderson insulator: all sites with energy $\epsilon_i < 0$ are doubly occupied. The case on the right corresponds to a Mott insulator: all sites are singly occupied. The case in the center represents an Anderson-Mott insulator. Here, a fraction of localized sites are doubly occupied or empty as in an Anderson insulator, but a finite number of sites are singly occupied, as in a Mott insulator.

value ϵ_i of a generic site r_i permits to know its occupation. However, the

actual energy level can be renormalized by the interaction, leading to a disorder screening, which will depend upon the local density $\hat{n}_i$. Let us uncover this concept in detail considering for simplicity just one site r_i with energy ϵ_i. If this site is doubly occupied, the corresponding state has energy $2\epsilon_i + U/2$. A single particle excitation consists in emitting one electron; after the electron emission, the site is singly occupied and the energy is ϵ_i. Therefore, the single-particle spectral function has an emission peak at $\omega = \epsilon_i + U/2$. We can define renormalized on-site energies $\tilde{\epsilon}_i$, such that the single-particle spectral function has a peak in $\tilde{\epsilon}_i$; in this case we have $\tilde{\epsilon}_i = \epsilon_i + U/2$. If the site r_i is empty, the corresponding state has an energy equal to $U/2$ and, to obtain an excited state, we have to absorb an electron, paying an energy $\epsilon_i - U/2$. Finally, the last case corresponds to a singly occupied site. The single particle spectral function has two peaks: an emission peak at $\epsilon_i + U/2$ and an absorption peak at $\epsilon_i - U/2$. In summary, the rule for replacing bare site energy ϵ_i by a renormalized one is

$$
\begin{cases}
\epsilon_i \rightarrow \epsilon_i + \dfrac{U}{2} & \text{if } \epsilon_i \leq -\dfrac{U}{2} \\[2ex]
\left.\begin{array}{l} \epsilon_i \rightarrow \epsilon_i + \dfrac{U}{2} \\[2ex] \epsilon_i \rightarrow \epsilon_i - \dfrac{U}{2} \end{array}\right\} & \text{if } -\dfrac{U}{2} < \epsilon_i \leq \dfrac{U}{2} \text{ with equal probability } \dfrac{1}{2} \\[3ex]
\epsilon_i \rightarrow \epsilon_i - \dfrac{U}{2} & \text{if } \epsilon_i > \dfrac{U}{2}
\end{cases}
\tag{3.4}
$$

From weak to intermediate Coulomb repulsions, these shifts lead to renormalization of the probability function $P(\tilde{\epsilon})$ with a reduced width. On the other hand, for large values of the interaction U, the distribution $P(\tilde{\epsilon})$ becomes bimodal, with two peaks centered one at $U/2$, the other at $-U/2$. Each peak is as large as the distribution $P(\epsilon)$, corresponding to $U = 0$, and, therefore, in the strong interaction regime, the atomic limit predicts no disorder screening.

A similar result is obtained within the Hartree-Fock approximation. In this approach, like in all weak coupling approaches, the redistribution of the on-site energies is related to the compressibility of the system [81]. In fact the screened random potential is

$$
\tilde{\epsilon}_{i,\sigma} = \epsilon_{i,\sigma} + U\langle \hat{n}_{i,-\sigma} \rangle,
\tag{3.5}
$$

which in the case of a paramagnetic solution, $\epsilon_{i,\uparrow} = \epsilon_{i,\downarrow} = \epsilon_i$, becomes:

$$\tilde{\epsilon}_i = \epsilon_i + \frac{U}{2}\langle\hat{n}_i\rangle. \tag{3.6}$$

In the weak coupling regime we can apply linear response theory and thus

$$\langle\hat{n}_i\rangle = \langle\hat{n}_i\rangle_0 + \sum_j \chi_{ij}\tilde{\epsilon}_j \tag{3.7}$$

where $\langle...\rangle_0$ means the average respect to the non-interacting clean Hamiltonian and $\chi_{i,j}$ is the proper density-density response function at $\omega = 0$. If we substitute Eq. (3.7) in Eq. (3.5) and we consider the half-filled case, i.e., $\langle\hat{n}_i\rangle_0 = 1$, we obtain

$$\tilde{\epsilon}_i = \epsilon_i + \frac{U}{2} + \frac{U}{2}\sum_j \chi_{i,j}\tilde{\epsilon}_j. \tag{3.8}$$

Neglecting the constant term $U/2$, the equation for the renormalized on-site energy becomes

$$\sum_j (\delta_{i,j} - \frac{U}{2}\chi_{i,j})\tilde{\epsilon}_j = \epsilon_i \tag{3.9}$$

that can be rewritten in a matrix form as

$$(\mathbf{I} - \frac{U}{2}\hat{\chi})\tilde{\epsilon} = \epsilon \tag{3.10}$$

where $\tilde{\epsilon}$ (ϵ) is the vector of components $\tilde{\epsilon}_i$ (ϵ_i) and $\hat{\chi}$ is the matrix of elements $\chi_{i,j}$. Therefore, it is straightforward to obtain a relation for the renormalized energies

$$\langle\tilde{\epsilon}_i\tilde{\epsilon}_j\rangle = \sum_k (\mathbf{I} - \frac{U}{2}\hat{\chi})^{-1}_{i,k}(\mathbf{I} - \frac{U}{2}\hat{\chi})^{-1}_{j,k}\langle\epsilon_k^2\rangle, \tag{3.11}$$

where we used that the original random energies are not correlated, i.e., $\langle\epsilon_i\epsilon_j\rangle = \langle\epsilon_i^2\rangle\delta_{ij}$. First of all, it has to be noticed that the screened disorder $\tilde{\epsilon}_i$ is correlated, namely that, contrary to the unscreened disorder $\langle\tilde{\epsilon}_i\tilde{\epsilon}_j\rangle \neq 0$ for $i \neq j$. Another important fact is that, within this weak-coupling approach, the disorder is no longer screened in the Mott phase. Indeed, whenever the charge gap is finite, $\chi(q, \omega = 0) = 0$ for every q, implying that $\chi_{i,j} = 0$. Therefore, in this limit, it is immediate to see that $\langle\tilde{\epsilon}_i\tilde{\epsilon}_j\rangle = \langle\epsilon_i^2\rangle\delta_{ij}$.

However, the fact that disorder is not suppressed in the regime of strong correlations, and in particular close to the Mott transition, is highly questionable. On the one hand, in the limit of $U = \infty$ one expects that translational

invariance is recovered, but, on the other hand, a substantial mass enhancement takes place, making plausible to have a behavior close to the atomic limit (where there is no screening for $U \gg D$). In this context, DMFT calculations are in sharp discrepancy with results obtained within Hartree-Fock or in the atomic limit [8, 82]. In fact, they show that the screening remains strongly enhanced also for large values of the interaction U, whereas Hartree-Fock and the atomic limit approximations predict a reduction and a complete cancellation of the disorder suppression. However, DMFT predicts that the randomness of the system is completely cancelled at the Mott transition, while, in realistic systems, we expect the disorder to be strongly but not perfectly screened, even in the vicinity of the Mott transition.

Within our variational approach, we evaluate the disorder suppression by calculating the variance of the distribution of the on-site energies of the mean-field Hamiltonian (3.2)

$$\Delta^2 = \frac{1}{N} \sum_i (\tilde{\epsilon}_i - \bar{\tilde{\epsilon}})^2, \tag{3.12}$$

where $\bar{\tilde{\epsilon}}$ is the average of $\tilde{\epsilon}_i$ over all sites, namely

$$\bar{\tilde{\epsilon}} = \frac{1}{N} \sum_i \tilde{\epsilon}_i. \tag{3.13}$$

Moreover, since Δ^2 is a purely mean-field quantity, we also calculate the density fluctuations

$$\delta n^2 = \frac{1}{N} \sum_i \langle \hat{n}_i - \langle \hat{n}_i \rangle \rangle^2 \tag{3.14}$$

that are related to the randomness of the full variational wave function (including the Gutzwiller and the Jastrow factors). Both Δ^2 and δn^2 are averaged over different disorder realizations. In Fig.(3.9) we report the variational results of Δ, compared with the one obtained by the Hartree-Fock approximation. The latter one leads to a disorder screening only for moderate interactions, while it gives almost unscreened on-site energies in the strongly-correlated regime. On the contrary, our variational approach is able to capture the physics of a realistic system, also for large interaction U, where the disorder, though finite, is highly suppressed. The redistribution of on-site energies leads to a decreased localization of the electronic state at the Fermi level. The fact that the single particle wave functions get more and more extended by increasing
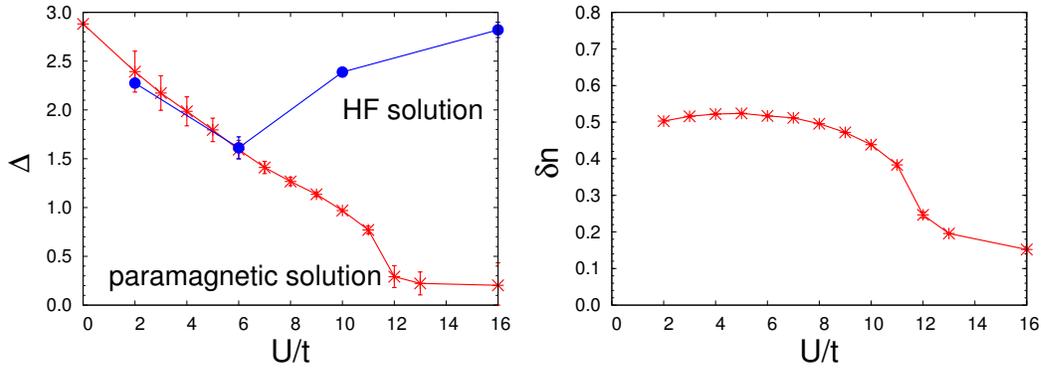
Figure 3.9: Left panel: standard deviation of the distribution of the mean field parameters $\tilde{\epsilon}_i$ (see text) obtained with the paramagnetic wave function (red curve) and within the Hartree-Fock approximation (blue curve). Right panel: standard deviation of the distribution of the on-site density δn (see text) for the paramagnetic state. Results are averaged over 12 different disorder configurations.

interaction, is evident from Fig.(3.10), where we report the $I.P.R. = \sum_i \langle i|\psi_f\rangle^4$ of the normalized eigenstate $|\psi_f\rangle$ at the Fermi level of the mean-field Hamiltonian (3.2). Even though within this approach we cannot access dynamical quantities like DC conductivity, hence we can not address the question of a possible stabilization of a conducting phase with moderate Coulomb repulsion, the previous outcome shows an increase in the "metallicity" of the ground state. This result is in agreement with the fact that the linear slope of N_q has a non-monotonic behavior as a function of U, showing a peak for $U/t \sim 7$ that indicates an accumulation of low-energy states around the Fermi energy, see Fig.(3.11). In fact, the linear slope of N_q is related to the compressibility of the system. At the same time, we observe that the charge fluctuations δn have a maximum for $U \sim D$, indicating that in the regime $U \sim D$ the wave function has its maximum extension, see Fig.(3.9) However, it has to be noticed that the Slater determinant $|SD\rangle$ is the ground state of a mean-field Hamiltonian that, no matter how large is the Coulomb repulsion, always describes non-interacting tight-binding electrons with on-site disorder. Therefore, even though the single-particle eigenstates may have a very long localization length
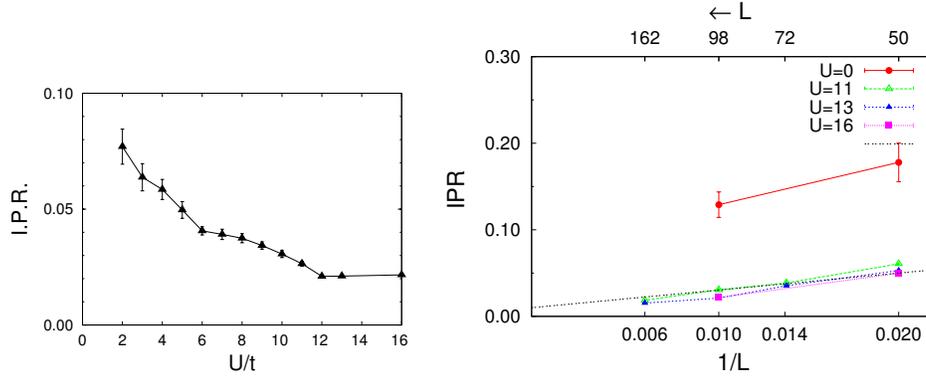
Figure 3.10: Left: I.P.R. of the single particle eigenstate $|\psi_f\rangle$ at the Fermi level of the mean field Hamiltonian for different values of the interaction U. Error bars correspond to the average over different disorder configuration. Right: size scaling of the I.P.R. for $U/t = 0, 11, 13, 16$. Lines are guides for the eye.
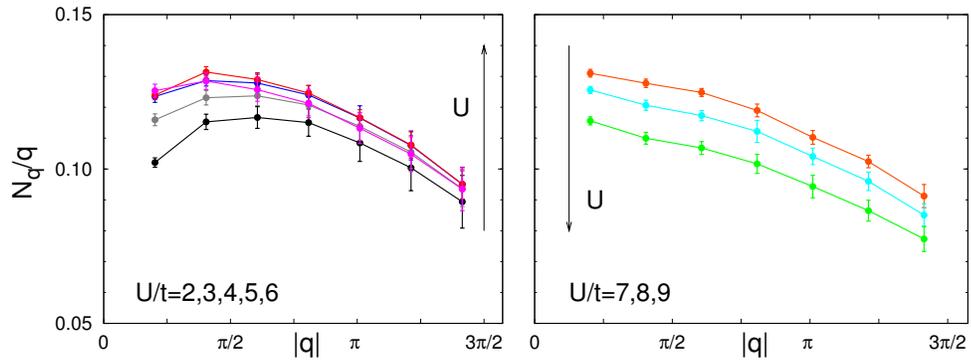
Figure 3.11: Static structure factor N_q divided by q vs q, for different values of the interaction U (left panel $U/t = 2, 3, 4, 5, 6$, right panel $U/t = 7, 8, 9$). Data points are averaged over different disorder configurations.

because of the suppression of the effective on site disorder $\tilde{\epsilon}_i$, yet this length remains finite in two dimensions, see also the size scaling of the I.P.R. reported in Fig.(3.10). Moreover, since the Jastrow factor is not expected to delocalize single particle orbitals, within this approach, the many-body wave function always describes an Anderson insulator below the Mott transition.

In conclusion, from our data the following picture of the paramagnetic Anderson-Mott transition emerges. At finite disorder D and $U = 0$ the ground state is an Anderson insulator, which is compressible, but with localized electron states. When the on-site interaction U is added, the Gutzwiller factors reduce the double occupancies and at the same time the local $\tilde{\epsilon}_i$ are renormalized. Thus, while the Gutzwiller factors introduce the correlations in the wave function, the Slater determinant $|SD\rangle$ becomes more and more "metallic", i.e., the single-particle localization length increases. At the transition the Jastrow factor induces long-range correlations between empty and doubly occupied sites and the wave function becomes a Mott insulator.
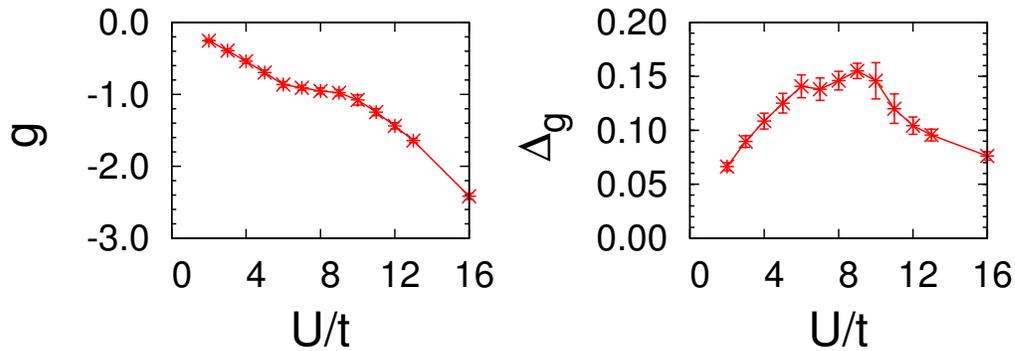
Figure 3.12: Average g (left panel) and standard deviation Δ_g (right panel) of the distribution of the Gutzwiller parameters.

3.4 Local quantities

In this section, we want to analyze in more detail the role of disorder at the Mott transition. A first glimpse of the basic effect of disorder on the transition was outlined by Mott, who pointed out that important consequences can even

be seen when the system is in the strongly localized regime, i.e., in the atomic limit. When $U \leq 2D$ there is a mixture of doubly occupied, empty and single occupied sites, see Fig.(3.8). In this regime the Mott gap vanishes, although a fraction of sites behaves as localized moments. We can describe this state as an inhomogeneous mixture of a Mott and an Anderson insulator. This physical picture is very transparent and intuitive. The non-trivial question is to understand the role of the kinetic term, given also the fact that mobility is increased by the interplay of disorder and interaction (see discussion above). In particular, one could expect strong inhomogeneities, in which sites of the system with a metallic character may coexist with localized electrons. This possibility has been discussed by Aguiar *et al.*, who approached the Anderson-Mott transition from the metallic side [83]. From their scaling analysis, a two-fluid behavior emerges at the critical point, where a fraction of sites turn into local moments, with a vanishing quasi-particle weight $Z_i \to 0$, while the remaining ones are either doubly occupied or empty, with $Z_i \to 1$. The fact of having important inhomogeneities up to the transition point (and even in the Mott phase) is also evident from our calculations. In Fig.(3.12), we report both the average g and the standard deviation Δ_g of the distribution of the parameters g_i. We have that $|g|$ increases with the interaction U in order to reduce the doubly occupied sites, while Δ_g has a non-monotonic behavior with a maximum close to the critical value U_c^{MI}.

In order to gain a deeper understanding on the local behavior, namely how each single site behaves across the Anderson-Mott transition, we introduce a local f-sum rule. In real space, the dynamical structure factor is defined as

$$S_{i,j}(\omega) = \int dt e^{i\omega t} \langle \hat{n}_i(t)\hat{n}_j(0) \rangle \tag{3.15}$$

and thus we can define a *local* dynamical structure factor

$$S_j(q,\omega) = \frac{1}{N} \int dt e^{i\omega t} \sum_i \langle \hat{n}_i(t)\hat{n}_j(0) \rangle e^{iq(r_i-r_j)}. \tag{3.16}$$

Using the fluctuation-dissipation theorem and the Heisenberg equation of motion (see appendix A), we calculate directly the first momentum of the "dynamical structure factor" of site r_j

$$\Sigma_j(q,\omega) = \int_0^{+\infty} \frac{d\omega}{\pi} \omega \, S_j(q,\omega) = \frac{1}{N}\sum_i \langle [[\hat{n}(r_i),H],\hat{n}(r_j)] \rangle e^{iq(r_i-r_j)}. \tag{3.17}$$

After some simple algebra, we obtain the relation

$$\Sigma_j(q) = -2t \sum_{<i>_j,\sigma} \langle c_{i,\sigma}^\dagger c_{j,\sigma} + h.c. \rangle e^{iq(r_i - r_j)} + 2t \sum_{<i>_j} \langle c_{i,\sigma}^\dagger c_i j, \sigma + h.c. \rangle. \quad (3.18)$$

where $\langle i \rangle_j$ indicates the sum over the first neighbors of site r_j. Defining a local static structure factor

$$N_j(q) = \frac{1}{N} \sum_i \langle \hat{n}_i \hat{n}_j \rangle e^{iq(r_i - r_j)} \quad (3.19)$$

we can recast the f-sum rule in a local form

$$\Delta_j(q) = \frac{\Sigma_j(q)}{N_j(q)}; \quad (3.20)$$

the $\lim_{q\to 0} \Delta_j(q)$ is a detector for a local gap, making it possible to clarify if at the Mott transition all sites become localized (with finite moments) simultaneously, or charge fluctuations are possible. The evaluation of both $\Sigma_j(q)$ and $N_j(q)$ requires the computation of equal-time correlations functions, which can be easily done in the variational Monte Carlo scheme.

In Fig.(3.13), we report the distribution of $\Sigma_j(q)$, evaluated at the smallest value of q available within a lattice of $N = 98$ sites, i.e., $q = (\pi/7, \pi/7)$. For small momenta $\Sigma_j(q)$ is proportional to the *local* kinetic term T_j:

$$T_j = t \sum_{\langle i \rangle_j,\sigma} \langle c_{i,\sigma}^\dagger c_{j,\sigma} + h.c. \rangle. \quad (3.21)$$

The average value of $\Sigma_j(q)$ slightly increases by increasing U and it has a maximum in the regime $U \sim D$, like $\lim_{q\to 0} N_q/q$ (see previous section). For small values of the interaction U the distribution of $\Sigma_j(q)$ (or equivalently, the one of T_j) is rather large and it shrinks for increasing interaction strength, in agreement with the fact that the disorder is suppressed by interaction. Just before the transition, i.e., $U/t \sim 10$, the distribution spreads out again, even though not as much as in the strong-D/small-U regime, and indeed the variance of the distribution has a maximum at $U = U_c^{MI}$. A summary of the average value of $\Sigma_j(q)$ and its standard deviation is reported in Fig.(3.14). This picture can be interpreted as a two-fluid like behavior, where a fraction of sites can be regarded as localized spins (i.e., with vanishing charge fluctuations), while
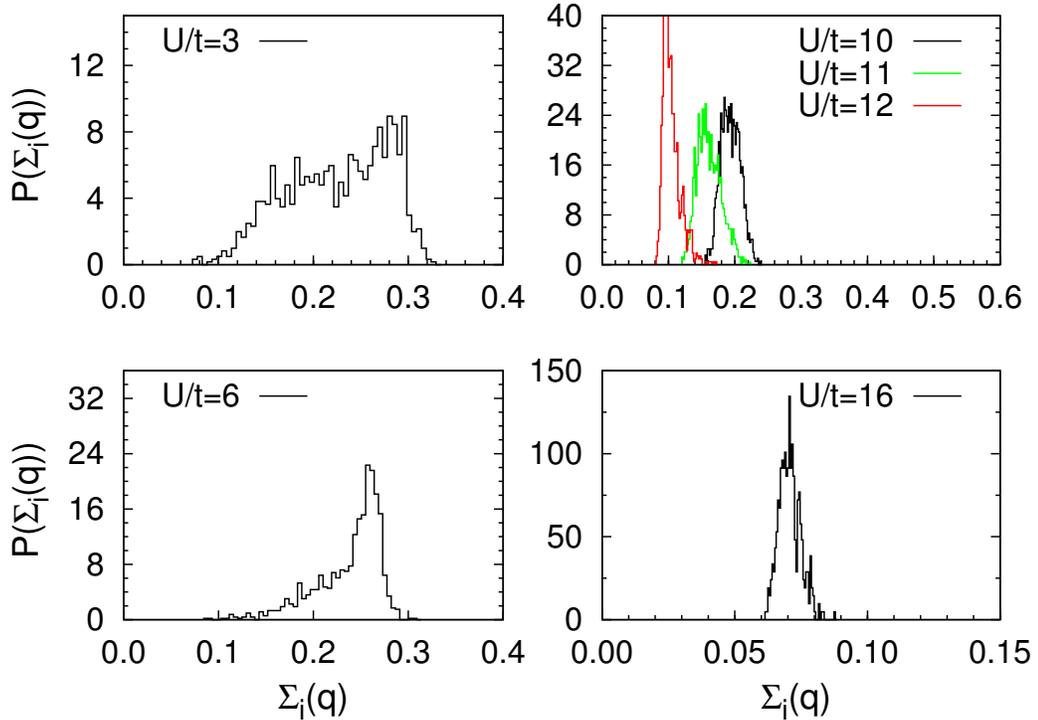
Figure 3.13: Distribution of $\Sigma_i(q) \sim q^2 T_i$ over the lattice sites and the disorder configurations, evaluated at $q = (\pi/7, \pi/7)$. Different curves correspond to different values of the interaction U. Calculations are done for $D/t = 5$. The accumulated statistics is the number of lattice sites($N = 98$) times the number of disorder configurations.

the remaining sites behave like in the Anderson insulator, i.e., they have finite charge fluctuations and no net magnetic moments. For $U > U_c^{MI}$, all the electrons are almost localized by the interaction and indeed the distribution of $\Sigma_j(q)$ has a very sharp peak.

Finally, in Figs.(3.15) and (3.16) we report the distributions of $N_j(q)$ and $\Delta_j(q)$. The behavior of the local structure factor is very similar to the one of the local kinetic term, namely a rather large distribution in the weak-coupling regime and a more peaked form for strong couplings. By contrast, the distribution of $\Delta_j(q)$ is rather narrow for $U < U_c^{MI}$, where $\lim_{q \to 0} \Delta_j(q) \sim 0$ due to a vanishing gap in the Anderson phase. For small values of the wave vector q,
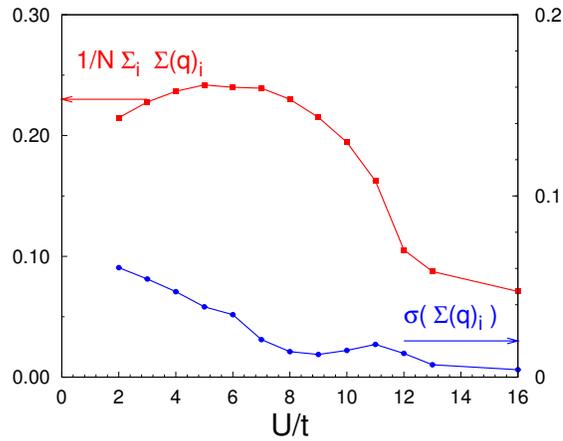
Figure 3.14: Average $\overline{\Sigma(q)} = \frac{1}{N}\sum_i \Sigma_i(q)$ and standard deviation σ of the distribution of $\Sigma_j(q)$ at different interaction values U. Here N is the number of accumulated statistics, i.e., the number of lattice sites times the number of disorder configurations.

the distribution of $\Delta_j(q)$ is peaked around a single value that tends to zero for $q \to 0$. Nevertheless, the distribution has very long tails (with almost invisible weight), which are related to disorder fluctuations; these tails tend to be suppressed by increasing values of the interaction U. For $U > U_c^{\mathrm{MI}}$, a charge gap opens up in the average density of states but the size of the gap turns out to be different from site to site, which implies a rather broad distribution, see Fig.(3.16).
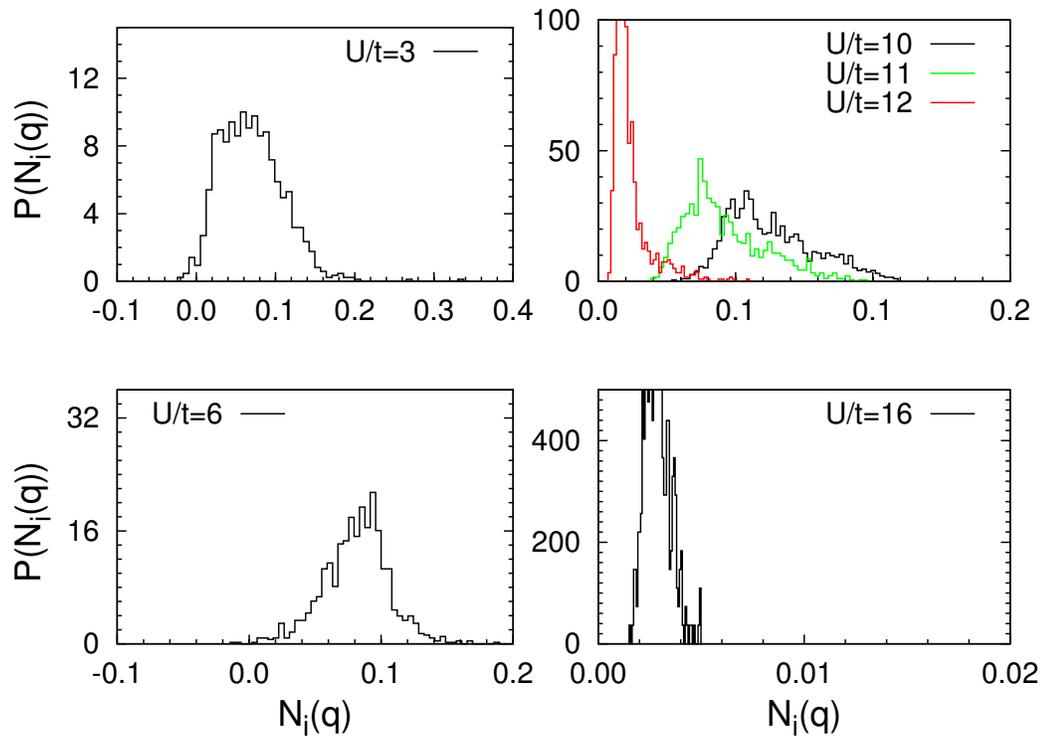
Figure 3.15: Distribution of the local structure factor $N_j(q)$ for different values of the interaction U.
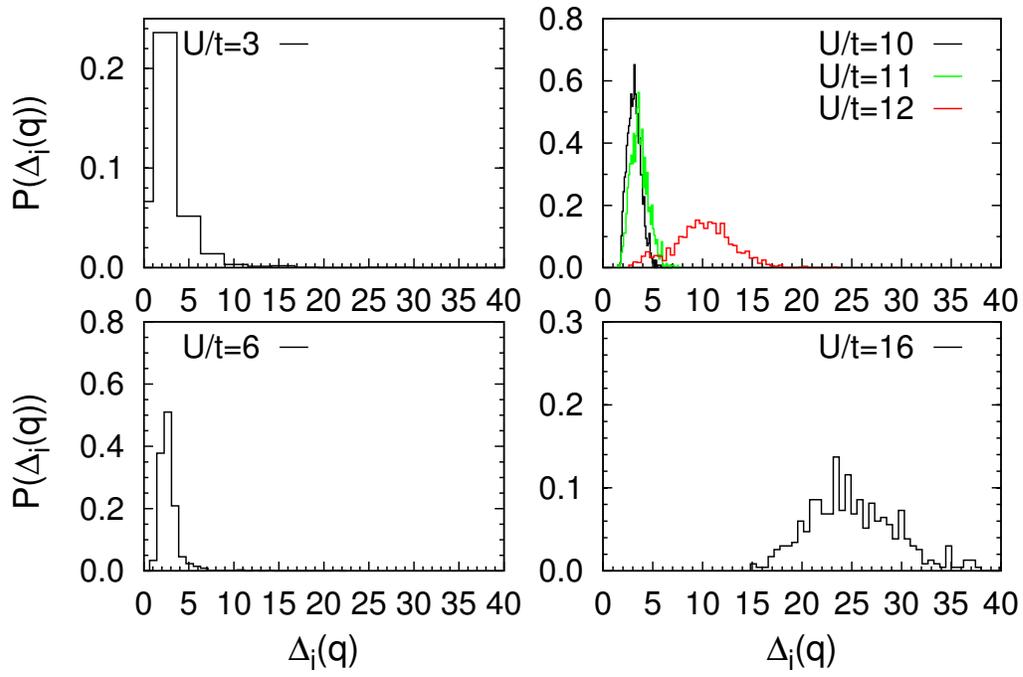
Figure 3.16: Distribution of $\Delta_j(q)$ for different values of the interaction U.

Chapter 4

Magnetic properties of the Anderson-Mott transition

On the square lattice at half filling, in the absence of frustration and disorder, an arbitrarily weak repulsive Hubbard interaction U is able to induce long-range antiferromagnetic order. In fact, in this case, the presence of a perfect nesting implies a diverging susceptibility at $Q = (\pi, \pi)$ that, in turn, opens up a finite gap at the Fermi level. Therefore, the ground state is a band insulator for every finite value of the interaction $U > 0$. By contrast, in the presence of a local random potential, the charge gap may be filled by (localized) energy levels, possibly destroying the long-range magnetic order. The full problem, with strong disorder and electron-electron correlation, is particularly difficult to tackle, since no perturbative approaches are possible. In this chapter, we will focus on this issue, starting from the simplest Hubbard Hamiltonian with local disorder and applying the improved variational technique introduced in the previous chapters, here generalized to describe also antiferromagnetic order. Therefore, the model is

$$H = -t \sum_{<i,j>,\sigma} \left(\hat{c}_{i,\sigma}^\dagger \hat{c}_{j,\sigma} + h.c. \right) + \frac{U}{2} \sum_i (\hat{n}_i - 1)^2 + \sum_i \epsilon_i \hat{n}_i, \qquad (4.1)$$

and the variational wave function is defined by $|\psi\rangle = \mathcal{J}\Pi_i \mathcal{G}_i |SD\rangle$. As usual, $\mathcal{G}_i$ are the local Gutzwiller projectors $\mathcal{G}_i = \exp[-g_i \hat{n}_i^2]$ and $\mathcal{J}$ the Jastrow factor $\mathcal{J} = \exp[1/2 \sum_{i,j} v_{i,j} (\hat{n}_i - 1)(\hat{n}_j - 1)]$ applied to the ground state of the

(non-interacting) Hamiltonian:

$$H_{\mathrm{MF}} = -t \sum_{<i,j>,\sigma} \left(\hat{c}_{i,\sigma}^{\dagger} \hat{c}_{j,\sigma} + h.c. \right) + \sum_{i,\sigma} \tilde{\epsilon}_{i,\sigma} \hat{n}_{i,\sigma}. \qquad (4.2)$$

Here, we allow for different local potential for up and down spins, i.e., $\tilde{\epsilon}_{i,\uparrow} \neq \tilde{\epsilon}_{i,\downarrow}$, in order to give the possibility of having a finite magnetization.

The variational energy landscape, for this generalized wave function, has different local minima. Nevertheless, we will show that, in the case of the simple unfrustrated Hamiltonian of Eq.(4.1), all physical properties corresponding to different minima are the same.

First, we will discuss the phase diagram of the disordered Hubbard model (4.1) with only a nearest-neighbor hopping t. In this case, a finite value of the interaction U_c^{AF} is needed for having the onset of long-range magnetic order: below U_c^{AF} the system is described by a standard paramagnetic (compressible) Anderson insulator, above U_c^{AF} a finite antiferromagnetic order parameter develops, that unexpectedly coexists with a gapless spectrum and, therefore, a finite compressibility. By further increasing the interaction U, the ground state encounters a second phase transition to an incompressible antiferromagnetic insulator with a finite charge gap. Interestingly, in the paramagnetic Anderson insulator, local moments with a finite value of $\hat{m}_i = \hat{n}_{i,\uparrow} - \hat{n}_{i,\downarrow}$ develop, suggesting that itinerant electrons may not be able to fully screen magnetic impurities created by disorder. Then, in the last part, we will add a next-nearest-neighbor (frustrating) hopping t'. Also in this case, we will show that the Mott insulating phase is always accompanied by magnetic order, though with a sufficiently large ratio t'/t many local minima appear in the energy landscape, with competing magnetic properties. In particular, although we find that the lowest-energy solution has magnetic long-range order, many other states with localized moments but no long-range order may be stabilized.

4.1 Local minima and accuracy of the wave function

The variational energy landscape of the disordered Hubbard model (4.1) is characterized by the presence of different local minima. In fact if we start from

different points in the parameter space, namely from different values of g_i, $v_{i,j}$ and $\tilde{\epsilon}_{i,\sigma}$, we converge to different solutions. For example in Fig.(4.1) we show the different energy evolution, as a function of optimization steps, obtained starting from two different points in the parameters space. In the following, we will consider two possibilities, either we start from a paramagnetic point, with $\tilde{\epsilon}_{i,\uparrow} = \tilde{\epsilon}_{i,\downarrow}$, or from a staggered point, with $\tilde{\epsilon}_{i,\sigma} = \tilde{\epsilon}_i + \sigma(-1)^{|x_i+y_i|}\delta$. In both cases, during the Monte Carlo simulation, these conditions are relaxed and the two on-site energies are optimized independently, so to allow a complete freedom to modify the starting configuration.
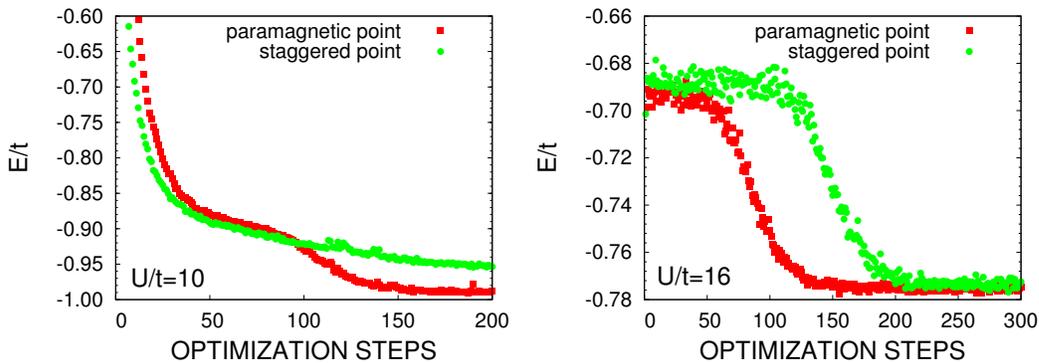
Figure 4.1: Energy evolution as a function of optimization steps for a typical disorder configuration, starting from a paramagnetic point, i.e., $\tilde{\epsilon}_{i,\uparrow} = \tilde{\epsilon}_{i,\downarrow}$ (red squares), and starting from a staggered point, i.e., $\tilde{\epsilon}_{i,\sigma} = \tilde{\epsilon}_i + \sigma(-1)^{|x_i+y_i|}\delta$ (green circles). Simulations have been done for $N = 98$, $D/t = 5$, $U/t = 10$ (left panel) and $U/t = 16$ (right panel).

In contrast to the paramagnetic case (where we force to have equal on-site energies, see the previous chapter), in which the energy landscape has just one minimum, when allowing a magnetic wave function different local minima may appear. This feature is particularly evident for large enough Coulomb repulsion, whereas in the weak-coupling regime we recover a simple picture with one minimum. In table (4.1), we report some example for different values of U/t and 98 sites. Remarkably, the appearence of different local minima is related to the presence of short-range or weakly long-range magnetic correlations. In fact, as it will be discussed in the following, by increasing the on-site Coulomb

repulsion, some sites acquire a finite magnetization and eventually, above a critical value U_c^{AF}, order, giving rise to the typical staggered pattern. Whenever local moments are present or the magnetization is very small, there are many different electronic arrangements that give similar energies but may be hardly connected by simple Metropolis (single-particle) moves, so to define metastable local minima.

	$U/t = 2$	
# 1	$-2.76483(3)$	$-2.76480(3)$
# 2	$-1.68989(3)$	$-1.68936(3)$
# 3	$-2.11823(3)$	$-2.11827(3)$
# 4	$-1.95084(3)$	$-1.95087(3)$
	$U/t = 10$	
# 1	$0.1007(1)$	$0.1016(1)$
# 2	$-0.3911(1)$	$-0.3858(1)$
# 3	$-0.8317(2)$	$-0.8300(1)$
# 4	$-0.9896(1)$	$-0.9905(1)$
	$U/t = 16$	
# 1	$0.0212(1)$	$0.0231(2)$
# 2	$-0.7770(1)$	$-0.7765(2)$
# 3	$-0.4901(2)$	$-0.4805(2)$
# 4	$-0.4780(2)$	$-0.4775(2)$

Table 4.1: Variational energy of the optimized wave function obtained starting from a paramagnetic point, i.e., $\tilde{\epsilon}_{i,\uparrow} = \tilde{\epsilon}_{i,\downarrow}$ (left column), and from a staggered point, i.e., $\tilde{\epsilon}_{i,\sigma} = \tilde{\epsilon}_i + \sigma(-1)^{|x_i+y_i|}\delta$ (right column), for $D/t = 5$, different disorder configurations and ratios U/t.

However, the presence of different local minima is not a dramatic problem in order to understand the physical properties of the disordered Hubbard model. In fact, generally, all physical quantities, as for instance the localization length or the density-density structure factor N_q, give similar results in all these cases. Therefore, we can safely conclude that all the optimized states share the same physical properties. As an example, in Fig.(4.2) we show the on-site magneti-
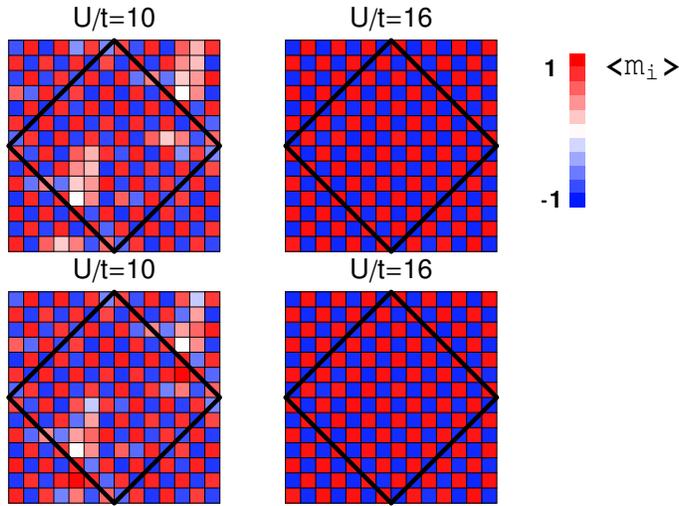
Figure 4.2: On-site magnetization $\langle \hat{m}_i \rangle = \langle \hat{n}_{j,\uparrow} - \hat{n}_{j,\downarrow} \rangle$ for a typical disorder configuration and interaction values $U/t = 10$ and $U/t = 16$. The upper panels correspond to the wave function obtained from the paramagnetic point, the lower panels correspond to the solution obtained from the staggered point.

zation $\langle \hat{m}_i \rangle = \langle \hat{n}_{j,\uparrow} - \hat{n}_{j,\downarrow} \rangle$ pattern, for the variational wave function optimized both starting from the paramagnetic point and from the staggered point. It is evident that there is no considerable difference between the two wave functions (notice that also for $U/t = 16$ the magnetization values are slightly different, though it does not appear from the color scale). We remark that, in most cases, we obtain a lower variational energy by starting from the paramagnetic point, see for instance table (4.1). Therefore, though in some particularly delicate cases we considered different starting points, we usually chose to initialize the simulation with a paramagnetic configuration.

Finally, we would like to discuss the accuracy in energy for a 4×4 lattice, where the exact ground state can be calculated by the Lanczos algorithm. In particular, we consider various wave functions: i) the magnetic state with on-site Gutzwiller and Jastrow factors (that corresponds to our best ansatz), ii) the paramagnetic state presented in the previous chapter (again with Gutzwiller and Jastrow terms), iii) a magnetic state with only Gutzwiller projectors, and iv) a magnetic mean-field state (i.e., without any correlation term) $|SD\rangle$. For
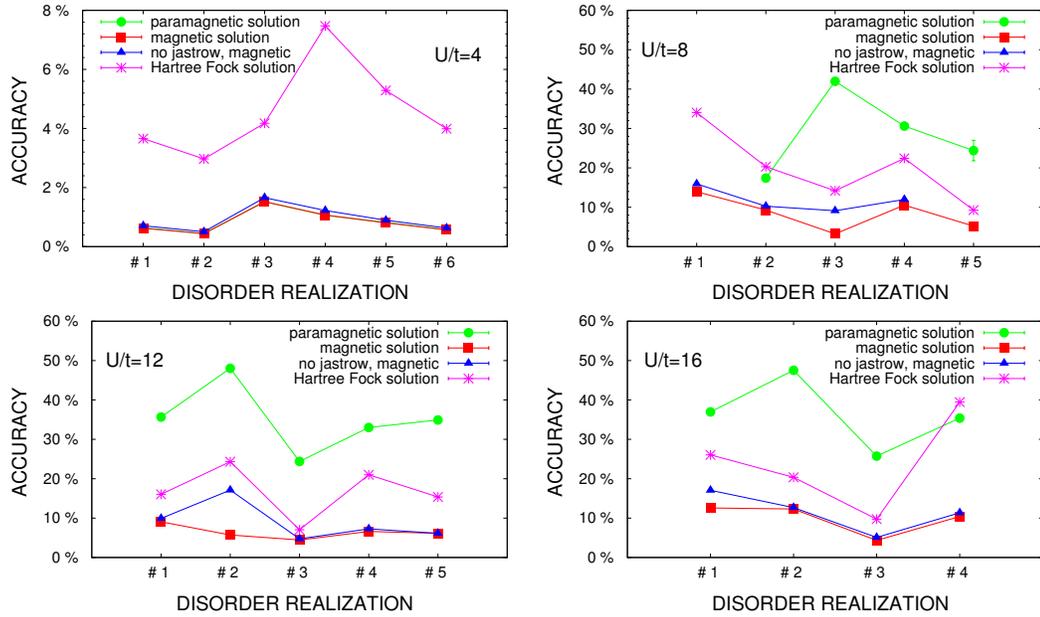
Figure 4.3: Accuracy in energy of different variational wave functions (w.f.) for a 4×4 lattice with $D/t = 5$: i) the magnetic w.f. (red squares),ii) the paramagnetic w.f. (green circles), iii) magnetic w.f. without Jastrow factors (blue triangles), iv) the Hartree Fock w.f. (violet stars). The exact ground-state energy is computed by the Lanczos algorithm.

$U = 0$, the exact ground state wave function can be obtained, implying a very good accuracy also for small but finite values of U/t. However, even for $U/t = 4$, the Hartree-Fock state, with no Gutzwiller and Jastrow factors, give a much poorer accuracy than the other three wave functions, see Fig.(4.3). For $U/t < U_c^{\mathrm{AF}}/t \sim 6.5$ there is no difference between the paramagnetic and the magnetic wave functions and for both of them the accuracy is lower than 4%. Moreover, we notice that both for small and large interaction values, e.g., $U/t = 4$ and $U/t = 16$, the Jastrow factor is not so crucial, since already the wave function iii) gives reasonably good accuracies. In fact, on the one hand, the on-site Gutzwiller factor can easily account for the small charge correlations induced by the Coulomb repulsion in the weak-coupling regime. On the other hand, for large U/t, the ground state has a finite magnetization and the charge-charge correlations can be already described within a (gaped) mean-field state. In the more difficult regime, when $U \sim D$, our magnetic state with

both on-site Gutzwiller projectors and the long-range Jastrow term may give a considerable improvement over the other states considered here. It should be stressed however that this Jastrow factor is essential to have a paramagnetic Mott insulator, whereas in the magnetic case it is not strictly necessary to capture the correct nature of the ground state (see also the discussion below), since the charge gap can be naturally opened by a finite antiferromagnetic mean-field parameter.

4.2 Magnetic phase diagram

Let us turn to the physical properties of the disordered Hubbard model (4.1). In order to assess the magnetic properties of the ground state, we consider the magnetization defined by:

$$M = \frac{1}{N} \sum_j e^{\imath Q r_j} \langle \hat{m}_j \rangle, \tag{4.3}$$

where $\hat{m}_j = \hat{n}_{j,\uparrow} - \hat{n}_{j,\downarrow}$. In analogy with the clean model, also in presence of disorder, by increasing the electron-electron repulsion, there is a tendency toward magnetic order at $Q = (\pi, \pi)$. Therefore, in the following we restrict the calculations to this momentum. Whenever $D > 0$, a finite value U_c^{AF} is needed to have a true long-range antiferromagnetic order.

In Fig.(4.4), we report our variational results for $D/t = 5$ and different values of the Coulomb repulsion and for $U/t = 4$ and various disorder strength. Fixing $D/t = 5$, we find that $U_c^{\mathrm{AF}}/t = 6.5 \pm 0.5$, and indeed for $U < U_c^{\mathrm{AF}}$ the magnetization vanishes. Moreover, as we discussed in the previous chapter, information about the compressibility can be obtained from the disconnected term of the density-density correlation function $N_q^{\mathrm{disc}} = \overline{\langle \hat{n}_q \rangle \langle \hat{n}_{-q} \rangle}$. In Fig.(4.4) we also observe that this quantity vanishes at $U_c^{\mathrm{MI}}/t = 10.5 \pm 0.5$, signalling the the opening of a charge gap. Remarkably, there is a finite region in which both the magnetization and the compressibility fluctuations are finite. This implies a stable regime that shows antiferromagnetic long-range order without any charge gap. We notice that this intermediate phase with finite magnetization and compressibility is reduced when we consider $U/t = 4$ and change the disorder strength, see Fig.(4.4). In this case, we can estimate that $D_c^{\mathrm{AF}}/t =$
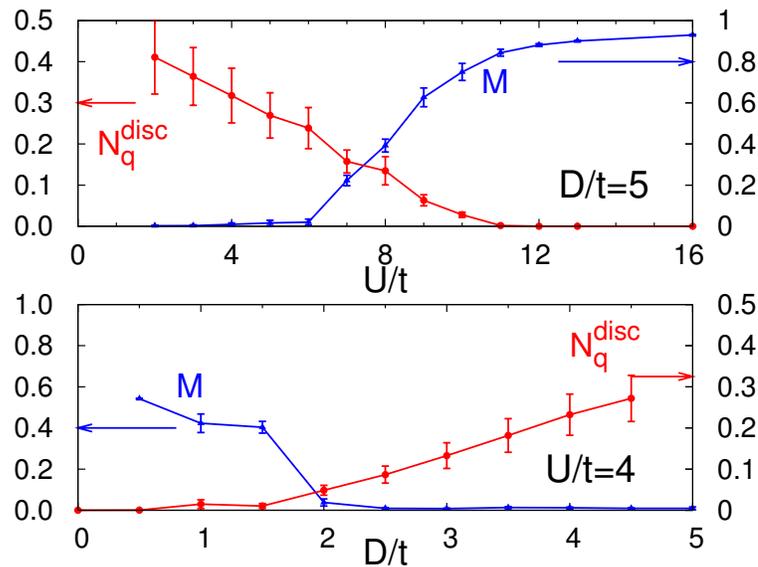
Figure 4.4: Upper panel: compressibility fluctuations N_q^{disc} with $q = (\pi/7, \pi/7)$ and staggered magnetization M for $D/t = 5$ and different values of the interaction U for a lattice of size $N = 98$. Data points are averaged over different disorder realizations. Lower panel: the same as above, but for $U/t = 4$ and different values of the disorder D.

2.5 ± 0.5 and $D_c^{\mathrm{MI}}/t = 1 \pm 0.5$. These results lead to the phase diagram sketched in Fig.(4.5), which is in close agreement with previous mean-field calculations [71, 84, 85]. For $U = 0$ the system is a (paramagnetic) Anderson insulator for every finite disorder $D > 0$, since for a non interacting bi-dimensional system is valid the scaling theory of localization [19]. In a similar way, for $D = 0$ the ground state is a Mott insulator with antiferromagnetic order for every $U > 0$. When both disorder and interaction are finite, there is an intermediate phase between the paramagnetic Anderson insulator and the antiferromagnetic Mott insulator. This phase is characterized by long-range magnetic order, but also by a finite compressibility. Though some authors identified this phase with a metal [71], we do not find any evidence in favor of it.

Let us now consider in more detail the nature of the Anderson-Mott transition that emerges from our variational approach, once we allow for spin-
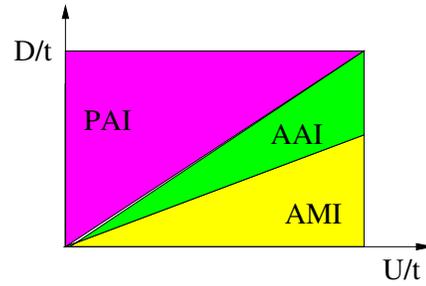
Figure 4.5: Variational phase diagram of the magnetic sector of the ground state. PAI stands for Paramagnetic Anderson Insulator, AAI for Antiferromagnetic Anderson Insulator and AMI for Antiferromagnetic Mott Insulator.
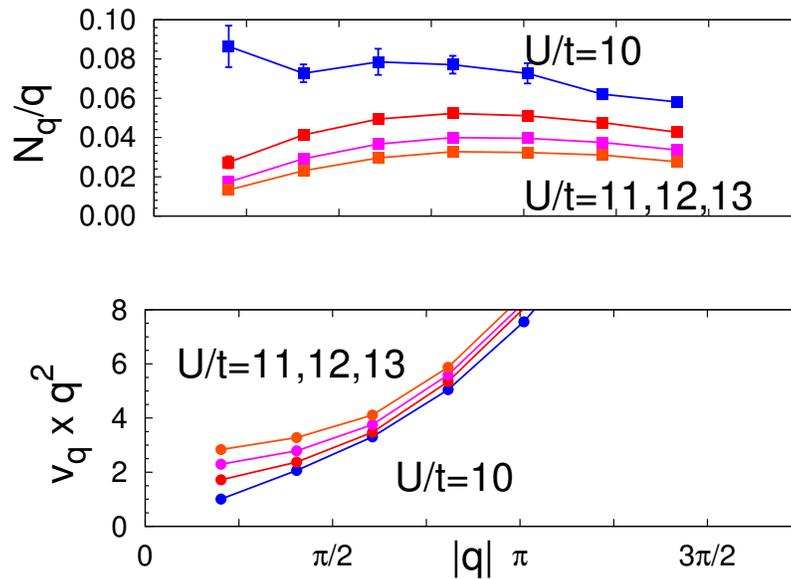
Figure 4.6: Upper panel: static structure factor of the variational magnetic wave function N_q divided by q versus $|q|$ in the $(1,1)$ direction. Lower panel: Fourier transform $v_q \times q^2$ of the Jastrow parameters versus $|q|$ in the $(1,1)$ direction. Calculations are done on a lattice of $N = 98$ sites for different values of the interaction and $D/t = 5$. Data points are averaged over different disorder realizations.

rotational symmetry breaking. We would like to remind the reader that in the paramagnetic case, the Mott insulator can be obtained only thanks to a singular Jastrow factor, i.e., $v_q \sim 1/q^2$. In this case, the mean-filed Hamiltonian is always gapless and the charge gap opens because of the strong correlations induced by the Jastrow term. In the magnetic case instead, two different mechanisms can open up a gap: i) the long-range charge correlations induced by the Jastrow factor and ii) the onset of long-range antiferromagnetic order. For $U < U_c^{MI} = (10.5 \pm 0.5) \, t$, the static structure factor behaves like $N_q \sim q$ and the Fourier transform of the Jastrow parameters like $v_q \sim 1/q$; on the other hand, for $U > U_c^{MI}$, we have that $N_q \sim q^2$ and $v_q \sim 1/q^2$. Thus in the intermediate phase with long-range magnetic order and finite compressibility, $N_q \sim q$ and $v_q \sim 1/q$, in agreement with the f-sum rule. Nevertheless, we notice that the change in the behavior of v_q at the Mott transition is less sharp with respect to the paramagnetic case studied in the previous chapter, see Fig.(4.6).

In order to understand which is the most relevant ingredient to open a charge gap, we calculate the static structure factor N_q and the compressibility fluctuations N_q^{disc} close to Mott transition for the full variational wave function $|\psi\rangle = \mathcal{J}\Pi_i\mathcal{G}_i|SD\rangle$ and for another state that only contains Gutzwiller terms $|\psi_g\rangle = \Pi_i\mathcal{G}_i|SD\rangle$. The Slater deterinant $|SD\rangle$ is independently optimized for the two cases. The results for N_q are reported in Fig.(4.7). Since the linear slope of N_q is related to the compressibility, we observe that $|\psi_g\rangle$ is less compressible than the full wave function $|\psi\rangle$ for $U < U_c^{\text{MI}}$. Nevertheless, the results for the two wave functions are not very different and the critical interaction value U_c^{MI} for the Mott transition is the same in the two cases. A similar outcome can be obtained by N_q^{disc}, see Fig.(4.8). Therefore, in the magnetic case, the charge gap opens mainly because of the presence of a sizable mean-field order parameter. However, the Jastrow parameters still behave like $v_q \sim 1/q^2$ in the Mott phase. In summary, the following scenario emerges: in the intermediate phase with antiferromagnetic order, but finite compressibility, the charge fluctuations are not completely suppressed and the mean-field density of state is large at the Fermi level. For larger U values, the Jastrow factor increases charge correlations and, at the same time, the mean-field density of states get suppressed at the Fermi level. Finally, a single-particle gap opens and the system becomes incompressible, see Fig.(4.9). We remark that the tendency

towards metallicity for intermediate values of U/t is suppressed by the presence of magnetic order: this can be seen by noticing a reduced density of states at the Fermi level for $U/t = 8$. The same information can be also extracted from the behavior of the Inverse Participation Ratio, which has a non monotonic behavior in function of U: in fact, for small values of the interaction, the localization length is short because of the strong disorder; then it becomes larger for higher values of the interaction U due to the disorder screening and then, at the antiferromagnetic transition, it decreases again. Moreover we notice that the single particle wave functions are more localized in the magnetic case than in the paramagnetic one, even in the regime of maximum "delocalization", i.e., $U \sim D$, compare Fig.(4.10) with Fig.(3.10).
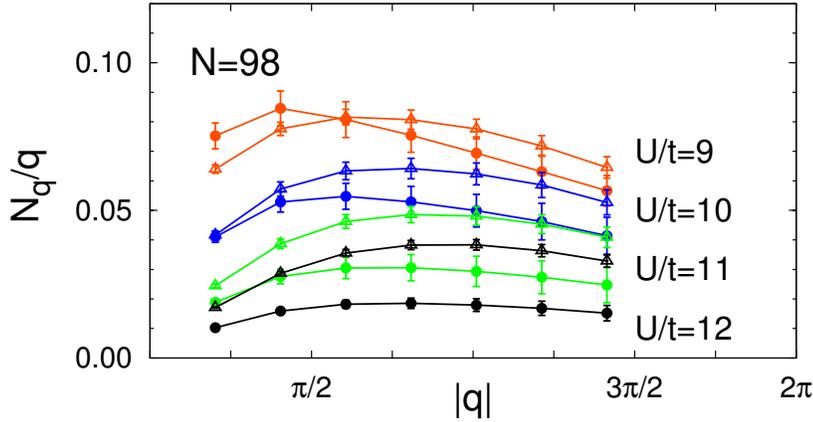
Figure 4.7: Static structure factor N_q divided by q versus q for the full variational wave function with Jastrow factor (circles) and with only Gutzwiller projectors (triangles).

In order to better quantify the disorder suppression, we calculate the fluctuations of the on-site density $\delta n^2 = 1/N \sum_i \langle \hat{n}_i - \langle \hat{n}_i \rangle \rangle^2$ and the variance $\Delta^2 = 1/N \sum_i (\delta_i - \overline{\delta})^2$ of the distribution of the variables δ_i defined as

$$\delta_i = \frac{1}{2}(\tilde{\epsilon}_{i,\uparrow} + \tilde{\epsilon}_{i,\downarrow}) \qquad (4.4)$$

where $\tilde{\epsilon}_{i,\sigma}$ are the variational parameters in the mean field Hamiltonian (4.2). The distribution of δ_i contains the relevant information for evaluating the ran-
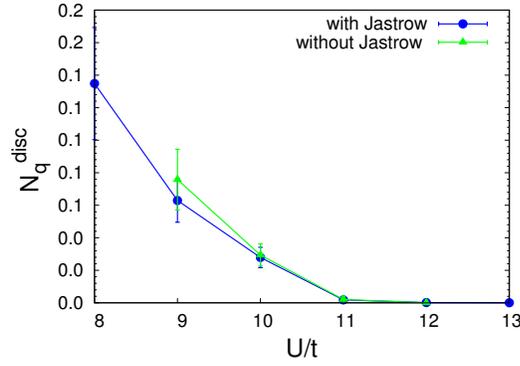
Figure 4.8: N_q^{disc} for different values of the interaction U. Circles (triangles) denote the results obtained from the variational wave function with (without) Jastrow parameters.
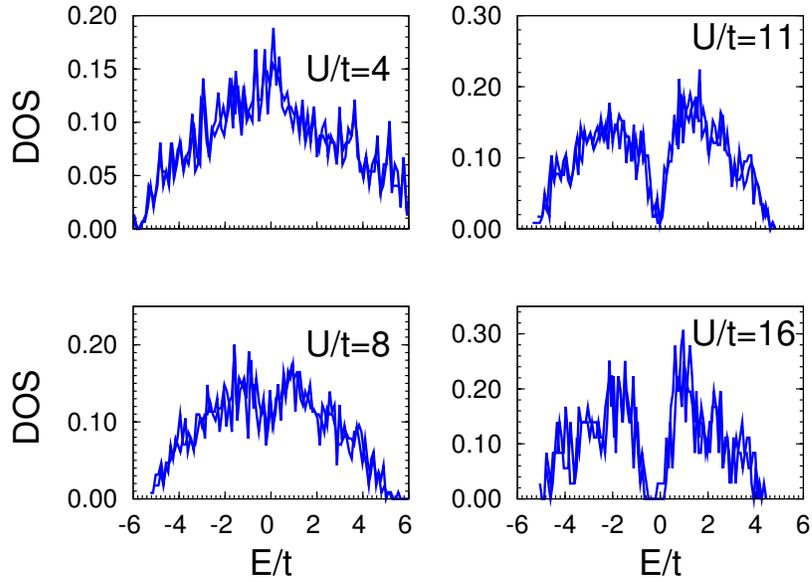
Figure 4.9: Density of states (DOS) of the mean-field Hamiltonian (4.2) with $D/t = 5$

domness of the Slater determinant, while $\epsilon_{\tilde{i},\sigma}$ contains also a constant (staggered) part, namely $\tilde{\epsilon}_{i,\sigma} = \sigma(-1)^{|x_i+y_i|}\Delta_{\mathrm{AF}} + \delta_i$, that should be eliminated in order to avoid spurious results. We observe that, though disorder is suppressed

in all interaction regimes, the screening is much more efficient in the param-
agnetic wave function than in the antiferromagnetic one, being Δ three times
smaller in the former case when $U > U_c^{\mathrm{MI}}$, see Fig.(4.11).
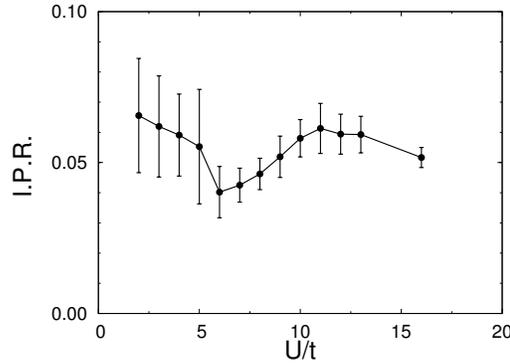
Figure 4.10: I.P.R. of the single particle eigenstate $|\psi_f\rangle$ at the Fermi level of
the mean field Hamiltonian for different values of the interaction U. Error bars
correspond to the average over different disorder configuration with $D/t = 5$.
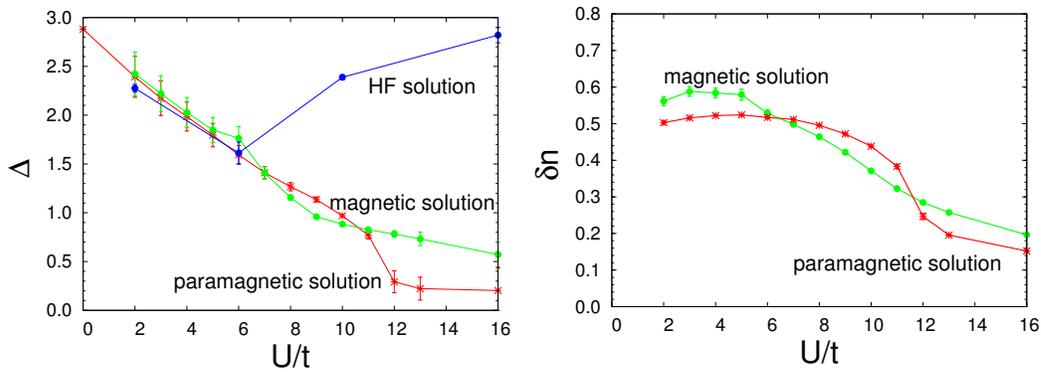
Figure 4.11: Left panel: standard deviation of the distribution of the variables
$\delta_i = (\tilde{\epsilon_{i,\uparrow}} + \tilde{\epsilon_{i,\downarrow}})/2$ defined for the magnetic wave function (green curve), of the
mean-field parameters $\tilde{\epsilon}_i$ obtained with the paramagnetic wave function (red
curve) and of the parameters $\tilde{\epsilon_{i,\sigma}}$ given by the Hartree Fock approximation
(blue curve). Right panel: fluctuation of the mean on site density δn. Results
are averaged over different disorder configurations, with $D/t = 5$.

As for the paramagnetic wave function discussed in the previuos chapter, also in presence of magnetism there is no evidence of a metallic phase, between the paramagnetic Anderson insulator and the magnetic Mott insulator. In fact, the single particle orbitals of the Slater determinant are even more localized than in the paramagnetic case and the Jastrow and Gutzwiller factors are not expected to delocalize the orbitals.

4.3   Local magnetic moments

In the first chapter, we mentioned that in three dimensional systems, where both disorder and interaction are strong (such as Si:P), local magnetic moments may appear before the metal-insulator transition, thus also deep in the metallic phase. The presence of local moments is a consequence of the competition between disorder and interaction. In principle, the presence of local moments may be a general property of disordered materials, not strictly related to a metallic behavior, so that they should be present also in two-dimensional systems. With our variational approach, we can address the regime of both strong disorder and interaction and indeed we find evidence for the appearance of local magnetic moments in the paramagnetic Anderson insulator.

In order to assess this issue, a simple inspection of the staggered magnetization M is not sufficient and the *local* magnetization

$$M_L = \sqrt{\frac{1}{N} \sum_i \langle \hat{m}_i \rangle^2} \tag{4.5}$$

must be also considered. In a paramagnetic state with local moments, namely a state in which some sites have an on-site magnetization $\langle \hat{m}_i \rangle \neq 0$, the total staggered magnetization (4.3) is vanishing, i.e., $M = 0$, while M_L is finite. On the contrary, in the antiferromagnetic phase $M_L \simeq M$. Therefore, once we compare M_L with M, it is possible to have a good feeling on the presence of local moments in the ground state. In Fig.(4.12) we compare the staggered magnetization M and the local magnetization M_L both for $D/t = 5$ and different values of the interaction U and for $U/t = 4$ and different disorder strengths D. Actually for $U > U_c^{\mathrm{AF}} = (6.5 \pm 0.5)\,t$ (and for $D < D_c^{\mathrm{AF}} = (2.5 \pm 0.5)\,t$) the two magnetization values coincide, while in the paramagnetic phase we
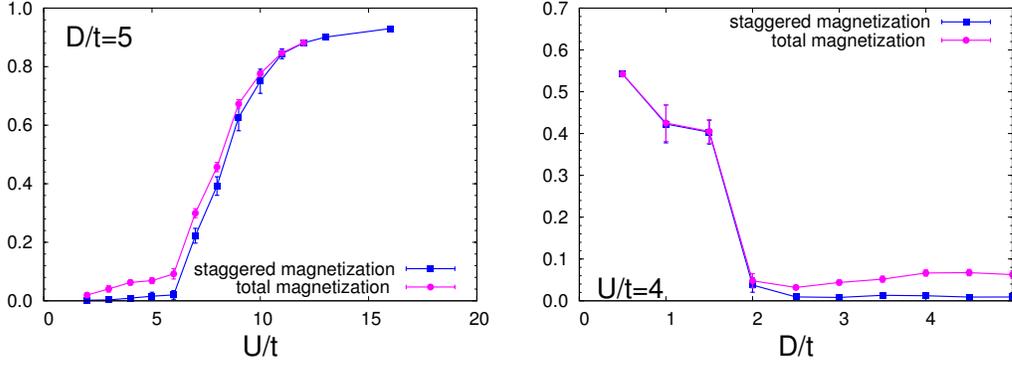
Figure 4.12: Left panel: staggered magnetization $M = 1/N \sum_i (-1)^{|x_i + y_i|} \langle \hat{m}_i \rangle$ and local magnetization $M_L = \sqrt{1/N \sum_i \langle \hat{m}_i \rangle^2}$ for $D/t = 5$ and different interaction values. Right panel: the same for $U/t = 4$ and different disorder values. Calculations are done on a lattice of size $N = 98$, data points are averaged over different disorder realizations.

observe that $M_L > M \simeq 0$. This indeed suggests a magnetically disordered phase (i.e., $M = 0$) in which the on-site magnetization $\langle \hat{m}_i \rangle$ is finite for some sites r_i. We identify those sites with $\langle \hat{m}_i \rangle \neq 0$ as local magnetic moments. The presence of local moments can be more appreciated by looking at the pattern of the on-site magnetization $\langle \hat{m}_i \rangle$, see Fig.(4.13), and at the distribution of $|\langle \hat{m}_i \rangle|$, see Fig.(4.14). In Fig.(4.13), the pattern of the local density $\langle \hat{n}_i \rangle$ and on-site magnetization $\langle \hat{m}_i \rangle$ are shown for a typical disorder realization. For $U/t = 4$, the ground state is an Anderson insulator with a large number of empty and doubly occupied sites with $\langle \hat{m}_i \rangle \sim 0$. However, some sites, which we identify as local magnetic moments, have finite magnetization; they are not spatially correlated hence long-range magnetism is absent. When the electron interaction U increases, the number of magnetic sites increases rapidly and the local moments eventually display the typical staggered pattern of Néel order. Nevertheless, charge excitations are still gapless and $N_q \sim q$. For $U/t = 12$ the system is a gaped insulator with antiferromagnetic order and a vanishing compressibility. In this phase $N_q \sim q^2$ and all the sites are localized spins, therefore $\langle \hat{n}_i \rangle \simeq 1$ and $\langle \hat{m}_i \rangle \simeq 1$ or -1. This picture is in agreement with the distribution of the absolute value of the on-site magnetization $|\langle \hat{m}_i \rangle|$, see Fig.(4.14). Here, we observe that for small interaction values, $U/t \sim 3$, the
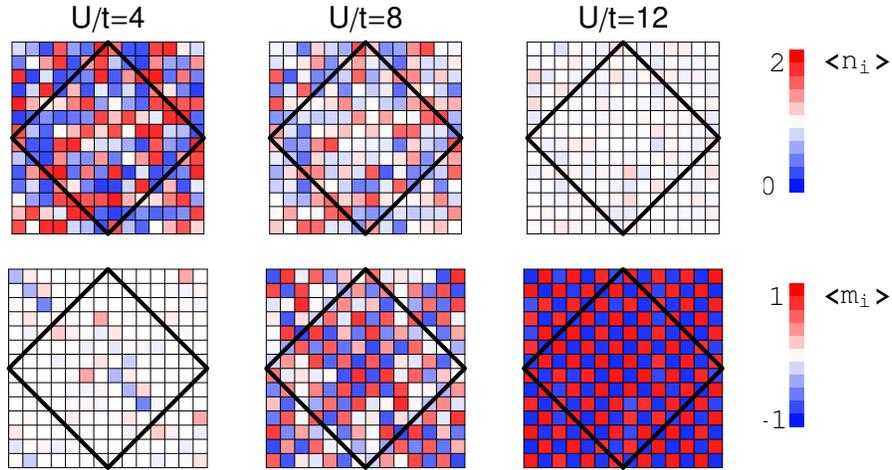
Figure 4.13: Local density $\langle \hat{n}_i \rangle$ (upper panels) and on-site magnetization $\langle \hat{m}_i \rangle$ (lower panels) for a given disorder realization with $D/t = 5$ and different values of U/t. The black contour shows the elementary cell of the lattice which it is repeated to mimic the infinite lattice with periodic boundary conditions.

distribution has a narrow peak in correspondence of $|\langle \hat{m}_i \rangle| = 0$, however at the same time it has long tails indicating the presence of local moments. For $U \simeq U_c^{\mathrm{AF}}$ the distribution is spread between 0 and 0.8, with a small peaks in correspondence of $|\langle \hat{m}_i \rangle| \sim 0$. By increasing the interaction strength, the peak at $|\langle \hat{m}_i \rangle| \sim 0$ disappears and the one at $|\langle \hat{m}_i \rangle| \sim 1$ becomes more pronounced. Finally, in the Mott insulating phase the distribution is completely peaked on $|\langle \hat{m}_i \rangle| = 1$.

The presence of both paramagnetic sites, with $\langle \hat{m}_i \rangle \sim 0$, and sites with finite magnetization can be connected with the *two-fluids* scenario. As we explained in the first chapter, the two-fluids picture was first introduced to explain the non-Fermi liquid behavior emerging in the thermodynamic measures of Si:P doped semiconductors, where the two fluids are the Fermi liquid quasiparticles and the local magnetic moments. The latter ones can be either free, i.e., non interacting with the Fermi liquid, or coupled to the conduction electrons by the Kondo interaction. Moreover, local moments can be totally screened or strongly suppressed at zero temperature by this Kondo interaction or even by their mutual magnetic interaction [4]. Here, we are considering a disordered
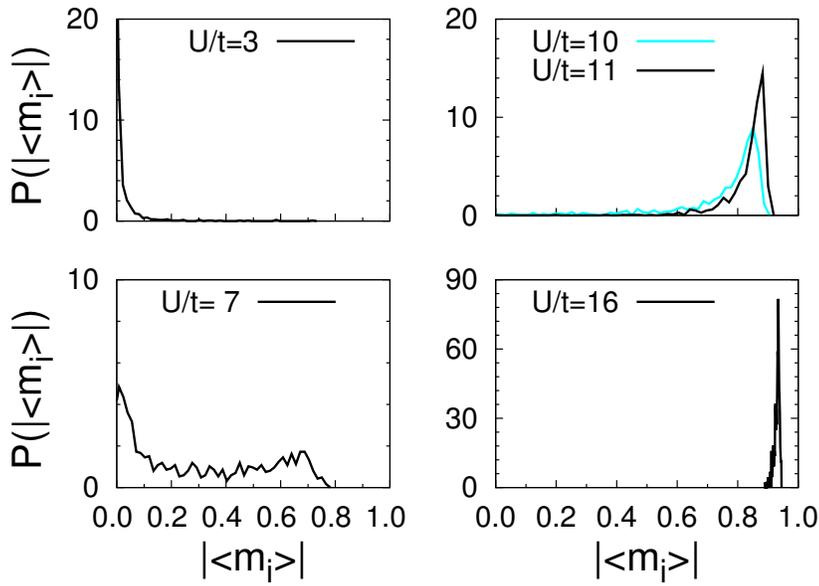
Figure 4.14: Distribution of the on-site magnetization $|\langle \hat{m}_i \rangle|$, over the lattice sites and the disorder configurations. Different curves correspond to different values of the interaction U. Calculations are done for $D/t = 5$. The accumulated statistics is the number of lattice sites, times the number of disorder configurations.

system of electrons in two dimensions, which, in absence of interaction, is an Anderson insulator with all localized states. Moreover, as we discussed within our approach, the localization length is always finite, even though it increases in presence of interaction. Therefore, we cannot identify part of the electrons as a metallic fluid. Nevertheless, the concomitant presence of local magnetic moments with other sites having finite charge fluctuations (when the localization length is larger than the lattice spacing) and an overall finite compressibility can be regarded as a system with two kind of particles. Indeed, in the regime $U \sim D$, i.e., where electron wave functions are maximally extended, we observe the coexistence of local moments and paramagnetic sites with $\langle \hat{n}_i \rangle = 0, 1, 2$, see Fig.(4.13). It should be emphasized that, within this picture, there are no truly itinerant fluids but all particles are localized. Although we cannot address the question of the Kondo coupling, from our calculations we can conclude that

there is a finite number of local magnetic moments in the ground state and thus that the local moments, at least in part, are not screened and survive at zero temperature.
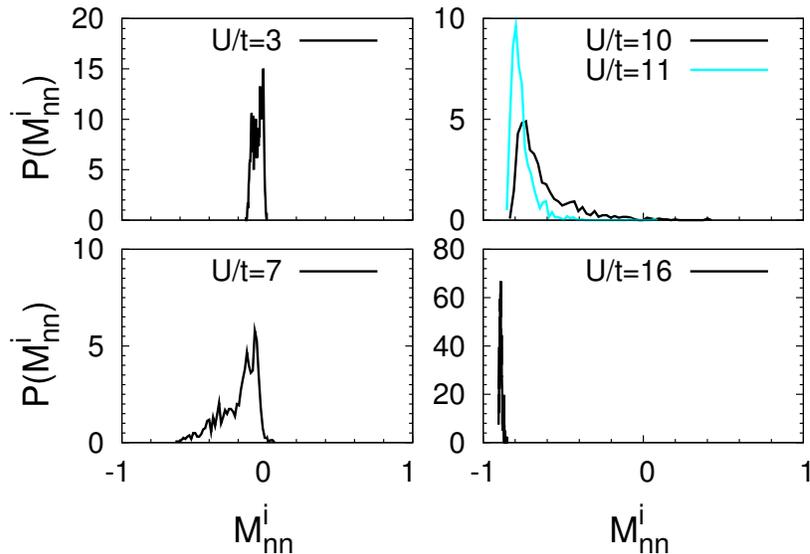

Figure 4.15: Distribution of the nearest-neighbor magnetic interaction $M_{nn}^i = 1/z \sum_{\langle j \rangle_i} \langle \hat{m}_i \hat{m}_j \rangle$, where z is the number of nearest neighbors, for $D/t = 5$.

Finally, we consider the nearest-neighbor spin-spin correlation function $M_{nn}^i = 1/z \sum_{\langle j \rangle_i} \langle \hat{m}_i \hat{m}_j \rangle$, z being the number of nearest-neighbor sites and $\langle j \rangle_i$ the sum over the neighbors of site r_i. This quantity gives information about the closeness of local moments: it is very small for isolated spins, whereas it is large if spins form clusters. We observe that in the regime of $U \sim D$, the distribution of M_{nn}^i is peaked around zero, indicating that local moments appear almost isolated. Then by increasing the Coulomb interaction, the peak shifts smoothly to negative values and saturates to $M_{nn}^i = -1$ in the antiferromagnetic phase. It should be noticed that, in all cases, the main interaction between localized spins is always antiferromagnetic and that a negligible ferromagnetic coupling is only present before the Mott transition.

4.4 The Anderson-Mott transition in presence of large frustration

In the previous sections, we showed that a disordered system of electrons on a square lattice undergoes a magnetic transition before becoming a Mott insulator. Therefore, the Mott insulator is always accompanied by magnetic order. However, in disordered materials, one could expect that long-range order may be strongly suppressed, leading to a *bona-fide* Mott transition, which is driven by the electron correlation alone. Since the tendency towards magnetic order is generally enhanced by an unfrustrated geometry of the lattice (that generally implies a strong nesting property of the non-interacting Fermi surface), the presence of a frustrated hopping may help to approach the Mott phase without any spurious magnetic effects. Moreover, from experimental point of view, most of the realizations of disordered materials, like for instance Si:P, can be described by electrons that hop and interact in a random lattice, since the "active" atoms are randomly placed in the underlying matrix. Here, we would like to approach the problem from a much simpler point of view and we consider a periodic lattice with translationally invariant hopping and frustration is only introduced by considering two different hopping processes, at first and second neighbors. In particular, we want to study the Hamiltonian

$$H = \sum_{i,j,\sigma} t_{i,j} \left(\hat{c}_{i,\sigma}^{\dagger} \hat{c}_{j,\sigma} + h.c. \right) + \frac{U}{2} \sum_i (\hat{n}_i - 1)^2 + \sum_i \epsilon_i \hat{n}_i \qquad (4.6)$$

where $t_{i,j} = -t$ or $-t'$ if r_i and r_j are first or second neighbors respectively, see Fig.(4.16). Similarly to what we did in the previous sections, we define a variational wave function $|\psi\rangle = \Pi_i \mathcal{G}_i \mathcal{J} |SD\rangle$, with $|SD\rangle$ the ground state of a mean-field Hamiltonian

$$H_{\text{MF}} = -t \sum_{<i,j>} \left(\hat{c}_{i,\sigma}^{\dagger} \hat{c}_{j,\sigma} + h.c. \right) - \tilde{t}' \sum_{<<i,j>>} \left(\hat{c}_{i,\sigma}^{\dagger} \hat{c}_{j,\sigma} + h.c. \right) + \sum_i \tilde{\epsilon}_{i,\sigma} \hat{n}_{i,\sigma}, \quad (4.7)$$

where, besides the spin-dependent local energies $\tilde{\epsilon}_{i,\uparrow}$ and $\tilde{\epsilon}_{i,\downarrow}$, we also consider a next-nearest-neighbor hopping $\tilde{t}'$ as a variational parameter to optimize $|\psi\rangle$.

The first important point is that a finite frustrating ratio t'/t makes the energy landscape very jagged. Furthermore, in contrast to the the disordered
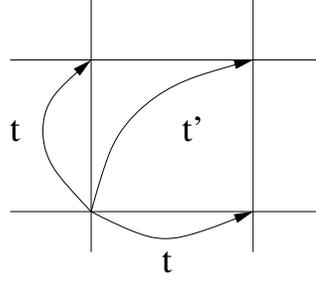
Figure 4.16: First neighbors hopping amplitude t and second neighbors hopping amplitude t'.

model with $t' = 0$, where different local minima share very similar physical properties, here different starting points in the parameter space give rise to rather different wave functions, especially in the intermediate/strong coupling regime. In fact, we will show that different minima correspond to states with different properties. In particular, as starting points for the energy optimization, we will consider i) a paramagnetic point, with $\tilde{\epsilon}_{i,\uparrow} = \tilde{\epsilon}_{i,\downarrow}$, ii) a staggered point, with $\tilde{\epsilon}_{i,\sigma} = \tilde{\epsilon}_i + \sigma(-1)^{|x_i+y_i|}\delta$, and iii) a collinear point, with $\tilde{\epsilon}_{i,\sigma} = \sigma(-1)^{|x_i|}$. Although the starting point in the first case has $\tilde{\epsilon}_{i,\uparrow} = \tilde{\epsilon}_{i,\downarrow}$, during the optimization different values for up and down spins can be achieved. It has to be noticed that with a 45 degrees tilted cluster (that has been used in this thesis), the collinear configuration has an intrinsic domain wall, see Fig.(4.17), since the reciprocal lattice does not contain $Q = (\pi, 0)$ and $Q = (0, \pi)$.
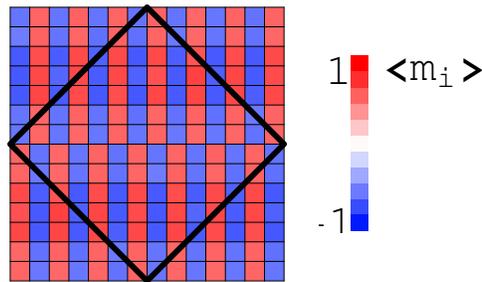
Figure 4.17: Example of a collinear configuration, $\langle \hat{m}_i \rangle = (-1)^{|x_i|}$, for a lattice with a tilted unit cell of $N = 98$ sites. The disorder is fixed to $D/t = 5$.

In the strong interacting regime, the super-exchange mechanism produces two (frustrating) antiferromagnetic interactions, i.e., $J_1 = t^2/U$ at nearest neighbors and $J_2 = t'^2/U$ at next-nearest neighbors. The classical ground state of a translational invariant Heisenberg model with both J_1 and J_2 can be easily found. In fact the energy can be always minimized by a planar helix

$$\vec{S} = \vec{e_1} \cos(Q \cdot r) + \vec{e_2} \sin(Q \cdot r) \tag{4.8}$$

provided that the wavevector Q minimizes the Fourier transform $J(Q)$ of the magnetic coupling. In the case of the $J_1 - J_2$ model, the energy is minimized by $Q = (\pi, \pi)$ if $J_2 < \frac{1}{2}J_1$, i.e., the ground state has Néel order, while if $J_2 > \frac{1}{2}J_1$ the energy is minimized for $Q = (\pi, 0)$, $Q = (0, \pi)$ or any linear combination of the two. At $J_2 = 1/2J_1$ the classical ground state is highly degenerate [86]. In presence of quantum fluctuations, a magnetically disordered phase with $M = 0$ is expected close to the first-order classical transition at $J_2 = \frac{1}{2}J_1$ [87]. Such a non-magnetic phase has been stabilized in a variational calculation for $0.4 \lesssim J_2/J_1 \lesssim 0.6$ [88]. In analogy, in the clean Hubbard model we expect to find the maximum frustration close to $t' = 0.7t$. Indeed, various numerical works addressed the physics of the frustrated Hubbard model on a square lattice and all of them succeeded in finding a non-magnetic phase, although in different regions of the $t' - U$ phase diagram [89, 90, 91, 92]. The above argument refers to a clean system, where there is translational invariance. In presence of disorder, we can expect that the maximal frustration may be slightly shifted, presumably towards higher values of t'/t. Here, we study the ground-state properties for two values of the frustrating hopping, namely $t'/t = 0.6$, which is close to the classical point of maximal degeneracy, and $t'/t = 1$. For all cases, we start the energy optimization from different points in the parameters space: the paramagnetic, magnetic, and collinear point. As we discussed above, starting from different points we converge to different local minima.

For $t'/t = 0.6$, we find that the solution describing a paramagnetic Anderson insulator is stable for $U < U_c^{\mathrm{AF}} \simeq 8t$. Up to this value of the Coulomb interaction, we find that the energy of the converged state does not depend upon the choice of the starting point (as for the unfrustrated case). We notice that, for $U/t \gtrsim 7$, different results for the staggered magnetization are found when considering paramagnetic or antiferromagnetic starting points, see
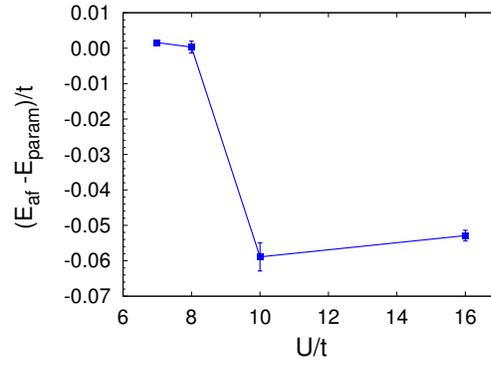
Figure 4.18: Difference between the variational energy of the wave function optimized starting from a paramagnetic point and from an antiferromagnetic point for $t'/t = 0.6$. Data points are averaged over different disorder realizations with a disorder strength $D/t = 5$.
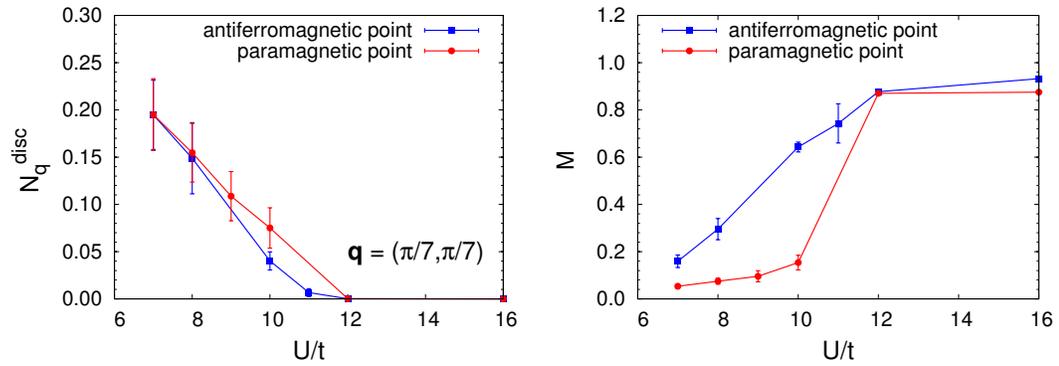

Figure 4.19: Compressibility fluctuations N_q^{disc} (left panel) and magnetization $M = 1/N \sum_j e^{iQr_j} \hat{m}_j$ with $Q = (\pi, \pi)$ (right panel) for $t'/t = 0.6$. Different curves correspond to variational wave functions obtained from different points in the parameter space, namely a paramagnetic point and an antiferromagnetic point. Data points are averaged over different disorder configurations with $D/t = 5$.

Fig.(4.19). In particular, the magnetization is strongly suppressed when considering a paramagnetic initial condition. This fact shows that, by increasing the frustrating ratio t'/t, different local minima may have rather different physical properties, in contrast to what happens in the weakly-frustrated case. For

$U_c^{\mathrm{AF}} < U \leq U_c^{\mathrm{MI}}$ the lowest minimum corresponds to a wave function with long-range antiferromagnetic order and finite compressibility and for $U > U_c^{\mathrm{MI}}$ the system is a Mott insulator with Néel order, see Figs.(4.19) and (4.18). These results suggest that the magnetic transition may become weakly first order, with a small jump in the magnetization. However, the case with $t'/t = 0.6$ does not show particularly strong frustration and the results are very similar to the ones found for $t' = 0$.
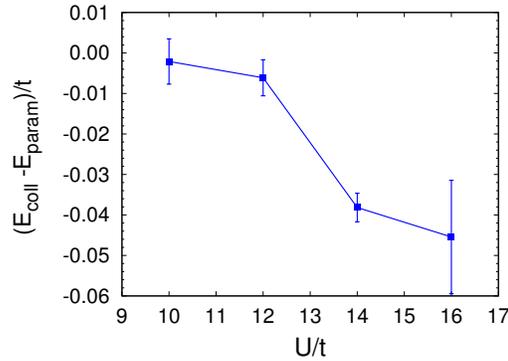
Figure 4.20: Difference between the variational energy of the wave function optimized starting from a collinear point and from a paramagnetic point for $t'/t = 1$. Data points are averaged over different disorder realizations with a disorder strength $D/t = 5$.

For $t'/t = 1$ the solution obtained starting from a staggered set of parameters $\tilde{\epsilon}_{i,\sigma}$ gives always the highest energy among the other ones used in this thesis, and, therefore, it will be excluded from the following analysis. Again, in the weakly-correlated regime, i.e., $U < U_c^{\mathrm{AF}} \simeq 11\,t$, we find similar energies for the paramagnetic and the magnetic starting points, see Fig.(4.20). By increasing the interaction value, the wave function with collinear order gives the best approximation of the ground state. Moreover, it clearly displays long-range magnetic order, see Fig.(4.21). It should be noticed that our approximated wave function may have either magnetic order at $Q = (\pi, 0)$ or at $Q = (0, \pi)$, depending upon the initial conditions of the optimization. By further increasing U/t, this solution corresponds to a gaped insulator for $U/t \geq U_c^{MI}/t = (13.5 \pm 0.5)$ and, indeed, $N_q^{\mathrm{disc}} = 0$ for $U/t > U_c^{MI}$, see

Fig.(4.21). We would like to stress that a larger frustrating ratio has mostly two effects: the first one is to enhance the first-order character of the magnetic transition, and second one is to reduce the stability region of the intermediate magnetic Anderson phase.
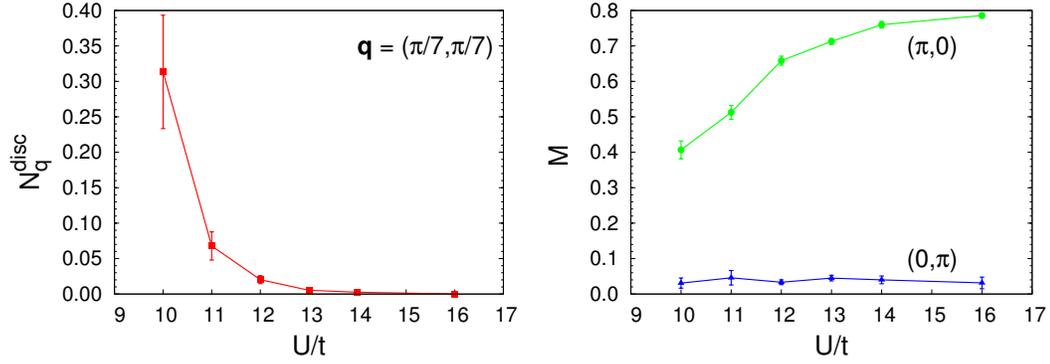

Figure 4.21: Compressibility fluctuations N_q^{disc} (left panel) and magnetization $M = 1/N \sum_j e^{iQr_j} \hat{m}_j$ calculated for $Q = (\pi, 0)$ and $Q = (0, \pi)$ (right panel) for $t'/t = 1$. N_q^{disc} and M are evaluated for a wave function optimized starting from a collinear point. Data points are averaged over different disorder configurations with $D/t = 5$.
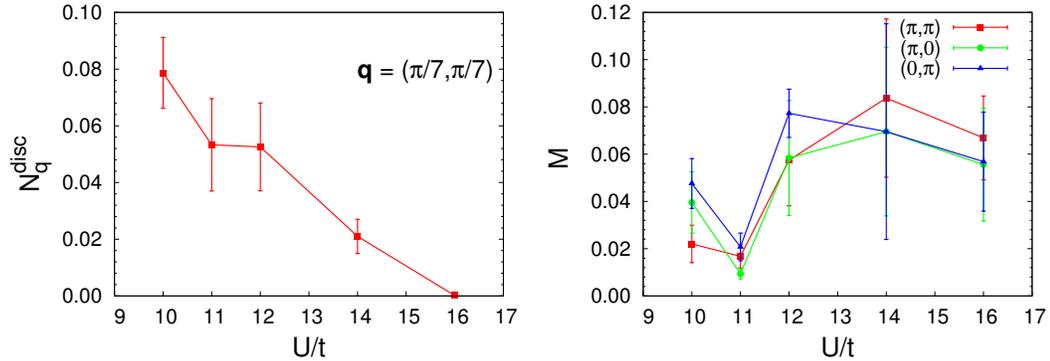
Figure 4.22: The same as in Fig.(4.21), but for a wave function optimized starting from a paramagnetic point.

The remarkable feature is that, in a wide range of Coulomb repulsions,

it is possible to find competing states just by starting from a paramagnetic wave function. The latter state gives rise to a pattern in which most of the sites have a net magnetization but an overall vanishing magnetic order, namely they show "glassy" spin patterns, see Figs.(4.22) and (4.23). For $U/t \sim 16$, these solutions are incompressible, i.e., $N_q^{\text{disc}} \sim 0$ and, therefore, may be viewed as disordered Mott insulators. By decreasing the interaction strength U, these metastable states turn compressible, still having a large number of local moments. Therefore, for $t'/t \sim 1$ we find evidence of a spin-glass behavior, in which metastable states with very different electron configurations have similar energies. Although the magnetically ordered solution has a lower energy, there are large energy barriers that separate different states and we observe a very slow dynamics. This is the primary reason that prevents one to smoothly converge to the lowest-energy state, by starting from a generic configuration. This glass behavior emerges for $t \sim t'$, in agreement with our expectations for the point of maximal frustration in a disordered system. However, once again, we would like to stress that the actual variational minimum shows, as in the unfrustrated case, a transition from a Mott to an Anderson insulator, both magnetically ordered, followed, at lower U, by a further transition into a paramagnetic Anderson insulator. The possibility to have a direct (probably first-order) transition between the magnetic insulator and the paramagnetic Anderson insulator cannot be ruled out for large enough frustration. The qualitative phase diagram (for fixed disorder $D/t = 5$) is shown in Fig.(4.24).

In summary, we conclude that, within our variational description and within the Hamiltonian (4.6), the frustrating hopping t' has two primary effects. The first one is the narrowing of the stability region of the magnetic Anderson insulator. In addition, there is some evidence that the magnetic transition turns to be weakly first order, in contrast to the unfrustrated case. The second and most important effect of a frustrating hopping term is the existence of a "glassy" phase at strong couplings, where many paramagnetic states, with disordered local moments, may be stabilized. Of course, these results may be due to the fact of having considered on-site disorder, whereas the frustrating hopping is taken to be translationally invariant. In this regard, a simple generalization to the Hamiltonian (4.6) can account for a truly disordered lattice, with random $t_{i,j}$, which is more pertinent to materials like Si:P.
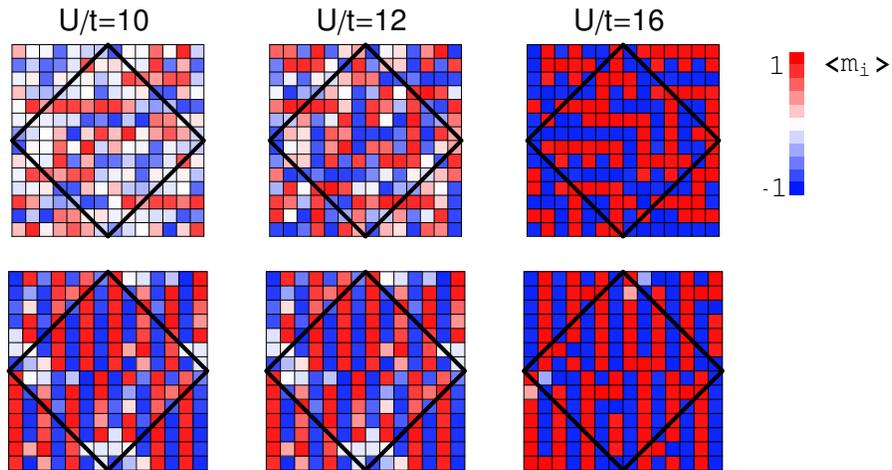
Figure 4.23: Local magnetization $\langle \hat{m}_i \rangle$ for the best variational state, i.e., the collinear solution, (lower panels) and for a metastable solution (upper panels), i.e., the paramagnetic solution, for a given disorder configuration with $D/t = 5$ and $t'/t = 1$.
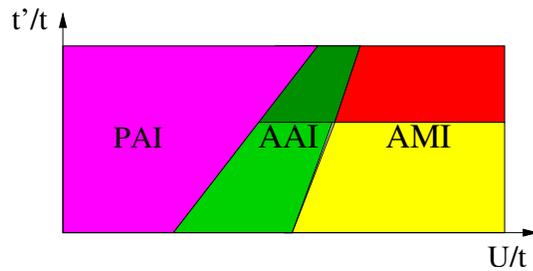

Figure 4.24: Sketched phase diagram for in the $(t' - U)$ plane. PAI stands for Paramagnetic Anderson Insulator, AAI for Antiferromagnetic Anderson Insulator, and AMI for Antiferromagnetic Mott Insulator. In the AAI and AMI phases, dark colors correspond to collinear order, while bright color to Néel order.

Conclusions and perspectives

In this thesis we have studied, by means of a variational Monte Carlo technique, the ground state properties, both magnetic and paramagnetic, of the disordered Hubbard model at half filling and in two dimensions. This model is the simplest example where disorder-driven Anderson localization and interaction-driven Mott localization are both active. This work was originally motivated by theoretical proposals according to which a metallic phase could intrude between the Anderson-insulator and the Mott-insulator in two-dimensions [80, 71], which might have been relevant in connection with the observed metal-insulator transition in high-mobility two-dimensional electron gases [3, 27]. Although the conductivity is a quantity that is not directly accessible by a variational calculations, other properties that we could calculate exclude that a true zero-temperature metallic phase exists. However, even though our calculation do not provide any insights on the observed metal-insulator transition in two dimensions, we think it might be relevant to another still alive puzzle in disordered systems, namely the metal-insulator transition in phosphorus doped silicon.

Concerning our specific calculations, first of all we have showed that a variational wave function is able to describe the Anderson-Mott transition without any symmetry breaking, i.e. a transition from a paramagnetic Anderson insulator to a paramagnetic Mott insulator. This is achieved thanks to a long-range charge correlations induced in the wave function by a Jastrow factor. We have showed that the transition can be easily detected within variational Monte Carlo by looking at the behavior of the static structure factor and of the Fourier transform of the Jastrow parameters, namely following the same criteria for the Mott transition in a clean system. Moreover, we found that for a disordered system the disconnected term of the density-density correlation function, i.e.,

$\lim_{q \to 0} N_q^{\text{disc}} = \lim_{q \to 0} \overline{\langle n_q \rangle \langle n_{-q} \rangle}$, acts as an easily accessible order parameter for the Anderson-Mott transition. We found that electron-electron repulsion partly screens disorder: for strong interaction the electrons "feel" an effectively very weak disorder potential that should imply an interaction-increased localization length. However, once interaction exceeds a critical value, a gap opens and the model turns into a Mott insulator. The model seems to be always insulating, yet, upon increasing the strength of interaction, the localization length may have a non monotonous behavior when we consider the full variational wave function, in which we allow for magnetism.

When magnetism is allowed, a compressible and magnetic Anderson insulating phase appears between the compressible paramagnetic Anderson insulator and the incompressible magnetic Mott insulator. When magnetism is not frustrated, all transitions are continuous. When frustration is included by means of next-to-nearest neighbor hopping, the paramagnetic to magnetic Anderson insulator transition turns first order. Moreover, we find many, almost degenerate with the actual lowest energy state, paramagnetic states in the magnetic region, which suggests a glassy behavior at finite temperature. Indeed, all paramagnetic states posses local moments, i.e. magnetic sites that are almost uncoupled to the rest of the system and would contribute with a finite $-K_B \ln 2$ term to the entropy at finite temperature. Although these results concern a two dimensional square lattice, when scaling theory does not predict any metal-insulator transition, yet they clearly show that local moments arises before the Mott transition, in accord with the actual behavior of three-dimensional Si:P.

Future perspectives of this work are many aspects of disordered and strongly correlated systems that we did not take into account. First of all, in connection with Si:P, the dimensionality: for our numerical convenience we considered two dimensional models but this system is instead three dimensional. Moreover, throughout this thesis, we have only considered diagonal disorder, while if the case of Si:P off-diagonal one is equally important, which could lead to a further increase of magnetic frustration and near the chemical potential to an anomalous increase of the localization length.

Second, in connection with high-mobility two-dimensional electron gases, we did not take into account possible inhomogeneities, our Jastrow factor was

taken, for numerical convenience, translationally invariant, as well as the long range Coulomb repulsion, which could play a relevant role in the real materials.

Nevertheless and in spite of its weak aspects in the context of Si:P and of two-dimensional high-mobility electron gases, our successful description of a disordered Mott transition in the Hubbard model could be relevant in connection with fermionic atoms trapped in optical lattices. The physics of these systems represents nowadays a very promising playground for strongly correlated physicists. In the experimental realisations of optical lattices, it is not difficult to add disorder thus realizing physical realization of the disordered Hubbard model that we have studied.

Acknowledgements

been beautiful. I would like to mention them all: the ones that are here with me, the ones in Genova and the ones around the world, but it would become a long list of names. A special thank to my flatmates Luca, Carlotta, Valeria, Giuliano and John. A special thank to my family for being always present.

Thanks to Francesco, because every day is a special day, but also because he advises and supports me actively with my work.

Appendix A

F-sum rule: a detailed calculation

The first momentum of the dynamical structure factor is defined as

$$\Sigma(q) = \int_0^\infty \frac{d\omega}{\pi} \omega S(q, \omega), \tag{A.1}$$

with the dynamical structure factor

$$S(q, \omega) = \int dt e^{i\omega t} \langle \hat{n}_q(t)\hat{n}_{-q}(0) \rangle. \tag{A.2}$$

We are interested in the calculation of the first momentum because it gives us information on the spectrum gap of the system. In fact the quantity

$$\Delta(q) = \frac{\int_0^\infty \frac{d\omega}{\pi} \omega S(q, \omega)}{\int_0^\infty \frac{d\omega}{\pi} S(q, \omega)} \tag{A.3}$$

is an estimate of the average energy of the low-lying charge density excitations. The fluctuations-dissipation theorem enunciates that

$$Im\chi(q, \omega) = -\frac{\pi}{2}(1 - e^{-\beta\omega})S(q, \omega); \tag{A.4}$$

where $\chi(q, \omega)$ is the Fourier transform of the response function

$$\chi(r - r', t - t') = -i\theta(t - t')\langle [\hat{A}(r, t), \hat{B}(r', t')] \rangle \tag{A.5}$$

with $\hat{A} = \hat{B} = \hat{n}$. Since in this case $\hat{A} = \hat{B}$, $Im\chi(\omega) = -\pi\chi''(\omega)$, where $\chi''(\omega)$ is the dissipative function defined as

$$\chi''(q, t - t') = \langle [\hat{n}_q(t), \hat{n}_{-q}(t')] \rangle. \tag{A.6}$$

Thus we can write the fluctuation-dissipation theorem as

$$S(q,\omega) = (1 - e^{-\beta\omega})^{-1}\chi''(q,\omega). \tag{A.7}$$

On the other hand it can be proved that

$$S(q,\omega) = (1 + e^{-\beta\omega})^{-1}F(q,\omega) \tag{A.8}$$

where $F(q,\omega)$ is the Fourier transform of the fluctuation function

$$F(q,t-t') = \langle\{\hat{n}_q(t),\hat{n}_{-q}(t')\}\rangle. \tag{A.9}$$

From the latter two relations (A.7), (A.8) we can see that at zero temperature, and thus for $\beta \to \infty$, the structure factor $S(q,\omega)$ is equal both to $\chi''(q,\omega)$ and $F(q,\omega)$, where ω is a positive frequency (notice that at zero temperature the structure factor is defined only for positive frequencies). Knowing that $\chi''(\omega)$ is an odd function of omega for a model with inversion symmetry, i.e., with $(\chi''(q,\omega) = -\chi''(-q,\omega))$, it follows that

$$\begin{aligned} i\frac{\partial}{\partial t}\chi''(q,t) &= \int_{-\infty}^{+\infty}\frac{d\omega}{2\pi}\,\omega\,e^{-i\omega t}\chi''(q,\omega) = \\ &= \int_0^{+\infty}\frac{d\omega}{\pi}\,\omega\,e^{-i\omega t}\chi''(q,\omega) = \\ &= \int_0^{+\infty}\frac{d\omega}{\pi}\,\omega\,e^{-i\omega t}S(q,\omega). \end{aligned} \tag{A.10}$$

Using the definition of the dissipative function and the Heisenberg equation of motion at equal time, we obtain

$$\Sigma(q) = \int_0^{+\infty}\frac{d\omega}{\pi}\,\omega S(q,\omega) = \langle[[\hat{n}_q,H],\hat{n}_{-q}]\rangle \tag{A.11}$$

At the same time we recognize that the integral at the denominator of expression (A.3) is, for definition, the static structure factor N_q. Since, in a system with inversion symmetry, $F(\omega)$ is an even function of ω we can write

$$N_q = \langle\hat{n}_q\hat{n}_{-q}\rangle - \langle\hat{n}_q\rangle\langle\hat{n}_{-q}\rangle = \int_0^\infty F(q,\omega)\frac{d\omega}{2\pi} = \int_0^\infty\frac{d\omega}{2\pi}S(q,\omega). \tag{A.12}$$

Thus, using the static structure factor and the commutator (A.11), we find the relation for the excitation energy (A.3)

$$\Delta(q) = \frac{\langle[[\hat{n}_q,H],\hat{n}_{-q}]\rangle}{N_q}. \tag{A.13}$$

For a tight binding model, with a cubic lattice of dimension d, it can be proved that $\Sigma(q) \sim (q^2/d)T$, with T the average value of the hopping term (absolute value). Therefore it follows that the static structure factor gives information on the energy spectrum of the system: if for $q \to 0$, we have that $N_q \sim q$, then $\Delta(q) \to 0$, otherwise, if $N_q \sim q^2$, the gap $\Delta(q)$ is finite.

Moreover from the relation

$$N_q = \int_0^\infty \frac{d\omega}{\pi} \omega \chi''(q, \omega) \tag{A.14}$$

we obtain $N_q \to 0$ for the particle number conservation. Infact we can write

$$\int_0^\infty \frac{d\omega}{\pi} \chi''(q, \omega) = \int_0^q \frac{d\omega}{\pi} \chi''(q, \omega) + \int_q^\infty \frac{d\omega}{\pi} \omega \chi''(q, \omega). \tag{A.15}$$

Since q is very small we can approximate the second integral as

$$\int_0^\infty \frac{d\omega}{\pi} \chi''(0, \omega) = \int_0^\infty \frac{d\omega}{\pi} \langle [\hat{n}(0, t), \hat{n}(0, 0)] \rangle \tag{A.16}$$

which it must be equal to zero since the density does not depend on time because of the electron number conservation. The first integral in the relation (A.15) is zero if $\chi''(q, \omega)$ does not diverge for $q \to 0$.

Bibliography

[1] P.W.Anderson, *Science* **177**, 393 (1972).

[2] A. von Oudenaarden, M.H. Devoret, Yu.V. Nazarov and J.E. Mooij, *Nature* **391**, 768 (1985).

[3] S.V.Kravchenko, G.V.Kravchenko, J.E.Furneaux and V.M.Pudalov and M.D'Iorio *Phys. Rev. B* **50**, 8039 (1994).

[4] D.Belitz and T.R.Kirkpatrick, *Rev. Mod. Phys.* **66**, 261 (1994).

[5] C.Castellani, C.Di Castro and P.A.Lee, *Phys. Rev. B* **57**, R9381 (1998).

[6] A.Punnoose and A.M.Finkel'stein, *Science* **310**, 289 (2005).

[7] A.Georges, G.Kotliar, W.Krauth and M.J.Rozenberg, *Rev. Mod. Phys.* **68**, 13, (1996).

[8] D.Tanasković, V.Dobrosavljević, E.Abrahams and G.Kotliar, *Phys. Rev. Lett.* **91**, 066603 (2003).

[9] M.Capello, F.Becca, M.Fabrizio, S.Sorella and E.Tosatti, *Phys. Rev. Lett.* **94**, 026406 (2005).

[10] N.F.Mott, *Proc. Phys. Soc. London* A **62**, 416 (1949).

[11] Y.Shimizu, K.Miyagawa, K.Kanoda, M.Maesato and G.Saito, *Phys. Rev. Lett.* **91**, 107001 (2003).

[12] Y.Kurosaki, Y.Shimizu, K.Miyagawa, K.Kanoda and G.Saito, *Phys. Rev. Lett.* **95**, 177001 (2005).

[13] M.Greiner, O.Mandel, T.Esslinger, T .W.Hansch and I.Bloch, *Nature* **415**, 39 (2002).

[14] R.Jördens, N.Strohmaier, K. Günter, H.Moritz and T.Esslinger, *Nature* **455**, 204 (2008).

[15] P.W. Anderson, *Phys.Rev.* **109**, 1492 (1957).

[16] W.Kohn and J.M. Luttinger, *Phys. Rev.* **108**, 590 (1957).

[17] N.F. Mott, *Philos. Mag.* **13**, 989 (1966).

[18] N.F.Mott and W.D.Twose, *Adv.Phys.* **10**, 107 (1961).

[19] E.Abrahams, D.C.Licciardello, P.W.Anderson and T.V.Ramakrishnan, *Phis. Rev. Lett.* **42**, 673 (1979).

[20] G.J.Dolan and D.D.Osheroff, *Phys. Rev. Lett.* **43**, 721, (1971).

[21] D.J.Bishop, D.C.Tsui and R.C.Dynes, *Phys. Rev. Lett.* **44**, 1153 (1980).

[22] M.J.Uren, R.A.Davies and M.Pepper, *J.Phys C* **13**, L985 (1980).

[23] B.L.Altshuler, A.G.Aronov and P.A.Lee, *Phys. Rev. Lett.* **44**, 1288 (1980).

[24] P.A.Lee and T.V.Ramakrishnan, *Rev. Mod. Phys.* **57**, 287 (1985).

[25] A.M.Finkelstein, *Z.Phys.B:Condensed Matter* **56**, 189 (1984).

[26] C.Castellani, C.Di Castro, P.A.Lee and M.Ma, *Phys Rev.B* **30**, 527 (1984).

[27] S.V. Kravchenko and M.P.Sarachik, *Rep. Prog. Phys* **67**, 1 (2004).

[28] E.Abrahams, S.V.Kravchenko, M.P.Sarachik , *Rev. Mod. Phys.* **73**, 251 (2001).

[29] S.He and X.C.Xie, *Phys. Rev. Lett.* **80**, 3324 (1998).

[30] B.Althshuler, D.L.Maslov, *Phys. Rev. Lett.* **82**, 145 (1999).

[31] S.Anissimova, S.V.Kravchenko, A.Punnose, A.M.Finkel'stein and T.M.Klapwijk, *Nature Physics* **3**, 707 (2007).

[32] J. Huang, J.S. Xia, D.C. Tsui, L.N. Pfeiffer, and K.W. West, *Phys. Rev. Lett.* **98**, 226801 (2007).

[33] M.J. Manfra, E.H. Hwang, S. Das Sarma, L.N. Pfeiffer, K.W. West, and A.M. Sergent, *Phys. Rev. Lett.* **99**, 236402 (2007).

[34] A.M.Finkel'stein, *Zh. Eksp. Teor. Fiz.* **84**, 168 (1983).

[35] A.M.Finkel'stein, *Zh. Eksp. Teor. Fiz.* **86**, 367 (1984).

[36] B.Altshuler and A.G.Aronov, *Solid state Comm* **46**, 429 (1983).

[37] C.Castellani and C.Di Castro , *Phys. Rev. B* **34**, 5935 (1986).

[38] C. Castellani, G. Kotliar and P.A. Lee, *Phys. Rev. Lett.* **59**, 323 (1987).

[39] M.J.Hirsch, D.F.Holcomb, R.N.Bhatt and M.A.Paalanen, *Phys. Rev. Lett.* **68**, 1418 (1992).

[40] M.A,Paalanen, J.E.Graebner, R.N.Bhatt and S.Sachdev, *Phys. Rev. Lett.* **61**, 597 (1988).

[41] M.A.Paalanen, S.Sachdev, R.N.Bhatt and A.E.Ruckenstein, *Phys. Rev. Lett.* **57**, 2061 (1986).

[42] R.N.Bhatt and P.A.Lee, *Phys. Rev. Lett.* **48**, 344 (1982).

[43] J.D.Quirt and J.R.Marko, *Phys. Rev. Lett.* **26**, 318 (1971).

[44] H.Ue and S.Maekawa, *Phys. Rev. B* **3**, 4232 (1971).

[45] M.Lakner, H.v.Löneysen, A.Langfeld, P.Wölfe, *Phys. Rev. B* **50**, 17064 (1994).

[46] M.Milovanović, S.Sachdev and R.N.Bhatt, *Phys. Rev. Lett.* **63**, 82 (1989).

[47] V.Dobrosavljevic and G.Kotliar, *Phys. Rev. Lett.* **71**, 3218 (1993).

[48] E.Miranda and V.Dobrosavljević, *Rep. Prog. Phys.* **68**, 2337 (2005).

[49] J.Hubbard, *Proc. Roy. Soc. London A*, 276, (1963).

[50] M.C.Gutzwiller, *Phys. Rev. Lett.* **10**, 159 (1963).

[51] J.Kanamori, *Prog. Theor. Phys.* **30**, 275 (1963).

[52] E.H.Lieb and F.Y.Wu, *Phys. Rev. Lett.* **20**, 1445 (1968).

[53] M.C.Gutzwiller, *Phys. Rev* **134** , A923 (1964).

[54] T.A.Kaplan, P.Horsch and P.Fulde, *Phys. Rev. Lett.* **49**, 889 (1982).

[55] H.Yokoyama and H.Shiba, *J. Phys. Soc. Japan* **56**, 3582 (1987).

[56] W.Metzner and D.Vollhardt, *Phys. Rev. Lett.* **59**, 121 (1987).

[57] R.Jastrow, *Phys. Rev.* **98**, 1479 (1955).

[58] W.L.McMillan, *Phys. Rev* **138**, A442 (1965).

[59] L.Reatto and G.V.Chester *Phys. Rev* **155**, 88 (1967).

[60] B.Sutherland, *Phys. Rev.A* **4**, 2019 (1971).

[61] F.D.M.Haldane, *Phys. Rev. Lett.* **60**, 635 (1988).

[62] B.S.Shastry, *Phys. Rev. Lett.* **60**, 639 (1988).

[63] R.B.Laughlin, *Phys. Rev. Lett.* **50**, 1395 (1983).

[64] M.Capello, F.Becca, S.Yunoki, M.Fabrizio, and S.Sorella, *Phys. Rev. B* **72**, 085121 (2001).

[65] W.Kohn, *Phys. Rev* **133**, A171 (1964).

[66] A.J.Millis and S.N.Coppersmith, *Phys. Rev. B* **43**, 13770 (1991).

[67] R.Roth and K.Burnett, J. Phys B **37**, 3893 (2004).

[68] D.Belitz, A.Gold, W.Gotze, and J.Metzger, *Phys.Rev.B* **27**, 4559 (1983).

[69] S.Sorella, *Phys. Rev. B* **64**, 024512 (2001). *Phys. Rev. B* **71**, 241103 (2005).

[70] S.Yunoki and S.Sorella, *Phys. Rev. B* **74**, 014408 (2006).

[71] D.Heidarian and N.Trivedi, *Phys. Rev. Lett.* **93**, 126401 (2004).

[72] V.Dobrosavljević and G.Kotliar, *Phys. Rev. B* **50**, 1430 (1994).

[73] V.Dobrosavljević and G.Kotliar, *Phys. Rev. Lett.* **78**, 3943 (1997).

[74] V. Dobrosavljević, A.A.Pastor and B.K. Nikolić, *Europhys. Lett..* **62**, 76 (2003).

[75] M.C.O. Aguiar, V. Dobrosavljevi/'c, E.Abrahams and G.Kotliar, *Phys. Rev. B* **71**, 205115 (2005).

[76] K.Byczuk, W.Hofstetter and D.Vollhardt, *Phys. Rev. Lett.* **94**, 056404 (2005).

[77] M.Capello, F.Becca, S.Yunoki and S.Sorella, *Phys. Rev. B* **73**, 245116 (2006).

[78] P.Henseler, J.Kroha and B.Shapiro, *Phys. Rev. B* **77**, 075101 (2008).

[79] P.J.H.Denteneer, R.T.Scalettar and N. Trivedi, *Phys. Rev. Lett.* **83**, 4610 (1999).

[80] P.B.Chakraborty, P.J.H.Denteneer and R.T.Scalettar *Phys. Rev. B* **75**, 125117 (2007).

[81] I.F.Herbut, *Phys. Rev. B* **63**, 113102 (2001).

[82] M.C.O.Aguiar,V.Dobrosavljević, E. Abrahams and G. Kotliar, arXiv:cond-mat/0704.0450 (unpublished).

[83] M.C.O.Aguiar,V.Dobrosavljević, E. Abrahams and G. Kotliar, *Phys. Rev. B* **73**, 115117 (2006).

[84] M.Ulmke, V.Janiś and D.Vollhardt, *Phys. Rev. B* **51**, 10411 (1995).

[85] V.Janiś, M.Ulmke and D.Vollhardt, *Europhys. Lett..* **24**, 287 (1993).

[86] G.Misguich and C.Lhuiller, arXiv:cond-mat/0310405

[87] P.Chandra and B.Doucot, *Phys. Rev. B* **38**, 9335 (1988).

[88] L.Capriotti, F.Becca, A.Parola and S.Sorella, *Phys. Rev. Lett.* **87**, 097201 (2001).

[89] H.Q.Lin, J.E.Hirsch, *Phys. Rev. B* **35**, 3359 (1987).

[90] T.Kashima and M.Imada, *J. Phys. Soc. Jpn.* **70**, 3052 (2001).

[91] H.Morita, S.Watanabe and M.Imada, *J. Phys. Soc. Jpn.* **71**, 2109 (2002).

[92] L.F.Tocchio, F. Becca, A.Parola and S.Sorella, *Phys. Rev. B* **78**, R041101 (2008).

[93] M.E.Pezzoli, F.Becca, M.Fabrizio and G.Santoro, arXiv:cond-mat/0808.0877

[94] M.E.Pezzoli, F.Becca and M.Fabrizio (in preparation).